Thesis

Aerodynamics of a 15-MW and a 5-MW Reference Wind Turbine Using Varying Fidelity Tools

C. Dos Santos Pereira Malveiro

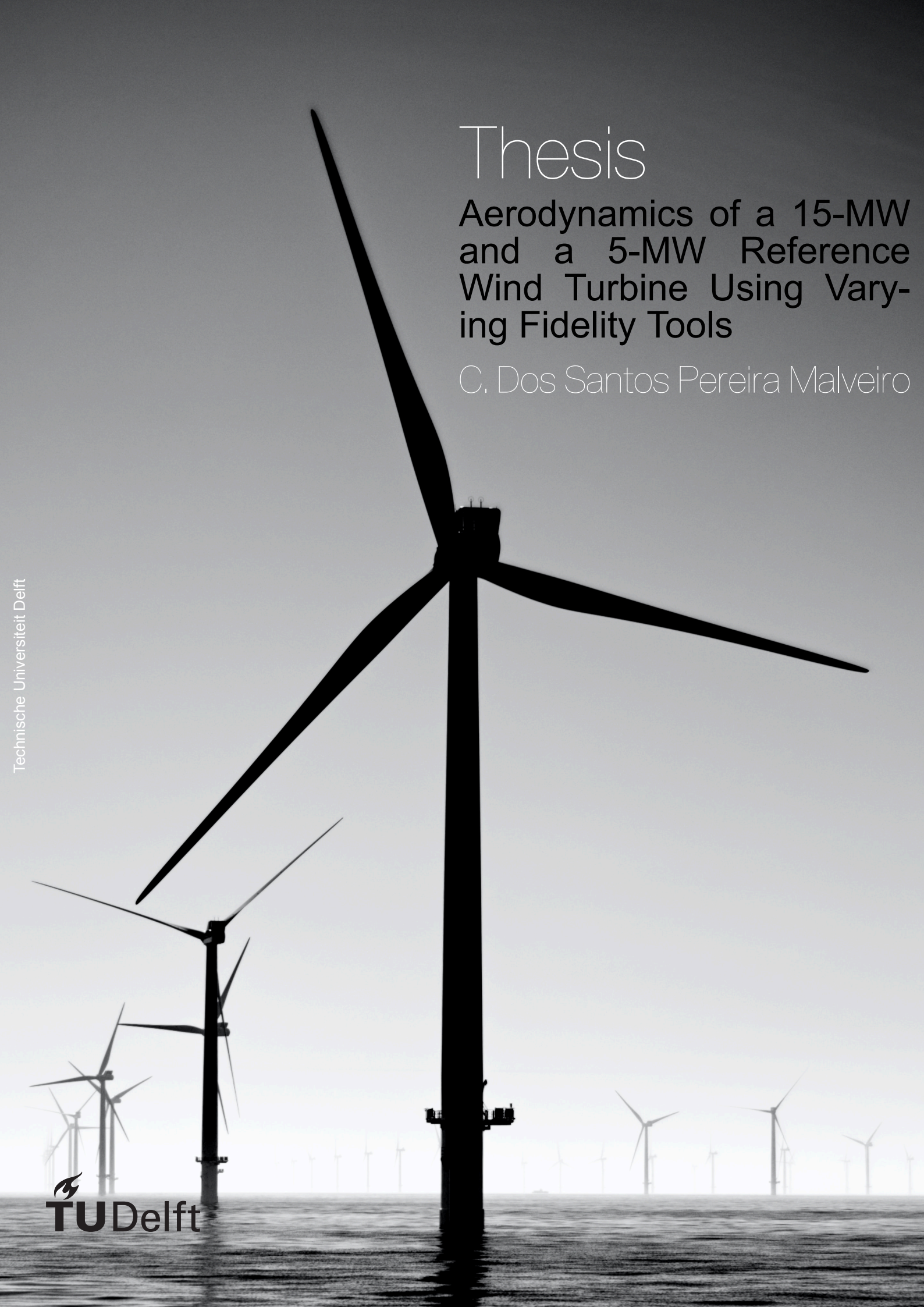

Technische Universiteit Delft

TU Delft

Thesis

Aerodynamics of a 15-MW and a 5-MW Reference Wind Turbine Using Varying Fidelity Tools

by

C. Dos Santos Pereira Malveiro

to obtain the degree of Master of Science
at the Delft University of Technology,
to be defended publicly on Tuesday June 22, 2022 at 09:30 AM.

Student number:	4534301	
Project duration:	August 30, 2021 – June 22, 2022	
Thesis committee:	Prof.dr. D.A. von Terzi,	TU Delft, chairman
	Dr.Ir. A.C. Viré,	TU Delft, supervisor
	Dr.Ir. M. Pini,	TU Delft, committee member

An electronic version of this thesis is available at http://repository.tudelft.nl/.

TU Delft

Preface

My six years at the TU Delft have come to an end and I find it difficult to believe. So much I have learned and so much I have still yet to learn. I have very much enjoyed working on this thesis project and I hope you will find it an interesting read.

Before jumping to the introduction, I first want to give my thanks to several people. First of all, my supervisor Axelle Viré who guided me with this thesis project and set me up with the right people for my questions. I also want to thank the AWEP board for all the interesting lunch lectures, excursions and drinks. Next, I want to thank the people who made my student years all worth it, these are of course the gentlemen from Pelikaan, Gier, Oude Delft 124 and my old high school buddies Pepijn, Bastiaan and Tim, all of whom I undoubtedly will still see far beyond my student years. From pelikaan, I would like to thank especially Alex, Arjen, Cotino, Dimitri, Hidde, Huib, Jan-Willem, Justin, Lars, Luuk, Sjaak and Tim for all the beer, holidays, fieldtrips, 21 diners, gymsessions and much more. I want to thank GIER (especially Jason, Quincy and Hidde) for all the memorable moments and I want to thank my housemates of the Oude Delft 124, Addick, Niels, Rick and Tobias for all the AVGs. Finally, I must also thank my family for supporting me in my student years. My parents who have always been there for me through thick and thin, my sisters who always give me the much needed unsolicited advice and my brother who borrowed me his old laptop to finish my thesis. I also want to thank my aunt and uncle Wil and Aart for all the good times and the good food and also my old nanny and her husband Grace and Theo for still keeping in touch after all these years. Finally, I want to thank my girlfriend, Lotte, for always filling my heart with love.

C. Dos Santos Pereira Malveiro
Delft, June 2022

Abstract

The most effective way to decrease the cost of energy of wind turbines is to increase the rotor diameter. This is true due to the economies of scale and the increasing energy capture per turbine. Also, a lower specific power (ratio diameter/power) corresponds to a higher capacity factor leading to more operating hours in full power. Therefore, this calls for the need of aerodynamic research on large wind turbines with a higher power rating than 10 MW.

This thesis project aimed to tackle the topics addressed by the IEA Wind Task 47 which is focused on the aerodynamic analysis and comparison of the newly proposed IEA 15-MW reference wind turbine using varying fidelity tools. Therefore, the main goal of this work was to analyse whether a low-fidelity approach is still feasible for aerodynamic analysis in comparison with a high-fidelity approach for uniform inflow conditions. The high-fidelity model was based on a RANS or LES CFD simulation with an actuator line model of the rotor and it was solved using the CFD solver OpenFOAM. Two low-fidelity models were also analysed, one was the free vortex wake method and the other was based on the BEM theory. Both low-fidelity methods were applied in OpenFAST.

The outcome of this thesis project is twofold as there are two research questions. First, it provides an understanding of the the effect of different sizes of wind turbines and its corresponding design on the wake aerodynamics. Secondly, the larger impact of this work is to show how critical it is to use high-fidelity methods, with respect to low-fidelity methods, to analyse the aerodynamics of large wind turbines. The answer to this question is important for wind turbine designers as they want to optimize a design based on the most accurate methods for the least computational effort. It can be concluded that there are quantitative differences between the different fidelity methods that increase with almost 50 % when comparing the NREL 5-MW RWT with the IEA 5-MW RWT. There are however qualitative similarities to be found for the same comparison. Therefore it is recommended to perform more research on this topic which could include different turbines, different fidelities and different fields (such as aero-elasticity and aero-acoustics) to identify whether the findings of this thesis project are on the right track.

Contents

Preface iii

Abstract v

List of Figures xi

List of Tables xiii

nomenclature xvi

1 Introduction 1

2 Wind Turbine High-Fidelity Aerodynamic Analysis Methods 3
2.1 Basic Overview of Horizontal Axis Wind Turbine Aerodynamics . . . 3
2.2 Computational Fluid Dynamics (CFD) . . . 4
2.2.1 RANS . . . 5
2.2.2 LES . . . 5
2.2.3 Conclusion . . . 6
2.3 Actuator Disc Method (ADM) . . . 6
2.4 Actuator Line Method (ALM) . . . 7
2.5 Blade Resolved Method (BRM) . . . 8
2.6 Comparison Between the Different Methods . . . 9
2.7 CFD Solver OpenFOAM . . . 10
2.7.1 Mesh Generation . . . 10
2.7.2 Models and Physical Properties . . . 10
2.7.3 Solver . . . 11
2.7.4 Actuator Line Modelling in OpenFOAM . . . 11

3 Wind Turbine Low-Fidelity Aerodynamic Analysis Methods 13
3.1 Blade Element Momentum (BEM) Method . . . 13
3.2 Free Vortex Wake (FVW) Method . . . 15

4 Introduction to the Reference Wind Turbines (RWTs) 17
4.1 The NREL 5-MW Reference Wind Turbine . . . 17
4.2 The IEA 15-MW Reference Wind Turbine . . . 20

5 Aerodynamic Analysis of the NREL 5-MW RWT 23
5.1 Actuator Line Method (ALM) of the NREL 5-MW RWT . . . 23
5.1.1 Numerical Setup . . . 23
5.1.2 Grid Refinement Study . . . 25
5.1.3 Temporal Convergence Study . . . 28
5.1.4 Number of Actuator Elements Study . . . 29
5.1.5 Verification Study . . . 30
5.1.6 Effect of the Ground, Tower and Hub . . . 32
5.1.7 Conclusion . . . 33
5.2 Blade Element Momentum Theory (BEM) of the NREL 5-MW RWT . . . 33
5.3 Free Vortex Wake (FVW) Method of the NREL 5-MW RWT . . . 34
5.4 Discussion of the Results of the Varying Fidelity Methods . . . 36
5.5 Conclusion . . . 37

6 Aerodynamic Analysis of the IEA 15-MW RWT **39**
6.1 Actuator Line Method (ALM) of the IEA 15-MW RWT . . . 39
6.1.1 Numerical Setup . . . 39
6.1.2 Grid Refinement Study . . . 40
6.1.3 Number of Actuator Elements Study . . . 41
6.1.4 Conclusion . . . 42
6.2 Blade Element Momentum Theory (BEM) of the IEA 15-MW RWT . . . 42
6.3 Free Vortex Wake (FVW) Method of the IEA 15-MW RWT . . . 43
6.4 Discussion of the Results of the Varying Fidelity Methods . . . 45
6.5 Conclusion . . . 46

7 Aerodynamic Comparison of the NREL 5-MW RWT and the IEA 15-MW RWT **47**
7.1 Comparison of Performance Parameters . . . 47
7.2 Comparison of Velocity Deficit Plots . . . 52
7.3 Comparison of Wake Visualization . . . 53
7.4 Comparison of Velocity Profiles . . . 56
7.5 Discussion and Conclusion . . . 57

8 Conclusions and Recommendations **59**
8.1 Summary of Conclusions . . . 59
8.2 Final Conclusions . . . 60
8.3 Recommendations . . . 61

List of Figures

2.1 Illustration of the angles and the forces that act on an airfoil element [11] 7

3.1 Illustration of the velocities and the forces that act on a blade element [5] 13

5.1 Cross-sectional front view of the baseline computational grid of the NREL 5-MW RWT . 24
5.2 Cross-sectional side view of the baseline computational grid of the NREL 5-MW RWT . 24
5.3 Plot of the power coefficient versus time to identify the time at which the solution has converged 24
5.4 Cross-sectional front view of the computational grid for the very fine cylinder region near the turbine 25
5.5 Cross-sectional front view of the computational grid for the very fine cylinder region near the turbine 25
5.6 Plot of the velocity deficit to compare the cases used to study the grid refinement 26
5.7 Zoomed in version of the plot of the velocity deficit to compare the cases used to study the grid refinement 27
5.8 Vorticity contour plot of the very coarse grid with Q-criterion = 0.001 27
5.9 Vorticity contour plot of the coarse grid with Q-criterion = 0.001 27
5.10 Vorticity contour plot of the baseline grid with Q-criterion = 0.001 28
5.11 Vorticity contour plot of the fine grid with Q-criterion = 0.001 28
5.12 Vorticity contour plot of the cylinder refinement grid with Q-criterion = 0.001 28
5.13 Vorticity contour plot of the cylinder refinement grid with Q-criterion = 0.01 28
5.14 Plot of the velocity deficit to compare the cases used to study the temporal convergence 29
5.15 Plot of the velocity deficit to compare the cases used to study the number of actuator elements 30
5.16 Plot of the lift coefficient along the span to compare the cases used to study the number of actuator elements 30
5.17 Velocity deficit plot of the coarse, baseline and refined grid (case 02) 31
5.18 C_p versus TSR plot used to verify the results from ALM with data from [24] 31
5.19 Cross-sectional front view of the new computational grid of the NREL 5-MW RWT including the ground as a wall boundary 32
5.20 Cross-sectional side view of the new computational grid of the NREL 5-MW RWT including the ground as a wall boundary 32
5.21 Velocity deficit plot to study the effect of including the ground, tower and hub in the baseline case 33
5.22 Visualization of the lifting lines 35
5.23 Visualization of the near wake for only one blade 35
5.24 Visualization of both the near wake and the far wake for only one blade 35
5.25 A complete visualization of both the near and the far wake for all blades 35
5.26 C_P versus TSR plot used to compare the results of the ALM, OLAF and BEM 36
5.27 C_T versus TSR plot used to compare the results of the ALM, OLAF and BEM 36
5.28 ALM vorticity contour plot of the fine grid with Q-criterion = 0.001 37
5.29 OLAF wake visualization of both the near and the far wake 37

6.1 Cross-sectional front view of the baseline computational grid of the IEA 15-MW RWT . . 40
6.2 Cross-sectional side view of the baseline computational grid of the IEA 15-MW RWT . . 40
6.3 Plot of the velocity deficit to compare the cases used to study the grid refinement 41
6.4 Vorticity contour plot of the very coarse grid with Q-criterion = 0.0001 41
6.5 Vorticity contour plot of the baseline grid with Q-criterion = 0.0001 41

6.6 Plot of the velocity deficit to compare the cases used to study the number of actuator elements . . . 42
6.7 C_P versus TSR plot used to compare the results of BEM with the definition of the RWT as defined in [2] . . . 43
6.8 C_T versus TSR plot used to compare the results of BEM with the definition of the RWT as defined in [2] . . . 43
6.9 Visualization of the near wake for only one blade . . . 44
6.10 Visualization of the lifting lines . . . 44
6.11 Visualization of both the near wake and the far wake for only one blade . . . 44
6.12 A complete visualization of both the near and the far wake for all blades . . . 44
6.13 C_P versus TSR plot used to compare the results of ALM, OLAF and BEM . . . 45
6.14 C_T versus TSR plot used to compare the results of the BEM with the definition of the RWT as defined in [2] . . . 45

7.1 C_T versus TSR plot of the NREL 5-MW RWT . . . 47
7.2 C_T versus TSR plot of the IEA 15-MW RWT . . . 48
7.3 C_P versus TSR plot of the NREL 5-MW RWT . . . 48
7.4 C_P versus TSR plot of the IEA 15-MW RWT . . . 49
7.5 C_T versus TSR plot of the IEA 15-MW RWT including the downscaled 5-MW turbine . . . 50
7.6 C_P versus TSR plot of the IEA 15-MW RWT including the downscaled 5-MW turbine . . . 50
7.7 Plot of the non-dimensional chord distribution along the span . . . 51
7.8 Plot of the twist distribution along the span . . . 51
7.9 Plot of the drag coefficient distribution along the span . . . 51
7.10 Plot of the lift coefficient distribution along the span . . . 52
7.11 Plot of the velocity deficit at a TSR of 9 for the IEA 15-MW RWT, the NREL 5-MW RWT and the downscaled version of the IEA 15-MW to a 5-MW version . . . 52
7.12 The same plot of the previous velocity deficit but now including the the line of the NREL 5-MW RWT at its design TSR of 7.5 . . . 53
7.13 Vorticity contour plot of the IEA 15-MW RWT with a very coarse grid and Q-criterion = 0.0001 . . . 54
7.14 Vorticity contour plot of the IEA 15-MW RWT with a baseline grid and Q-criterion = 0.0001 54
7.15 Vorticity contour plot of the NREL 5-MW RWT with a very coarse grid and Q-criterion = 0.001 . . . 54
7.16 Vorticity contour plot of the NREL 5-MW RWT with a very coarse grid and Q-criterion = 0.001 . . . 54
7.17 Vorticity contour plot of the downscaled version of the IEA 15-MW RWT with a very coarse grid and Q-criterion = 0.0001 . . . 54
7.18 Vorticity contour plot of the IEA 15-MW RWT and the downscaled version with a baseline grid and Q-criterion = 0.0001 . . . 54
7.19 Example of two ways to discretize the grid when scaling the turbine . . . 55
7.20 Visualization of both the near wake and the far wake of the NREL 5-MW RWT for only one blade . . . 55
7.21 Visualization of both the near wake and the far wake of the IEA 15-MW RWT for only one blade . . . 55
7.22 Velocity profile plot of the IEA 15-MW RWT with the baseline grid resolution ($2mx2mx2m$) 56
7.23 Velocity profile plot with overlapping grid of the IEA 15-MW RWT with the baseline grid resolution ($2mx2mx2m$) . . . 56
7.24 Velocity profile plot of the NREL 5-MW RWT with the baseline grid resolution ($2mx2mx2m$) 56
7.25 Velocity profile plot with overlapping grid of the NREL 5-MW RWT with the baseline grid resolution ($2mx2mx2m$) . . . 56
7.26 Velocity profile plot of the downscaled version of the IEA 15-MW RWT with the baseline grid resolution ($2mx2mx2m$) . . . 56
7.27 Velocity profile plot with overlapping grid of the downscaled version of the IEA 15-MW RWT with the baseline grid resolution ($2mx2mx2m$) . . . 56
7.28 Velocity profile plot of the IEA 15-MW RWT with the very coarse grid resolution ($4mx4mx4m$) 57

7.29 Velocity profile plot with overlapping grid of the IEA 15-MW RWT with the very coarse grid resolution ($4mx4mx4m$) 57
7.30 Velocity profile plot of the NREL 5-MW RWT with the very fine grid resolution ($1mx1mx1m$) 57
7.31 Velocity profile plot with overlapping grid of the NREL 5-MW RWT with the very fine grid resolution ($1mx1mx1m$) 57

List of Tables

4.1 Key parameters of the NREL 5-MW RWT [23] 18
4.2 Key parameters of the IEA 15-MW RWT [2] 21

5.1 Overview of all the cases analyzed in this section 25
5.2 Cases used to study the grid refinement 25
5.3 Cases with their corresponding power and thrust coefficient 26
5.4 Cases used to study the temporal convergence 29
5.5 Cases used to study the number of actuator elements 29
5.6 Cases used to study the effect ground, tower and hub 32

6.1 Overview of all the cases analyzed in this section 40

7.1 Overview of the computation time required for each turbine and fidelity tool 58

Nomenclature

Abbreviations

2D	Two Dimensional
3D	Three Dimensional
ADM	Actuator Disk Method
ALM	Actuator Line Method
BEM	Blade Element Momentum Theory
BRM	Blade Resolved Method
CAD	Computer Aided Design
CFD	Computational Fluid Dynamics
DDES	Delayed Detached Eddy Simulation
DES	Detached Eddy Simulation
FVW	Free Vortex Wake Method
IEA	International Energy Agency
LES	Large Eddy Simulation
MRF	Multiple Reference Frame
NREL	National Renewable Energy Laboratory
OLAF	cOnvectinig LAgrangian Filaments
PIMPLE	Pressure-Implicit Method for Pressure Linked Equations
PISO	Pressure-Implicit with Splitting of Operators
RANS	Reynolds Averages Navier-Stokes Equations
RWT	Reference Wind Turbine
SGS	subgrid-scale stresses
SIMPLE	Semi-Implicit Method for Pressure Linked Equations
SMI	Sliding Mesh Interface
SRF	Single Reference Frame
SST	Shear Stress Transport
TSR	Tip Speed Ratio

Symbols

α	Angle of attack
ϵ	Regularization parameter
η_ϵ	Regularization function
Γ	circulation
λ	Tip speed ratio
$\mathbf{e}_D$	Drag unit vector
$\mathbf{e}_L$	Lift unit vector
$\mathbf{f}$	Force vector
$\mathbf{f}_{2D}$	Two dimensional force vector
$\mathbf{f}_\eta$	Regularized force vector
$\mathbf{n}$	Normal vector
$\mathbf{u}$	Velocity vector
$\mathbf{x}$	Location vector
μ	Dynamic viscosity of air
ν	Kinematic viscosity
ν_{SGS}	Subgrid-scale stress viscosity
ν_T	Turbulent eddy viscosity
Ω	Rotational velocity or domain
ϕ	Flow angle
ψ	Azimuthal angle
ρ	Density
τ_{SGS}	Subgrid-scale stress
θ	Pitch angle
$\vec{\omega}$	Vorticity vector
$\vec{r}$	Distance vector
$\vec{u}$	Velocity vector
$\vec{v}$	Velocity vector
$\vec{V}_0$	Free stream velocity vector
$\vec{v}_\omega$	Induced velocity vector
A	Area
a	Axial induction factor

a'	tangential induction factor
A_∞	Cross-sectional area of the streamtube upstream
A_d	Cross-sectional area of the streamtube at the disc
A_w	Cross-sectional area of the streamtube at the far wake
c	Chord length
C_D	Three dimensional drag coefficient
C_d	Two dimensional drag coefficient
C_L	Three dimensional lift coefficient
C_l	Two dimensional lift coefficient
C_P	Power coefficient
C_T	Thrust coefficient
Co	Courant number
d	Distance
$d\vec{l}$	Length along a filament
dx	Characteristic cell size
F_v	Regularization parameter
L'	Lift per unit span
p	Pressure
R	Radius
r	Spanwise distance
S	Surface
t	Time
U_∞	Free stream velocity
U_d	Velocity at the disc
U_{tip}	Tip speed
U_w	Velocity at far wake
V_θ	Tangential velocity
V_{ref}	Reference velocity
V_{rel}	Relative velocity
V_z	Axial velocity
W	Resultant velocity
B	Number of blades
D	Drag
L	Lift
Q	Torque
T	Thrust
V	Velocity
W	Velocity

1 Introduction

The most effective way to decrease the cost of energy of wind turbines is to increase the rotor diameter. This is true due to the economies of scale and the increasing energy capture per turbine. Also, a lower specific power (ratio diameter/power) corresponds to a higher capacity factor leading to more operating hours in full power. Therefore this calls for the need of aerodynamic research on large wind turbines with a higher power rating than 10 MW [1].

A lot of the wind turbine research worldwide is performed on so-called reference wind turbines (RWTs) which are theoretical wind turbines. There are a variety of reasons for this. First of all, they are used as the baseline for the wind energy community to perform optimization studies on or to explore new technologies. Secondly, it allows for collaboration between industry and academia as the intellectual property of the industry is protected while they can still research new developments. Third and last of all, RWTs are a good starting point for newcomers to understand fundamental design. Several of these RWTs have been proposed since the beginning of this century by the National Renewable Energy Laboratory (NREL) and to be relevant with the increasing wind turbine size, a new RWT has to be the new baseline for research. In this light, a new wind turbine has been proposed by the NREL in collaboration with the International Energy Agency (IEA) which is a 15-MW RWT for use in offshore wind energy and it has been designed for both bottom-fixed and floating support structures [2].

The thesis project will tackle the topics addressed by the IEA Wind Task 47 which is focused on the aerodynamic analysis and comparison of this RWT using varying fidelity tools. The aerodynamic analysis will be performed using the open-source CFD solver OpenFOAM [3] and the open-source wind turbine simulation tool OpenFAST [4]. This project is at the forefront of the research undertaken in the offshore wind energy field as this RWT has just been proposed. The main goal of this work is to analyse whether a low-fidelity approach is still feasible for aerodynamic analysis in comparison with a high-fidelity approach. The main research questions to be solved in reaching the project goal are listed below. With each main research question, there are also sub-questions that together give an answer to the main research question.

1. How does the IEA 15-MW RWT compare with the previous NREL 5-MW RWT in terms of the steady state analysis and the unsteady wake simulation?
   (a) Does the 15-MW RWT show more complex aerodynamics?
   (b) What is the direct effect of the increased rotor size on the wake aerodynamics?
2. How well do different fidelity models perform in analysing the 15-MW RWT?
   (a) Are there significant differences in the performance parameters when using the different fidelity models?
   (b) Is the use of CFD critical for analysing the 15-MW RWT with uniform inflow conditions?

The main research objective of this thesis is to perform an aerodynamic analysis and comparison of the IEA 15-MW RWT and the NREL 5-MW RWT by using varying fidelity tools such as the actuator line method (ALM) with the CFD solver OpenFOAM, the blade element momentum (BEM) method and the free vortex method (OLAF) with the simulation tool OpenFAST. To achieve this main objective multiple sub-goals can be created. The first sub-goal is to make a model of the 5-MW RWT in OpenFOAM using the actuator line method. Also, the blade element momentum theory and the free vortex method model of this RWT should be made in OpenFAST. The results from these models should then be analysed and verified using literature. Once these models are verified it is possible to make a similar high-fidelity and low-fidelity model for the 15-MW RWT for which there is almost no literature available. The last step is then to answer the research questions by performing an aerodynamic analysis and comparison of this 15-MW RWT with the 5-MW RWT and to compare the results of the different fidelity models.

This thesis report will continue with the discussion of the state-of-the-art about different topics that are related to this research. It starts with a literature review of the high-fidelity aerodynamic analysis methods after which the low-fidelity methods are discussed. The fourth chapter contains the literature review of the NREL 5-MW RWT and the IEA 15-MW RWT. The latter is a newly proposed wind turbine and therefore not a lot of research has yet been published about it but the state-of-the-art regarding this wind turbine should still be discussed. The NREL 5-MW RWT on the other hand, offers much more literature and will therefore serve as the basis for verification of the model used to analyse the IEA 15-MW RWT. Following the introduction of the RWTs, the aerodynamic analysis of the NREL 5-MW RWT and of the IEA 15-MW RWT are covered in chapter 5 and chapter 6, respectively. With the two turbines discussed in detail it is possible to compare them in chapter 7 and finally a conclusion with recommendations for future research is given in chapter 8.

2

Wind Turbine High-Fidelity Aerodynamic Analysis Methods

This chapter will introduce and discuss the state-of-the-art of the high-fidelity aerodynamic analysis methods for wind turbine wake analysis. High-fidelity, in this case, means that computational fluid dynamics (CFD) is used which can accurately solve the Navier-Stokes equations that are the governing equations in fluid mechanics. There are in general two methods to model the wind turbine when solving these equations. The first method is to use actuator models which model the blades of the wind turbine either as for example a disc or a line which simplifies the problem and reduces the computational requirements. The other method is to fully resolve the blades of the wind turbine which means that the geometry of the blades are discretized on the computational grid. This increases the computational cost but allows for better blade calculations that could include the simulation of transition, separation and stall. This chapter will go into detail about these methods and find out which method fits best to this thesis project. To do this, this chapter will first start with a basic overview of wind turbine aerodynamics. Secondly a basic overview of computational fluid dynamics will be provided. After that the actuator disc method will be described. Then the actuator line method is explained, after which that the blade resolved method will be described. In the end, a comparison is given for these different methods and a conclusion is provided for with which method to continue the thesis project.

2.1. Basic Overview of Horizontal Axis Wind Turbine Aerodynamics

This section will explain how horizontal axis wind turbines (HAWT) are used to extract kinetic energy from the wind as described in the Wind Energy Handbook [5]. Starting with the one-dimensional momentum theory and modelling the rotor as a disc (and calling it the actuator disc), a streamtube can be drawn where no mixing occurs between the flow that is inside the streamtube (which enters the actuator disc) and the flow outside the streamtube (which does not enter the actuator disc). As the flow inside the streamtube goes through the actuator disc, its kinetic energy is reduced, and therefore the velocity of the flow is reduced which causes the cross-sectional area of the streamtube to increase due to the mass conservation of the incompressible fluid. Mass conservation means that, assuming constant density and an absence of a mass source or loss inside the streamtube, the mass flow rate should be the same at every plane of the streamtube. This can be written as the continuity equation as shown in Equation 2.1.

$$\rho A_\infty U_\infty = \rho A_d U_d = \rho A_w U_w \tag{2.1}$$

Where ρ is the density, A is the cross-sectional area at a plane of the streamtube and U is the velocity. Subscript ∞ refers to the free stream conditions, subscript d refers to the disc and subscript w is used for the wake. The relation between the velocity at the disc U_d and the freestream velocity U_∞ can be related by the so-called induction factor a as shown in Equation 2.2.

$$U_d = U_\infty(1-a) \tag{2.2}$$

Using the momentum theory, a relation between the velocity at the wake U_w and the free stream velocity U_∞ can be derived as well which is shown in Equation 2.3. This equation shows that half of the velocity is lost upstream of the actuator disc and half is lost downstream.

$$U_w = U_\infty(1-2a) \tag{2.3}$$

The momentum theory can be used to calculate the power coefficient of the disc which is shown in Equation 2.4. The maximum power coefficient (also known as the Betz limit) can be derived by taking the derivative of the C_P with respect to the induction factor and finding for which induction factor this equals zero. This happens when the induction factor equals $a = \frac{1}{3}$ and this gives a power coefficient of $C_{p,max} = \frac{16}{27} = 0.593$

$$C_P = \frac{Power}{\frac{1}{2}\rho U_\infty^3 A_d} = 4a(1-a)^2 \tag{2.4}$$

The thrust that the actuator disc exerts can also be non-dimensionalised to the thrust coefficient which is defined in Equation 2.5. This equation is only valid for induction factors lower than 0.5 because for higher induction factors the wake velocity as shown in Equation 2.3 becomes negative and the momentum theory cannot be used anymore.

$$C_T = \frac{Thrust}{\frac{1}{2}\rho U_\infty^2 A_d} = 4a(1-a) \tag{2.5}$$

The last topic that should be addressed before explaining the higher fidelity methods is the blade element momentum (BEM) theory. The blade element momentum theory uses a global momentum balance with 2D c_l and c_d airfoil data to calculate forces on the blade. Each blade is split into individual blade elements that have no interaction with each other. The main assumption is that the force on each element is solely responsible for the change in momentum of the flow that passes through the annulus swept by this element. From BEM it is possible to calculate blade and turbine characteristics such as the power coefficient of the wind turbine as a function of the tip speed ratio.

The equations above provide guidelines in creating numerical codes to simulate and model wind turbines. The rest of this section will continue with the higher fidelity models. These higher fidelity models are based on computational fluid dynamics and a certain modelling method such as actuator line, actuator disc or blade resolved.

2.2. Computational Fluid Dynamics (CFD)

The incompressible Navier-Stokes equations can be used to describe the wake aerodynamics of wind turbines as long as tip speed is below a Mach number of 0.25. This is just about the case with this RWT where the tip speed is given in Table 4.2 as 95 m/s. It does mean however that care must be given when fully resolving the blades since then it might be required to solve the compressible Navier-Stokes equations at the tip of the blades (see section 2.5). The incompressible Navier-Stokes equations are given below [6].

$$\nabla \cdot \mathbf{u} = 0 \tag{2.6}$$

$$\frac{\partial \mathbf{u}}{\partial t} + (\mathbf{u}\cdot\nabla)\mathbf{u} = -\frac{1}{\rho}\nabla p + \nu\nabla^2\mathbf{u} \tag{2.7}$$

These are the governing equations which have no analytical solutions and are not easy to solve numerically. The non-linear convective term creates a wide range of time and length scales that can range from 1 km to 1 mm for the atmospheric boundary layer. For this reason, it is not feasible to resolve all scales in the flow using direct numerical simulations. This, therefore, calls in the need for turbulence models which use the behaviour of the large scales to model the effect of the unresolved small scales. It

is important to note however that it is not possible to resolve the boundary layer and the turbulent wake structures at the same time [6]. The rest of this section will explain the two most important classes of turbulence modelling (RANS and LES) and close off with a comparison and conclusion of which method is deemed must suitable for this thesis project.

2.2.1. RANS

The Reynolds-averaged Navier-Stokes (RANS) approach is used to calculate and solve for the mean flow. this can be done by splitting the velocity and pressure into a mean and a fluctuation component which is also known as the Reynolds decomposition as shown in Equation 2.8.

$$\mathbf{u}(\mathbf{x}, t) = \overline{\mathbf{u}}(\mathbf{x}) + \mathbf{u}'(\mathbf{x}, t) \tag{2.8}$$

The above Equation 2.8 can be substituted into Equation 2.7. Then using ensemble averaging (which states that the average of the average is the average and that the average of the fluctuations equals zero) the averaged Navier-Stokes equations can be written as Equation 2.9.

$$\frac{\partial \overline{\mathbf{u}}}{\partial t} + (\overline{\mathbf{u}} + \cdot\nabla)\overline{\mathbf{u}} + = -\frac{1}{\rho}\nabla\overline{p} + \nu\nabla^2\overline{\mathbf{u}} - \nabla \cdot (\overline{\mathbf{u}'\mathbf{u}'}) \tag{2.9}$$

In the above equation, the term $\overline{\mathbf{u}'\mathbf{u}'}$ is known as the Reynolds stress tensor which is the averaged momentum transfer because of the turbulent fluctuations. This term will be modeled in terms of the mean flow quantities to close the system of equations. There are different models that do this. The first approach was proposed by [7], which relates the Reynolds stress to the mean velocity gradients via a turbulent eddy viscosity v_T as shown in Equation 2.10 [6].

$$\overline{\mathbf{u}'\mathbf{u}'} = \nu_T\left(\nabla\overline{\mathbf{u}} + (\nabla\overline{\mathbf{u}})^T\right) \tag{2.10}$$

This method is computationally efficient since the Reynolds stress tensor is only weakly dependent on the Reynolds number. There are some issues with the validity of this method however as there is no physical evidence for Equation 2.10. this makes this method unsuitable for a variety of cases such as sudden changes in mean strain rate, anisotropic flows and 3D flows. Nevertheless, different methods have been proposed to calculate the turbulent eddy viscosity v_T. Two important ones for wind turbine applications are the $k-\epsilon$ the $k-\omega$ model. The $k-\epsilon$ is a two-equation model used frequently for wind turbine wake calculations and the $k-\omega$ model is used frequently for blade calculations [6].

2.2.2. LES

The large eddy simulation (LES) approach is used to calculate large eddies of the flow while the eddies that are smaller than the grid are modeled with the so-called subgrid-scale models. This separation is performed by filtering the velocity field and by applying it to the Navier-Stokes equations which leads to Equation 2.11 where $\widetilde{\mathbf{u}}$ is defined as the filtered velocity (also known as resolved, large scale or simulated velocity) [6].

$$\frac{\partial \widetilde{\mathbf{u}}}{\partial t} + (\widetilde{\mathbf{u}} \cdot \nabla)\widetilde{\mathbf{u}} = -\frac{1}{\rho}\nabla\widetilde{p} + \nu\nabla^2\widetilde{\mathbf{u}} - \nabla \cdot (\widetilde{\mathbf{u}\mathbf{u}} - \widetilde{\mathbf{u}}\widetilde{\mathbf{u}}) \tag{2.11}$$

In the above equation, the term $(\widetilde{\mathbf{u}\mathbf{u}} - \widetilde{\mathbf{u}}\widetilde{\mathbf{u}})$ is known as the subgrid-scale stresses (SGS) which are the effect of the unresolved scales on the large scales. One important model that is frequently used is the Smogorinsky model which is shown in Equation 2.12 [8].

$$\tau_{SGS} = \widetilde{\mathbf{u}\mathbf{u}} - \widetilde{\mathbf{u}}\widetilde{\mathbf{u}} = -\nu_{SGS}\left(\nabla\widetilde{\mathbf{u}} + (\nabla\widetilde{\mathbf{u}})^T\right) \tag{2.12}$$

One big downside of the LES model is that the computational cost approximately scales with the Reynolds number squared and at the boundary layer it requires refinement in three directions (RANS only requires it normal to the wall) [6].

2.2.3. Conclusion

The LES approach can calculate unsteady, anisotropic turbulent flows with large-scale structures and turbulent mixing which the RANS approach is not able to do. That makes it troublesome to use the RANS approach for wind turbine wake calculations as the flow is highly unsteady and, due to the averaging of the Navier-Stokes equations, these unsteady features are lost (keep in mind that, also for blade aerodynamic, RANS will not always be able to capture the flow physics accurately for instance if there is large flow separation). However, the computational costs for the LES approach are also much higher than the RANS approach as the RANS approach is only weakly dependent on the Reynolds number and the LES approach scales approximately with the Reynolds number squared [9]. Keeping all this in mind, the choice has been made to go with the RANS approach particularly because the computational time for performing an LES would be out of the scope of this thesis project. If it turns out that it is possible to perform an LES simulation then that would be preferred.

Now that the computational fluid dynamics theory has been discussed it is possible to discuss the different high-fidelity modelling methods. This starts with the momentum equation as shown in Equation 2.7 but then the force that is exerted by the actuator disc (or line) is added as a momentum sink as shown in Equation 2.13 [6].

$$\int_{\Omega} \frac{\partial \mathbf{u}}{\partial t} \cdot d\Omega + \int_{\partial\Omega} \mathbf{u}\mathbf{u} \cdot \mathbf{n} \cdot dS = -\int_{\partial\Omega} \frac{1}{\rho} p\mathbf{n} \cdot dS + \int_{\partial\Omega} \nu \nabla \mathbf{u} \cdot \mathbf{n} \cdot dS + \int_{A\cap\Omega} \mathbf{f} \cdot dA \tag{2.13}$$

Because of the discontinuity in pressure, this is written in the weak form. Apart from adding the momentum sink also the sources of turbulence that would normally be generated by the pressure of the blades should be added [6]. In the following sections, the formulation of this momentum sink term will be discussed for the different modelling approaches.

2.3. Actuator Disc Method (ADM)

The actuator disc method (ADM) uses an actuator disc that exerts forces on the fluid that passes through. These forces can be the thrust or a combination of the thrust with a tangential force. This way it is possible to model the blades of a wind turbine as a rotor disc and to simulate the wake it would produce. However, it is important to note that the ADM cannot simulate the tip vortices that would be produced by the blades [9].

The thrust force for a uniformly loaded actuator disc is given by Equation 2.14 [6]. This thrust is based on a one-dimensional approximation and it does not take into account the rotation in the flow caused by the blades. Notice that this equation is virtually the same as Equation 2.5. However, the V_{ref} may not just be the U_∞ since the wind turbine could be in the wake of a different wind turbine. This is important because the ADM is especially effective when used in wind farm analysis and therefore the situation of one turbine being in the wake of another is one that should be considered [10].

$$\rho\mathbf{f} = \frac{1}{2}\rho V_{ref}^2 C_T \tag{2.14}$$

In the case of a non-uniformly loaded disc, the force is considered to be constant over an annulus but can change depending on the radial position. The sectional lift and drag coefficients are then used to find the forces on the annulus as shown in Equation 2.15 (just like with the blade element momentum theory as explained in section 3.1) [6]. In this equation, c_l and c_d are the lift and drag coefficients while $\mathbf{e}_L$ and $\mathbf{e}_D$ are the unit vectors for the lift and the drag, respectively. Also, note that the lift and drag coefficient are both functions of the angle of attack and the Reynolds number. The relative velocity V_{rel} can be determined by interpolating the velocity field in the surrounding computational cells or by determining it using Equation 2.16 and the velocity triangle as shown in Figure 2.1 [11].

$$\rho\mathbf{f}_{2D} = \frac{1}{2}\rho V_{rel}^2 c(c_l\mathbf{e}_L + c_d\mathbf{e}_D) \tag{2.15}$$

$$V_{rel} = \sqrt{V_z^2 + (\Omega r - V_\theta)^2} \tag{2.16}$$

In this equation, Ω is the angular velocity, V_z is the axial velocity and V_θ is the tangential velocity. The flow angle between the relative velocity and the rotor plane can be calculated using Equation 2.17.

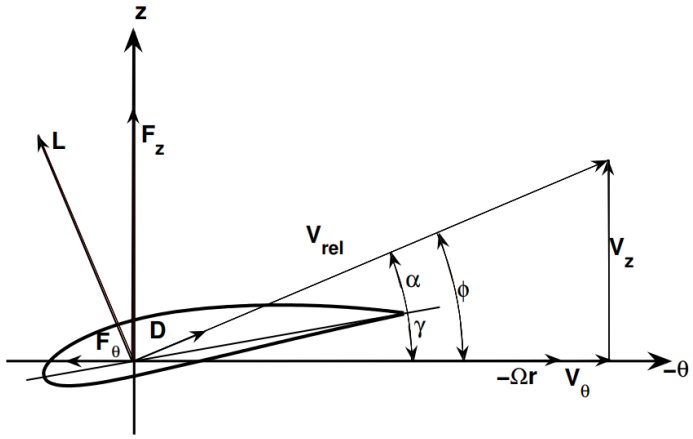

Figure 2.1: Illustration of the angles and the forces that act on an airfoil element [11]

$$\varphi = \arctan\left(\frac{V_z}{\Omega r - V_\theta}\right) \tag{2.17}$$

When comparing the actuator disc model with fully resolved blade simulations, it shows that it can be a good approximation for the mean flow values at distances that are at least one rotor diameter away from the wind turbine [12]. It can be said that the ADM is not suited to calculate the near wake of a wind turbine since it does not capture tip and root vortices and vortical structures in the near wake. However, since the results average out in the far wake it can be used effectively for wind farm calculations since then the distances are larger and more wakes need to be calculated [9].

2.4. Actuator Line Method (ALM)

The actuator line method (ALM) uses actuator lines to model the blades which exert forces on the fluid that passes through. These forces are calculated using the 2D airfoil c_l and c_d data for each element along the actuator line. Since the vorticity is not shed as a continuous sheet as with the actuator disc model, it is possible to calculate tip vortices. However, since 2D airfoil data is used it is necessary to correct for the Coriolis, centrifugal and tip effects [6]. The force per spanwise unit length is given by Equation 2.18 [13].

$$\mathbf{f}_{2D} = \frac{d\mathbf{F}}{dr} = \frac{1}{2}\rho U_{rel}^2 c(C_l \mathbf{e}_L + C_D \mathbf{e}_D) \tag{2.18}$$

Notice that this equation is almost virtually identical to Equation 2.15 used for the actuator disc model. This is because even though a different actuator method is used, the forces that are to be modelled are still the lift and the drag and thus, since the 2D c_l and c_d airfoil data are used for both methods also the equation for the momentum sink will be similar. To avoid singular behaviour, the forces need to be distributed smoothly on several mesh points. This can be done by performing the convolution of the computed local load $\mathbf{f}$ and regularization function η_ϵ as shown in Equation 2.19 [11].

$$\mathbf{f}_\epsilon = \mathbf{f} \otimes \eta_\epsilon \tag{2.19}$$

The regularization function η_ϵ is given by Equation 2.20.

$$\eta_\epsilon(d) = \frac{1}{\epsilon^2 \pi^{3/2}} \cdot \exp\left[-\left(\frac{d}{\epsilon}\right)^2\right] \tag{2.20}$$

In this equation, the $d = |\mathbf{x} - s\mathbf{e}_i|$ equals the distance between the cell-centred grid points and the points at the i'th actuator line. ϵ is a parameter that can be used to change the concentration of the

regularized load. It would be best if ϵ could be chosen as such that the applied forces would represent the chordwise pressure distribution. This is however not possible due to limited computer resources and therefore the sensitivity of this parameter is important to understand. This has been studied by [11] and he finds that the values of ϵ are scaled with the resolution of the actuator lines Δr and that choosing $\epsilon = 2\Delta r$ seemed to be a good compromise between reducing oscillations and limiting the smoothing of the loading.

The ALM yields good results but it does have the drawback that it is difficult to accurately simulate the real force distribution over the chord of an element. The three-dimensional Gaussian projection can be used which removes numerical instabilities but it does not reproduce the actual force distributions on the blades. Still, it is possible to use the ALM to resolve flow structures that are caused by the presence of blades, to capture the root and tip vortices and to capture the helical and asymmetric structures across the wake [9].

2.5. Blade Resolved Method (BRM)

The blade resolved method (BRM) or direct method uses fully resolved blades to model the rotor. This can be seen as the best method to compute the flow around a turbine as the blades fitted to the computational grid exactly as they are in real life. This means that the boundary layer can be simulated accurately including effects such as transition, separation and stall (keep in mind that, this will also depend on the accuracy of the turbulence model, see section 2.2). However, the issue with this method is that the higher accuracy comes at the price of a higher computational cost. In addition to this, the mesh generation of a high-quality moving mesh is difficult [6].

A RANS and DDES blade resolved simulations of a horizontal-axis wind turbine under stalled flow conditions using OpenFOAM were performed by [14]. The complex and unsteady root flow are studied in detail and the numerical results are compared with experimental data which shows a good agreement.

The effect of temporal convergence for blade-resolved simulations of a model wind turbine was studied by [15] and guidelines for best practices were established here as well. The performance of three turbulence models are investigated (Spalars-Allmaras, Meter SST and the DES version of the Menter SST). The numerical results are compared with experimental data. It was found that temporal convergence has a considerable effect on the power and thrust coefficients. In terms of power and thrust coefficients, all models perform well. However, for predicting the mean and fluctuating components of the velocity in the wake the DES model performs significantly better than the other two turbulence models.

The geometric approximations of the NREL 5-MW RWT and how well those approximations perform using a CFD analysis and comparison for steady-state cases was analysed by [16]. The Reynolds Averaged Navier-Stokes (RANS) equations are used and the blades are fully resolved using a Computer Aided Design (CAD) model of the blade. The turbulence models used in the setup are the $k-\epsilon$, $k-\omega$ and Spalars-Allmaras models based on the RANS equations. The reason for the usage of RANS is because the resolving of the eddies that have large spatial and temporal variations requires too much computational effort. Finally, five cases are analysed using OpenFOAM with either the PIMPLE algorithm for transient cases or the semi-implicit-method for pressure-linked-equations (SIMPLE) algorithm for steady-state cases. In terms of the numerical techniques, three different methods are used: the single reference frame (SRF), the multiple reference frame (MRF) and the sliding mesh interface (SMI). In the SRF and the MRF methods, the maintained stationary and appropriate source/sink terms are added to the governing equations to model the steady-state behaviour of the flow implicitly. In the SMI method, the turbine rotation is explicitly resolved using a rotating mesh and unsteady simulations. A more detailed description of the three methods can be found below:

- Single Reference Frame (SRF): Used when there is only one centre of rotation and the wall surfaces are rotating with the same rotational speed. The flow is described from a reference frame attached to the rotating body and therefore the governing equations are rewritten in the rotating reference frame. This leads to two additional terms in the momentum equation (the centripetal and the Coriolis forces)

- Multiple Reference Frame (MRF): The SRF method requires all the walls to be rotating around the same axis with the same speed but in the current context the ground surfaces and the support structures have to be stationary while the turbine rotates. So the SRF is not useful in this scenario and that is where the MRF comes in. The computational domain is subdivided into different non-overlapping zones with their own rotational speed. So in the fixed zones, the absolute reference frame is used and in the rotating zones, the rotating reference frame is used where the governing equations are similar as shown in the SRF. At the boundaries between the different zones, a transformation is applied to the flow variables to estimate the fluxes. This is not done for the scalar quantities
- Sliding Mesh Interface (SMI): The previous two methods pursue steady-state solutions to problems that are unsteady. The SMI method is used to capture the transient behaviour. The methods works as follows, flow around a rotating turbine at any instance is calculated, then the mesh is rotated by an angle equal to the rotational speed of the turbine times a time step. The previously computed flow field is then projected onto the resolved mesh and solved for the new time step. The governing equations remain in their original form but there is an additional step of mesh motion and projection at every time step.

A numerical analysis of the NREL 5-MW RWT using different modelling approaches (SMI and MRF) to get insight into the wake dynamic in the near and far regions with different TSRs and incoming turbulence intensities was performed by [17]. In the MRF approach for the turbulence modelling, the $k-\omega$ and $k-\epsilon$ models with standard wall functions are used. In the SMI approach, the turbine and mesh are rotating with time, and the k epsilon turbulence models are used with standard wall function. For the domain and mesh, only the 120 degrees sector is used including just one blade. A hybrid finite element mesh is used with structured hexahedral elements close to the blade to model the boundary layer accurately and to have good control over the y^+ (according to the wall function). Everywhere else is a tetrahedral mesh because it is easier to optimize the local refinement. This hybrid mesh is also good for a smooth transition between the structured and the unstructured mesh. In the end, the total mesh has about three million cells. As said before, there is a stationary zone and a rotating zone separated by a non-overlapping interface with a low relative tolerance between the zone faces to ensure that the interface boundary is as tight as possible. The boundary conditions used are: uniform inlet velocity profile, standard outlet boundary condition, free slip boundary condition on the curved surface, periodic boundary condition on the adjacent faces, no-slip boundary condition on the blade surface and the wall function is used along with the k epsilon and k omega equations to work with the relatively coarse mesh close to the blade surface. OpenFOAM is used to solve the equations using the Semi-Implicit Method for Pressure-Linked Equations (SIMPLE) algorithm. The conclusion is given as follows: SMI has to ability to capture unsteadiness while MRF ignores it. MRF can be used on a desktop machine while SMI requires supercomputing. There is little influence on the incoming turbulence intensity on the performance.

It can be concluded that the BRM is especially useful when the blade aerodynamics is important. This could be the case for instance when analysing transition, separation, stall or the complex and unsteady root flow. However, it can be unnecessary computationally expensive to use the BRM when analysing the wake. Especially since at the tips, the compressible Navier-Stokes equations might have to be solved due to compressibility effects while the wake is essentially incompressible. The main contribution of the blade resolved approach is to contribute to the understanding of flow physics on the blades [6].

2.6. Comparison Between the Different Methods

The main advantage of the ADM is its low computational cost and its good results for the far wake which makes it effective in wind farm calculations for which the near wake is not important and many wakes need to be calculated. However, the results for the near wake are poor as the method does not capture the tip and root vortices or the helical and asymmetric structures across the wake or the cortical structures in the near wake or the flow structures that are caused by the presence of the individual blades [9].

The main advantage of the ALM is that it allows for detailed study of the wake structures such as the tip and root vortices without having a large number of grid points. It also eases grid generation as simple structured grids can be used. The main drawback of this method is that the 2D c_l and c_d airfoil data are required especially when also correction models are used in this data (such as dynamic stall, transition or 3D effects) [11].

The main advantage of the BRM is that the results are the best results that could be obtained from any computational method as the blades are discretized precisely as they are in real life. This means that important effects such as transition, separation and stall can be accurately simulated. The downside of this method is the high computational cost and the difficult mesh generation [6].

It was found by [18], who performed a comparison of different CFD models for wake calculations of the NREL 5-MW RWT, that for uniform inflow the actuator line and disc are in agreement with each other but differ greatly from the BRM. However, when analysing the turbulent inflow conditions the three methods were in close agreement for the wake characteristics. This shows that when choosing a turbulent inflow condition the differences observed for uniform inflow conditions do not play an important role. Similar results have been found by [19] who performed the same comparison. He did find however that the BRM has a more sustained velocity deficit.

It can be concluded that a higher accuracy comes with higher computational costs. Performing accurate blade resolved calculations can be very challenging and since the focus lies on performing near wake calculations as opposed to blade calculations or far wake calculations, the choice will be to go with the ALM.

2.7. CFD Solver OpenFOAM

This section will discuss the important aspects of the CFD solver OpenFOAM [3] which will be used to first set up the actuator line model of the NREL 5-MW RWT and second to do the same for the IEA 15-MW RWT. The actuator line theory has already been discussed in section 2.4 and the articles that implemented the ALM using OpenFOAM for the 5-MW RWT will be discussed in section 4.1. But before that can be done first the CFD solver needs to be introduced. This section will start with an explanation of the mesh generation, then the models and physical properties will be discussed and finally the solving itself will be discussed. All the information in this section is taken from the OpenFOAM user guide [3] and the information given here is limited to what is deemed interesting for the thesis project and kept brief on purpose.

2.7.1. Mesh Generation

The mesh generation can be done by using the blockMesh utility, the snappyHexMesh utility or by using a third-party product that can transform that into an OpenFOAM mesh.

The blockMesh utility can be used for simple meshes of blocks of hexahedral cells by creating parametric meshed with grading and curved edges. Blockmesh splits the domain geometry into three dimensional hexahedral blocks where the edges of each block can be straight lines, arcs or splines.

The snappyHexMesh utility can be used for generating complexly meshed of hexahedral and split-hexahedral cells automatically from triangulated surface geometries in Stereolithography (STL) format. SnappyHexMesh uses an iterative procedure to conform the mesh to the surface by refining using splitting. The specification of mesh refinement is very flexible and snappyHexMesh runs in parallel with a load balancing step every iteration.

2.7.2. Models and Physical Properties

There are many solvers in OpenFOAM each made for specific scenarios with different equations and algorithms. Therefore it is important to identify which solver in OpenFOAM would fit well to the problem at hand based on the initial choices on the modelling. The choice of the solver determines the parameters and physical properties that are required to be defined. The models and physical properties that are deemed to be important for this thesis project are discussed in this section.

There are more than 70 boundary conditions that are subdivided into three categories, basic (basic types), constraint (geometrical constraints) and derived (specialised conditions). Setting up the correct boundary conditions are important for the simulation to be a success.

The turbulence modelling is done by using three models, laminar (no turbulence model), RAS (Reynolds-averaged stress modelling) or LES (Large-eddy simulation where also detached-eddy simulation modelling can be chosen which is defined as a subset of the LES model). In the OpenFOAM files, the model coefficients can be defined and also a range of wall function models can be applied as boundary conditions.

2.7.3. Solver

As stated before there are many solvers in OpenFOAM and also many numerical schemes that can be chosen which will be discussed in this section.

The user is completely free in choosing the interpolation scheme where the Gaussian finite volume integration is chosen most often. This interpolation scheme is based on summing the values of the cell faces which are interpolated from the cell centres.

The most common algorithms that are used to solve fluid dynamics using OpenFOAM are the pressure-implicit split-operator (PISO) and the semi-implicit method for pressure-linked equations (SIMPLE) algorithms. These algorithms both use iterative methods to solve for velocity and pressure. PISO is used for when a transient solution is wanted and SIMPLE is used for when a steady-state solution is wanted.

2.7.4. Actuator Line Modelling in OpenFOAM

Actuator line modelling in OpenFOAM will be done using turbinesFoam [20] which is a library for OpenFOAM. This library contains a tutorial for the axial flow of a wind turbine using the ALM which will be discussed in this section. There are three folders in this tutorial just like many OpenFOAM cases which are the ”0.org”, ”constant” and ”system” folders. The commands that are used to run the case are shown in the file ”allrun”. The folders and the commands will be discussed one by one below.

The initial conditions are given in the ”0.org” folder and should be copied and renamed to ”0” so this is now considered to be the initial conditions folder. The initial conditions can be changed to whatever values are needed for the initial velocity, pressure and turbulence coefficients.

The constants are given in the ”constant” folder which contains the RAS model (in this case the $k-\epsilon$ model) and the value of the kinematic viscosity ν.

The folder ”system” contains many important files which will be discussed briefly below:

1. The first one is ”blockMeshDict” which contains the locations of the vertices and the block that make up the domain of the grid. It also defines the type of boundaries are used and where they are located (in this case the inlet and outlet are of the ”patch” type and the rest is all of the ”wall” type).
2. The second file is ”controlDict” which defines the control variables such as the start time, end time, time step size, the application which should be run (in this case pimpleFoam), the interval of when to write something, etc.. Also if any libraries should be imported it should be done here (in this case the library ”libturbinesFoam.so” should be imported).
3. The third file is ”decomposeParDict” which can be used to run a simulation in parallel with multiple processors to obtain the solution faster.
4. The fourth file is ”elementData” which contains the axial distance, radius, azimuth angle, chord size, chord mount angle and twist angle for each blade element.
5. The fifth file is ”fvOptions” which is where the turbine is defined as actuator lines. In this file, the origin and axis of rotation are defined as well as the free stream velocity, tip speed ratio and the rotor radius. It is also possible to activate a dynamic stall model and tip effects corrections here.

The rest of this file defines the blades, the hub and the tower. For the blades, only one blade has to be defined (number of elements and airfoil type for each element) and then the second and third blade can be copied from the first blade but then they should have an azimuthal offset of 120 and 240 degrees, respectively.

6. The sixth file is ”fvschemes” shows the numerical schemes that are used to solve the equations. In this case, all the schemes are set to their default option.

7. The seventh file is ”fvSolution” which is where the solvers and the tolerances for the iterations are defined.

8. The eighth file is ”snappyHexMeshDict” which defines where all the surfaces of the geometry and where the mesh will be refined. The surfaces are used to specify refinement for any mesh cell intersecting it, to specify refinement for any mesh cell and to snap the mesh boundary to the surface. Different types of refinement are performed such as explicit feature edge refinement, surface-based refinement and region-wise refinement. Also, the settings for the snapping are defined in this file which are mainly the number of different types of iterations that have to be performed. Finally, the settings for the layer addition and the mesh quality settings are defined.

9. the ninth and last file in the ”system” folder is ”topoSetDict” which is used to define the cellset of the turbine.

The last file that should be discussed is ”Allrun”. Here are the applications that should be run are listed in order. First, the blockMesh application should be run to set up the main block and grid. Secondly, the snappyHexMesh application is run to define the surfaces and the mesh refinements. Then the topoSet application should be run to set up the cellset of the turbine. Finally, the pimpleFoam command can be used to solve the equations. It is possible to run the solver in parallel which will save time but this is not necessary.

To conclude, it is possible to model a wind turbine using actuator lines in OpenFOAM and this tutorial from turbinesFoam will help with the setup of the actuator line models for the NREL 5-MW RWT and the IEA 15-MW RWT.

3

Wind Turbine Low-Fidelity Aerodynamic Analysis Methods

This chapter will introduce and discuss the state-of-the-art of the low-fidelity aerodynamic analysis methods for wind turbine analysis. Low-fidelity in this case means without the use of computational fluid dynamics but with simpler methods to solve for the performance parameters of the wake of the wind turbine. Two methods will be described which are the blade element momentum (BEM) method and the free vortex wake (FVW) method. In BEM the wake is not modelled but this method can be useful to compare performance parameters with the high-fidelity method (such as the C_P and the C_T versus tip speed ratio). In FVW, the wake is modeled using the vorticity as the main flow variable for which it is possible to also calculate the performance parameters but also to visualize the wake. This chapter will continue first with the BEM method and then with the vortex method.

3.1. Blade Element Momentum (BEM) Method

This section first summarizes the BEM method based on [5] and then discusses one article that has used the BEM method on the IEA 15-MW RWT. The blade element momentum (BEM) method works similarly as the ADM as they both assume that the forces on blade elements can be determined using the 2D c_l and c_d data and the angle of attack. Figure 3.1 shows how the velocities and forces are relative to the blade angles where α is the angle of attack, β is the pitch angle and ϕ is the flow angle. Using this figure the lift force for a blade element with length δr can be determined using Equation 3.1. Similarly the drag force, axial thrust and torque can be determined using Equation 3.2, Equation 3.3 and Equation 3.4, respectively. In these equations, B is the number of blades and it is assumed that there is no radial interaction between the blade elements [5]

$$\delta L = \frac{1}{2}\rho W^2 c C_l \delta r \tag{3.1}$$

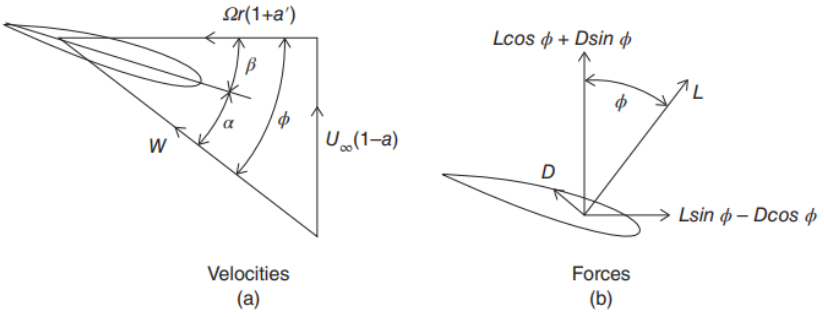

Figure 3.1: Illustration of the velocities and the forces that act on a blade element [5]

$$\delta D = \frac{1}{2}\rho W^2 c C_d \delta r \tag{3.2}$$

$$\delta T = \delta L \cos\phi + \delta D \sin\phi = \frac{1}{2}\rho W^2 B c (C_l \cos\phi + C_d \sin\phi)\delta r \tag{3.3}$$

$$\delta Q = (\delta L \sin\phi + \delta D \cos\phi) r = \frac{1}{2}\rho W^2 B c r (C_l \cos\phi + C_d \sin\phi)\delta r \tag{3.4}$$

It is possible to rewrite Equation 2.5 to Equation 3.5 with $A_D = 2\pi r \delta r$. Which in turn can be substituted on the left-hand side of Equation 3.3 to obtain Equation 3.6.

$$\delta T = 4\rho U_\infty^2 \pi r \delta r (1-a) a \tag{3.5}$$

$$\delta T = \delta L \cos\phi + \delta D \sin\phi = \frac{1}{2}\rho W^2 B c (C_l \cos\phi + C_d \sin\phi)\delta r = 4\rho U_\infty^2 \pi r \delta r (1-a) a \tag{3.6}$$

Then for the torque, it is known that the change in torque on an annulus is equal to the rate of change of the angular momentum of the air that passes through the annulus as given by Equation 3.7. This can in turn be substituted on the left hand side of Equation 3.4 to obtain Equation 3.8.

$$\delta Q = \rho U_\infty (1-a) 4\pi r^3 a' \Omega \delta r \tag{3.7}$$

$$\delta Q = (\delta L \sin\phi + \delta D \cos\phi) r = \frac{1}{2}\rho W^2 B c r (C_l \cos\phi + C_d \sin\phi)\delta r = \rho U_\infty (1-a) 4\pi r^3 a' \Omega \delta r \tag{3.8}$$

Equation 3.6 and Equation 3.8 can be rewritten to Equation 3.9 and Equation 3.10, respectively. In these equations, λ is the tip speed ratio and μ is the non-dimensional radial position ($\frac{r}{R}$).

$$\frac{W^2}{U_\infty^2} B \frac{c}{R} (C_l \cos\phi + C_d \sin\phi = 8\pi a (1-a)\mu \tag{3.9}$$

$$\frac{W^2}{U_\infty^2} B \frac{c}{R} (C_l \sin\phi - C_d \cos\phi = 8\pi \lambda a' (1-a)\mu^2 \tag{3.10}$$

The above two equations need to be solved iteratively to determine the induction factors a and a'. From these induction factors, it is possible to determine an estimation of the performance parameters of the wind turbine that is analyzed (such as the C_P and the C_T versus tip speed ratio).

One major shortcoming of the BEM method is that the discrete number of blades are not considered because the method only works with annuli of an actuator disk. This can be solved by using the Prandtl correction for the tip-loss factor given by Equation 3.11.

$$f(r) = \frac{2}{R} \cos^{-1}\left[e^{-\pi\left(\frac{R_W - r}{d}\right)}\right] \tag{3.11}$$

In this equation, the $R_w - r$ is the distance measured from the edge of the wake and d is the distance between two vortex sheets which can be calculated using Equation 3.12.

$$d = \frac{2\pi R_W}{B} \frac{U_\infty (1-\overline{a})}{W_s} \tag{3.12}$$

For this thesis project, the simulation tool OpenFAST will be used [4]. An analysis of loads from OpenFAST for the IEA 15MW RWT has already been performed by [21]. The article mainly focuses on the aeroelastic loads with different fidelities in OpenFAST but it nevertheless gives a good impression of how the BEM model could be implemented. The aeroelastic codes use the AeroDyn model in OpenFAST to calculate the aerodynamic forces. The baseline potential flow model is used to model the tower shadow and the Beddoes-Leishman dynamic stall model is used to calculate the unsteady aerodynamics. For the BEM model, empirical corrections are used such as the Prandtl tip loss model. This article shows that BEM can indeed be used for low-fidelity modelling since it has already been done for the 15-MW RWT. This article is discussed in more detail in section 4.2.

3.2. Free Vortex Wake (FVW) Method

This section will discuss the vortex method based on the user guide of OLAF [22]. The abbreviation OLAF stands for cOnvecting LAgrangian Filaments (OLAF) and it is a free vortex wake (FVW) module used to compute the aerodynamic forces of horizontal-axis wind turbines. It is not a simulation tool on its own but is a module incorporated in the simulation tool OpenFAST also from the NREL. It can be chosen as an alternative to the BEM method in the Aerodyn model (which is explained in the previous section) and both models return the same information. However, OLAF provides more accurate calculations where the BEM assumptions are violated and it is therefore useful when complex aerodynamics such as dynamic inflow, skewed wake, tip losses or ground effects should be accounted for.

OLAF uses a lifting-line representation of the blades which is defined by the bound vortex that sheds a vortex sheet into the wake. This wake is discretized into Lagrangian markers and is represented by a hybrid lattice/filament method. The position of such a marker depends on the wake age ζ and its azimuthal position ψ. Every marker is linked to the adjacent marker by the straight-line vortex filaments. The discretization of the wake is defined by the blade sections and the time step size. However, after the initialization, the wake can move and distort as the markers move downstream.

The vorticity equation can be used to describe the change of the wake vorticity in the FVW method. This equation is shown in Equation 3.13 and can be derived from the Navier-Stokes equations when assuming incompressible homogeneous flow in the absence of non-conservative forces. In this equation, ν is the vorticity, $\vec{u}$ is the kinematic viscosity and $\vec{\omega}$ is the vorticity which is equivalent to the curl of the velocity ($\vec{\omega} \equiv \nabla \times \vec{u}$).

$$\frac{d\vec{\omega}}{dt} = \frac{\partial \vec{\omega}}{\partial t} + (\vec{u} \cdot \nabla)\vec{\omega} = (\vec{\omega} \cdot \nabla)\vec{u} + \nu \Delta \vec{\omega} \tag{3.13}$$

Vortex filaments are used to model the continuous vorticity distribution using a finite number of elements. These vortex filaments are delimited by two points and it creates a vorticity tube along the unit vector $\vec{e_x}$ with cross-section dS. The total vorticity of the tube and the vortex filament are equal to each other as shown in Equation 3.14, where $\vec{\Gamma}$ is the circulation intensity of the vortex filament.

$$\vec{\omega} dS = \vec{\Gamma} \tag{3.14}$$

The lifting line method works similarly as the BEM method and the actuator line method as it does not consider the geometry of the airfoil but only considers the forces using the 2D C_l and C_d data. In this case, the blades are modeled as a ”lifting line” which means it is modeled as a single line where the line is discretized into elements according to the blade elements. Each element has a certain circulation according to the loads acting on the blade element. This line is referred to as the ”bound circulation”. This circulation can be determined by using the lift in the Kutta-Joukowski theorem as shown in Equation 3.15. In this equation, L' is the lift per unit span.

$$L' = \rho_\infty V_\infty \Gamma \tag{3.15}$$

Due to the spanwise variation in the bound circulation as calculated with the equation above, there will be vorticity shed into the wake. This is called the ”trailing vortex”. Due to the temporal changes in the bound circulation, there will also be vorticity shed into the wake which is referred to as ”shed vorticity”.

The convection of the vortex filaments can be determined by the convection of the Lagrangian marker as shown in Equation 3.16. In this equation, $\vec{r}$ is the position of the Lagrangian marker. Since the convection of the filaments stretches the filaments it automatically takes the strain of the vorticity equation into account.

$$\frac{d\vec{r}}{dt} = \vec{V}(\vec{r}, t) \tag{3.16}$$

The velocity in the above equation is a combination of the freestream and induced velocities. These induced velocities are caused by the filaments and can be determined using the Biot-Savart law as shown in Equation 3.17. in this equation $\vec{x}$ is a certain point on the grid, $d\vec{l}$ is the length along the filament and $\vec{r}$ is the vector between $\vec{x}$ and the filament.

$$d\vec{v}(\vec{x}) = \frac{\Gamma}{4\pi}\frac{d\vec{l}\times\vec{r}}{|\vec{r}|^3} \tag{3.17}$$

This equation can be integrated along the length of the filament (from $\vec{x}_1$ to $\vec{x}_2$) which leads to Equation 3.18.

$$\vec{v}(\vec{x}) = F_v\frac{\Gamma}{4\pi}\frac{(r_1+r_2)}{r_1r_2(r_1r_2+(\vec{x}-\vec{x}_1)\cdot(\vec{x}-\vec{x}_2)}(\vec{x}-\vec{x}_1)\times(\vec{x}-\vec{x}_2) \tag{3.18}$$

In the above equation, F_v is the regularization parameter for which different regularization functions are possible. These regularizations improve the regularity of the discrete vorticity field that is needed because of the singularity that exists in Equation 3.17 which affects the numerical accuracy.

Finally, the velocity at any point on the grid can be determined by adding all the velocities induced by all the vortex filaments to the free stream velocity as shown in Equation 3.19.

$$\vec{V}(\vec{x}) = \vec{V}_0(\vec{x}) + \vec{v}_\omega(\vec{x}), \qquad \text{where} \qquad \vec{v}_\omega(\vec{x}) = \sum_k \vec{v}_k(\vec{x}) \tag{3.19}$$

4

Introduction to the Reference Wind Turbines (RWTs)

A lot of the wind turbine research worldwide is performed on so-called reference wind turbines (RWTs) which are theoretical wind turbines. There are a variety of reasons for this. First of all, they are used as the baseline for the wind energy community to perform optimization studies on or to explore new technologies. Secondly, it allows for collaboration between industry and academia as the intellectual property of the industry is protected while they can still research new developments. Third and last of all, RWTs are a good starting point for newcomers to understand fundamental design. Several of these RWTs have been proposed since the beginning of this century by the National Renewable Energy Laboratory (NREL) and to be relevant with the increasing wind turbine size, a new RWT has to be the new baseline for research. In this light, a new wind turbine has been proposed by the NREL in collaboration with the International Energy Agency (IEA) which is a 15-MW RWT for use in offshore wind energy and it has been designed for both bottom-fixed and floating support structures [2]. As stated before, in this thesis project the wake aerodynamics of the IEA 15-MW RWT and the NREL 5-MW RWT will be analysed.

Before it is possible to analyse these RWTs it is important to discuss their design and the aerodynamic wake research that has already been performed on each turbine. This is done in two sections. The NREL 5-MW RWT is discussed in section 4.1 and the IEA 15-MW RWT is discussed in section 4.2.

4.1. The NREL 5-MW Reference Wind Turbine

This section will discuss the current knowledge about the 5-MW RWT which will serve as the baseline for the development of the model for the IEA 15-MW RWT which will be discussed in the next section. This wind turbine was proposed in 2009 and an overview of this wind turbine can be found in the technical report from the NREL [23]. The rotor diameter is 126 meters and the hub height is 90 meters. An overview of the important design parameters can be found in Table 4.1. The NREL has provided input files for various analysis tools in their report as well.

Naturally, since this RWT is already 10 years old, much more (aerodynamic) research has been performed on it. Below is a summary of the three articles of which the content was deemed interesting for this thesis project. They all have to do with the aerodynamic analysis of the 5-MW RWT using the actuator line method and the CFD solver OpenFOAM [3]. What is especially interesting for this thesis topic is the numerical method, the simulation setup and the results as that can be used for comparison and validation.

The first article [24] is about a comparison of the RANS based Actuator Line method (ALM) with the sliding mesh interface and the multiple reference frame method (the last two methods are different methods of the blade resolved method which is explained in section 2.5. These methods are applied to the NREL 5-MW RWT with different tip speeds ratios (TSRs). A summary of the numerical method used for the ALM is provided below:

Table 4.1: Key parameters of the NREL 5-MW RWT [23]

Description	Units	Value
Rating	MW	5
Rotor orientation	-	Upwind
Number of blades	-	3
Control	-	Variable speed Collective pitch
Rotor diameter	m	126
Hub diameter	m	3
hub height	m	90
Cut-in wind speed	m/s	3
Rated wind speed	m/s	11.4
Cut-out wind speed	m/s	25
Cut-in rotor speed	rpm	6,9
Rated rotor speed	rpm	12.1
Rated tip speed	m/s	80
Overhang	m	5
Shaft tilt	deg	5
Precone	deg	2.5
Rotor mass	kg	110000
Nacelle mass	kg	240000
Tower mass	kg	347460
Coordinate location of overall CM	m	(-0.2, 0.0, 64.0)

- The $k-\omega$ SST turbulence model is used.
- The domain size of the ALM simulation is 200 m x 190 m (streamwise) x 200 m.
- A grid of 1.5 million cells is used with approximately 40 grid points across the rotor diameter (minimum grid length is about 3m which should be sufficient to resolve wake tip vortices)
- Uniform inlet wind velocity of 9 m/s.
- At the outlet, a standard outlet boundary condition is used (fixed pressure value and zero normal gradients for the rest).
- The free slip boundary condition is applied at the rest of the surfaces.
- Approximately 40 actuator segments were used
- The regularization parameter (ϵ is approximately two times the cube root of the grid volume size in that region.
- The simulation time is 100s which corresponds to 17 revolutions and 5 times the flow passage at the wind free stream velocity.
- The time step size is 0.007 s which corresponds to a Courant number of 0.1 (constrained by the tip speed).
- The computational time for the ALM equalled 1 week (done on a high-end desktop) whereas the computational time for the blade resolved methods equaled 3 weeks (done at a computational facility).
- The CFD solver OpenFOAM was used and the equations are solved in a segregated manner using the Semi-Implicit Method for Pressure-Linked Equations (SIMPLE) algorithm. The details and theory of this solver are explained in section 2.7.

The article concludes that the comparison shows quantitative differences but qualitative similarities in trends between the three methods for the near-wake region. The ALM predicts a relatively milder variation of C_P with TSR and the analysis done with ALM only shows a slight variation in the flow pattern near the hub region with different TSRs which could be caused by the fact that the blades are not resolved. The author recommends future studies to involve LES in ALM to see if that improves the results.

The second article [25] is a numerical study of the wake interaction and its effect on wind turbine aerodynamics on the NREL 5-MW RWT based on the actuator line model. The simulations which are performed using LES consider uniform inflow conditions and six different layouts are implemented to study the evolving process of the interacting wakes. A summary of the numerical method used for the ALM is provided below:

- LES is used as it shows better performance in dealing with the large-scale unsteady anisotropy turbulence appearing in the turbine wake.
- The domain length L_x (flow direction) equals 17D (D = diameter = 126 m), domain height L_z equals 3.2D and the domain width varies from case to case.
- The computational domain is divided into three regions with increasing grid resolutions.
- Uniform inflow conditions are used with a velocity of 11.4 m/s.
- At the top boundary, a free-slip constraint is imposed. At the bottom, a wall condition is imposed, the left and right side boundaries are set to symmetry and at the outlet plane, the zero-gradient condition is applied.
- The simulation time is 320 s and the time step size is 0.025 seconds.
- The CFD solver OpenFOAM was used and the equations are solved using the PISO (pressure implicit with splitting operators) algorithm. The details and theory of this solver is explained in section 2.7.

The article concludes that the interacting region of wakes contains a higher level of turbulent flow than the single wake. The diffusion of turbulence causes the merging of wakes and thus the velocity is redistributed among the whole wake region. The article recommends performing simulations of typically arranged wind farms with complex inflow conditions for future work.

The third article [19] is about a comparison of the actuator disc, actuator line and the blade resolved method applied to the NREL 5-MW RWT. The simulations are performed using RANS to investigate the interactions of the wind turbine models in the neutrally stratified atmospheric boundary layer (ABL). A summary of the numerical method used for the ALM is provided below:

- Transient simulations used the PISO algorithm.
- The $k - \epsilon$ model was used.
- Spatial discretizations were set to Gauss linear for gradient and divergence terms and Gauss linear corrected for Laplacian terms.
- First-order implicit Eulerian discretization was used for temporal terms.
- The computational domain is 2772 x 630 x 378 m (for two turbines)
- The fully developed inlet profiles of mean streamwise velocity, turbulent kinetic energy and dissipation rate turbulent kinetic energy of Richard and Hoxey were applied at the domain inlet
- The domain outlet was specified as a pressure outlet with a constant value of 0 Pa, the top and side surfaces of the computational domain were assigned a slip condition which ensures zero-gradient for scalar quantities. For vector quantities, the normal component is set to zero and tangential components are assigned zero-gradient.

The article concludes that the three methods compare well qualitatively with the literature for this RWT. However, the blade resolved method has a more sustained velocity deficit. The author suggests considering stably stratified ABLs for future research as it can introduce high shear rates, low-level jets, and wave motions in the ABL which can lead to higher loads on blades and increase shear forces over the wind turbine.

From these articles, it becomes clear that a lot of (rotor and wake aerodynamics) research has been performed on the NREL 5-MW RWT. It is, therefore, safe to say that this RWT can function well as the baseline for the model to be developed for the 15-MW RWT and it can also serve as validation for the results of the 15-MW RWT wake analysis.

4.2. The IEA 15-MW Reference Wind Turbine

This section is dedicated to providing the current understanding of the 15-MW reference wind turbine (RWT) with a focus on what is important for an aerodynamic analysis which has been discussed in the previous section. This reference wind turbine is a collaboration between the International Energy Agency (IEA) and the National Renewable Energy Laboratory (NREL). The details and a complete description of this RWT are provided in their technical report [2]. The rotor diameter is 240 meters and the hub height equals 150 meters. An overview of the important design parameters can be found in Table 4.2. The blade and rotor are deemed to be technically feasible and has a blade length of 117 meters with a tip speed of 95 m/s. Finally, the NREL and IEA have made a collaboration folder where input files can be found for various analysis tools.

As stated before this is a new reference wind turbine and as such not a lot of research has been done yet on this specific turbine. However, two articles were published that did an aerodynamic analysis on this RWT and these will be discussed in this section.

The first article [21] is about a comparison of loads of this RWT using the software HAWC2 and OpenFAST. The article mentions that RWTs that reflect the state-of-the-art are required for innovation in wind turbine design and that they worked on task 37 (offshore floating-foundation applications). The article also mentions that the two codes which are implemented use different structural models and therefore the aeroelastic responses are compared for three cases (steady wind, step wind and turbulent wind) and the results show good agreement for the loads dominated by thrust and force, but not for asymmetric loading. For this thesis project the part where OpenFAST is used and the BEM theory is applied is particularly interesting as can be used to compare the pure aerodynamic analysis in this thesis with the aeroelastic analysis in the article. The article does not mention the importance of including aeroelasticity in the analysis of the 15-MW RWT which could therefore be a valuable addition to this thesis.

The second article [26] is about an investigation of this RWT in the floating scenario using the vortex methods. The article mentions that the BEM model might not be well suited when analysing the dynamic phenomena that occur when a rotor moves in and out of its own wake. Therefore, the article compares the standard BEM code with a vortex solver to clarify the capabilities and limitations of both methods. Even though the floating condition is not relevant for this thesis project, it provides good background information for the modelling strategy of both the low-fidelity solvers. The article mentions that the BEM method is the industry standard but it is not capable to simulate complex blade geometries or complex flow cases such as yaw and shear. This can be solved however by using sub-models to account for these complexities but these need to be calibrated with high-fidelity codes or experimental data. Nevertheless, the results can differ greatly when using different model fidelities for floating wind turbines. This drives the question whether these differences will also be evident for large bottom-fixed wind turbines or if it is only a phenomenon only attributed to the dynamic behaviour of floating turbines.

To conclude this section about the 15-MW RWT, there is enough information available from the NREL to model the wind turbine and input files for various analysis tools are also available. From the literature research, it can be concluded that some aerodynamic analysis has been done using the BEM method and the vortex method. This is useful for verification and validation of the low-fidelity models. None of the three articles has any mention of CFD analysis of the RWT which puts this thesis project at the forefront of the research currently undertaken in the offshore wind energy field.

Table 4.2: Key parameters of the IEA 15-MW RWT [2]

Parameter	Units	Value
Power rating	MW	15
Turbine class	-	IEC Class 1B
Specific rating	W/m^2	332
Rotor orientation	-	Upwind
Number of blades	-	3
Control	-	Variable speed Collective pitch
Cut-in wind speed	m/s	3
Rated wind speed	m/s	10.59
Cut-out wind speed	m/s	25
Design tip-speed ratio	-	9.0
Minimum rotor speed	rpm	5.0
Maximum rotor speed	rpm	7.56
Maximum tip speed	m/s	95
Rotor diameter	m	240
Airfoil series	-	FFA-W3
Hub height	m	150
Hub diameter	m	7.94
Hub overhang	m	11.35
Rotor precone angle	deg	-4.0
Blade prebend	m	4
blade mass	t	65
Blade length	117	m
Root diameter	5.20	m
Root cylinder length	2.34	m
Max chord	5.77	m
Max chord spanwise position	27.2	m
Tip prebend	4.00	m
Precone	4.00	deg
Blade mass	65250	kg
blade centre of mass	26.8	m
Design tip-speed ratio	9.00	-
First flapwise natural frequency	0.555	Hz
First edgewise natural frequency	0.642	Hz
Design C_P	0.489	-
Design C_T	0.799	-
Annual energy production	77.4	GWh

5

Aerodynamic Analysis of the NREL 5-MW RWT

This chapter contains an aerodynamic analysis of the NREL 5-MW RWT using varying fidelity methods. The analysis starts off with the actuator line method (ALM) in OpenFOAM (section 5.1), after which the blade element momentum (BEM) theory is applied in OpenFAST (section 5.2) and lastly the free vortex wake (FVW) method is applied in OpenFAST (section 5.3). The comparison and discussion of the results of the different fidelity methods is presented in section 5.4. Finally a conclusion of the analysis is given in section 5.5.

5.1. Actuator Line Method (ALM) of the NREL 5-MW RWT

This section is dedicated to analysing the NREL 5-MW RWT using the ALM in the CFD solver OpenFOAM [3]. To analyse this RWT first some studies need to be performed to figure out the best simulation setup. This section will start with an overview of the numerical setup after which it is clear which variables can be analysed and have to be fine-tuned. The first study is the grid refinements study, where different grid refinements will be analysed to find out which levels of refinement are required for acceptable (converged) results. Secondly, the temporal convergence study will be performed which looks at if there is a noticeable effect of having a lower time step size with the same grid to find out what the optimal Courant number is. Thirdly, the effect of the number of actuator elements are studied to find out how much the results diverge from each other for different number of elements and which number of actuator elements seems to be best.

Since no experimental data is available for this RWT, it is not possible to perform validation studies but performing a verification study is possible. Therefore, with the results obtained in the previous three studies, a comparison will be performed based on the obtained results and the results found in literature. In the literature that is used for this comparison ([19], [24], [25]), the effect of including the tower, the hub and the addition of a ground wall boundary conditions are not analysed and it is not clear how large the effect of including these obstacles in the domain is. For this reason, the effect of including these elements are also studied. Then at last, a conclusion is provided which should present the final and concluding thoughts of the discussions based on the aforementioned studies.

5.1.1. Numerical Setup

The finite volume solver OpenFOAM is used to solve the Navier-Stokes equations using the PISO algorithm (Pressure Implicit with Splitting of Operators). The turbulence model used in this ALM CFD simulation will be the $k-\epsilon$ model as in the literature study this came up to be well suited for near wake aerodynamic analysis.

For the initial baseline computational setup, the domain is outlined as shown in Figure 5.1 and Figure 5.2. Here the height (z-axis) and width (y-axis) of the domain are both equal to six times the diameter while the length (x-axis) is equal to nine times the diameter. The turbine is placed at the origin

which is in the centre of the yz-plane and 3 times the diameter along the x-axis. Since the turbine is in the middle of the yz-plane, it follows that the ground, hub and tower are not modelled here but will be modelled in a different computational setup (see subsection 5.1.6). In this so-called clean configuration there are three main regions with different refinements. At all times in this thesis, the cell size is a cube where dx = dy = dz. For this initial grid (henceforth the baseline grid), the characteristic length of the cells in region 1 (the outer and light blue region) equals 8 m, in region 2 (the middle and darker blue region) this equals 4 meters and in region 3 (the inner and dark blue region) this equals 2 meters. Uniform inflow conditions are used with a velocity of 9 m/s and a tip to speed ratio of 7.5. The bottom, top and sides all have the slip boundary condition while the inlet has a prescribed velocity and the outlet has the inletOutlet boundary condition.

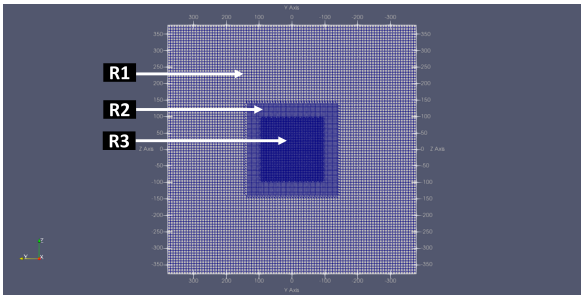

Figure 5.1: Cross-sectional front view of the baseline computational grid of the NREL 5-MW RWT

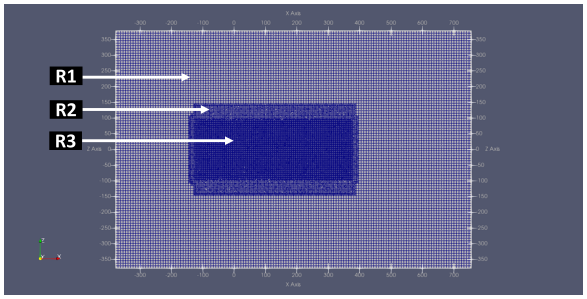

Figure 5.2: Cross-sectional side view of the baseline computational grid of the NREL 5-MW RWT

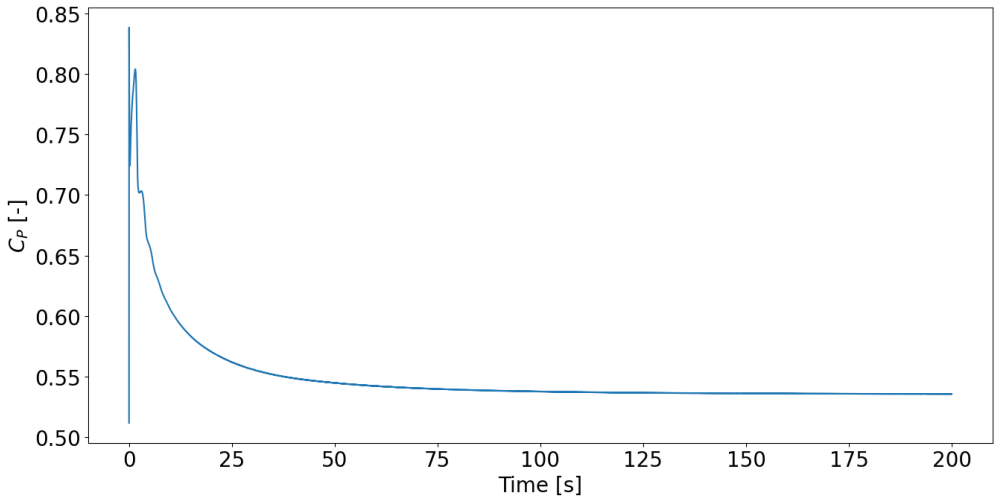

Figure 5.3: Plot of the power coefficient versus time to identify the time at which the solution has converged

The simulation time equals 200 seconds as it was observed that the solution has converged after 150 seconds as shown in Figure 5.3. Most comparisons will therefore be made at 200 seconds. The Courant number is chosen to equal 0.75 which leads to a time step size of 0.22 as shown below in Equation 5.1.

$$Co = \frac{U_{tip} \cdot \Delta t}{\Delta x} = \frac{U_\infty \cdot TSR \cdot \Delta t}{\Delta x} \tag{5.1}$$

$$\Delta t = \frac{Co \cdot \Delta x}{U_\infty \cdot TSR} = \frac{0.75 \cdot 2}{9 \cdot 7.5} = 0.022$$

An overview of all the cases that will be analysed for the NREL 5-MW RWT and for which study are shown in Table 5.1.

Table 5.1: Overview of all the cases analyzed in this section

Case #	Case name	dx R1 [m]	dx R2 [m]	dx R3 [m]	dx R4 [m]	dr [m]	dt [s]	Courant [-]	U_∞ [m/s]	TSR [-]	# cells [-]	Tend [s]
Case 01	Very coarse	8	4	4	NA	4	0,0444	0,75	9	7,5	1,96E+06	200
Case 02	Coarse	6	3	3	NA	4	0,0333	0,75	9	7,5	4,61E+06	200
Case 03	Baseline	8	4	2	NA	4	0,0222	0,75	9	7,5	4,36E+06	200
Case 04	Fine	6	3	1,5	NA	4	0,0167	0,75	9	7,5	1,01E+07	200
Case 05	Cylinder refinement region near turbine	8	4	2	1	2	0,00926	0,75	9	7,5	7,95E+06	200
Case 06	Baseline Co 0,10	8	4	2	NA	4	0,00296	0,1	9	7,5	4,36E+06	50
Case 07	Refined Co 0,10	6	3	1,5	NA	4	0,00222	0,1	9	7,5	1,01E+07	50
Case 08	Baseline # elements 34	8	4	2	NA	2	0,0222	0,75	9	7,5	4,36E+06	200
Case 09	Refined # elements 34	6	3	1,5	NA	2	0,0167	0,75	9	7,5	1,01E+07	200
Case 10	Refined # elements 68	6	3	1,5	NA	1	0,0167	0,75	9	7,5	1,01E+07	200
Case 11	Baseline ground wall boundary	8	4	2	NA	4	0,0222	0,75	9	7,5	3,19E+06	200
Case 12	Baseline ground wall boundary, tower and hub	8	4	2	NA	4	0,0222	0,75	9	7,5	3,19E+06	200

5.1.2. Grid Refinement Study

The first study is to determine the correct grid size for an accurate aerodynamic analysis. From literature the initial grid minimum length at the turbine was chosen to 3 meters by [25], 2 meters by [24] and 1 meter by [19]. Therefore a study will be performed that will compare the dependency of the results on the grid size. The baseline grid has already been discussed in subsection 5.1.1. In addition to this also a super coarse, coarse, refined and a very refined grid near the turbine have been made. An overview of these cases can be found in Table 5.2 with the grid details. For the very refined grid near the turbine a new cylinder-shaped refinement region has been made to increase the refinement only near the turbine. This is shown in Figure 5.4 and Figure 5.5. The reason for adding this new refinement region is because it was found that having more refinement outside this region does not contribute to any more accurate results thus to save time only the inner region is refined. This inner region is also the region of interest since this is where the wake develops. A wake deficit plot can be seen in Figure 5.6 which is used to analyse the grid dependence.

Table 5.2: Cases used to study the grid refinement

Case #	Case name	dx R1 [m]	dx R2 [m]	dx R3 [m]	dx R4 [m]	dr [m]	dt [s]	Courant [-]	U_∞ [m/s]	TSR [-]	# cells [-]	Tend [s]
Case 01	Very coarse	8	4	4	NA	4	0,0444	0,75	9	7,5	1,96E+06	200
Case 02	Coarse	6	3	3	NA	4	0,0333	0,75	9	7,5	4,61E+06	200
Case 03	Baseline	8	4	2	NA	4	0,0222	0,75	9	7,5	4,36E+06	200
Case 04	Fine	6	3	1,5	NA	4	0,0167	0,75	9	7,5	1,01E+07	200
Case 05	Cylinder refinement region near turbine	8	4	2	1	2	0,00926	0,75	9	7,5	7,95E+06	200

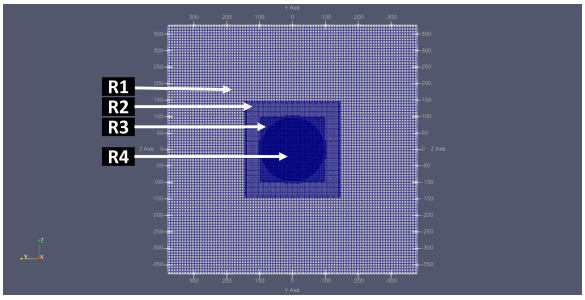

Figure 5.4: Cross-sectional front view of the computational grid for the very fine cylinder region near the turbine

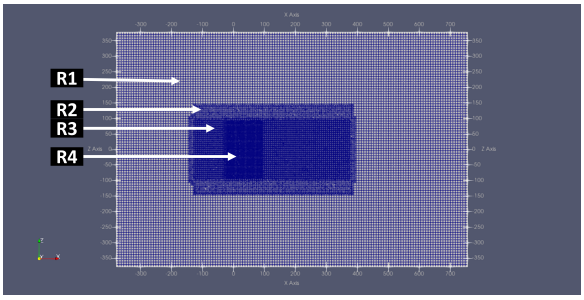

Figure 5.5: Cross-sectional front view of the computational grid for the very fine cylinder region near the turbine

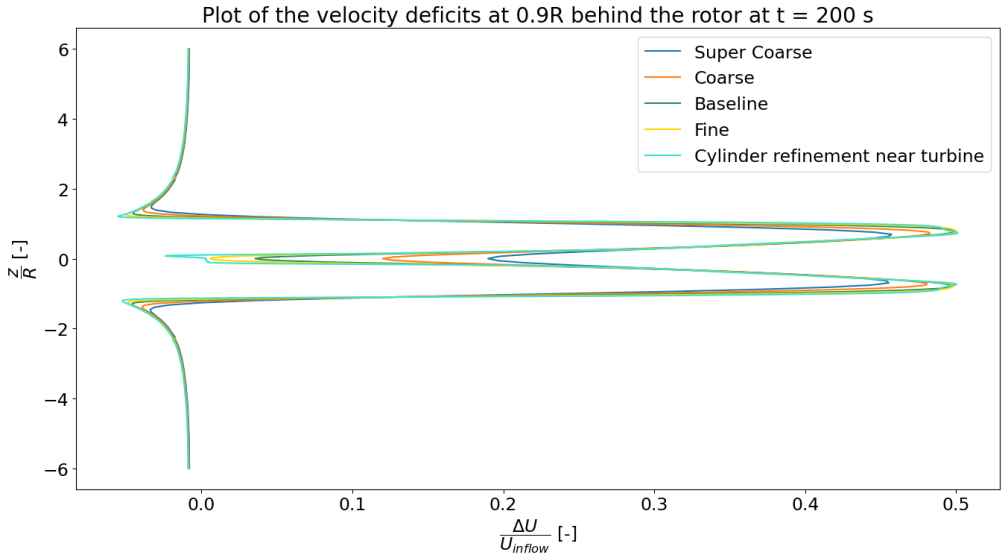

Figure 5.6: Plot of the velocity deficit to compare the cases used to study the grid refinement

First of all, this figure shows that indeed outside the inner region (above and below 1.5 R) the results do not differ to a large extent which makes sense as the wake does not reach outside this region (under these inflow conditions). Secondly, there are obvious large deviations between the different grid sizes. The coarse and super coarse grid deviate a lot from the baseline and higher grids. It therefore seems that using the baseline and higher grids are necessary to obtain accurate results. This can also be seen when comparing the power and thrust coefficients as shown in Table 5.3. In this table, the baseline, refined and cylinder refinement cases lie close in terms of the power and thrust coefficients. However, it does show that using a finer grid leads to a lower power coefficient which means that for accurate comparison the cylinder refinement is deemed to be the best.

Thirdly, the cylinder refinement grid shows some oscillations or disturbances which is shown more clearly in the zoomed in version of the plot in Figure 5.7. Since the velocity deficit is plotted at 0.9 R behind the rotor at 200 seconds, it is a fully developed wake that is being analysed without the effect of the ground, tower or hub. Therefore it is expected that the results are symmetrical. This is indeed the case, except of the cylinder refinement case where, due to the very fine grid, disturbances arise. This means that the results should be averaged over time for the best result of the wake deficit plot instead of taking an instantaneous snapshot.

Table 5.3: Cases with their corresponding power and thrust coefficient

Case	C_P	C_T
Super Coarse	0,57	0,79
Coarse	0,55	0,78
Baseline	0,53	0,78
Fine	0,53	0,77
Cylinder refinement near turbine	0,52	0,77

The wake can also be visualized for the different grid sizes using vorticity contours. These are shown in the figures below where the Q-criterion is set such that the vortices are visible at 0.001 for T = 200 s. From the coarser grids (Figure 5.8 and Figure 5.9) it is not possible to see the blades or distinguish the three tip and root vortices. From the baseline grid in Figure 5.10, these elements are already more visible and for the fine grid in Figure 5.11 the blades, tip vortices and root vortices are much more refined and clearly visible. In the cylinder refinement case the instabilities can be seen as well which interfere with the root and tip vortices. Showing this grid at a lower Q-criterion of 0.01 leads to a plot without

the instabilities. These plots illustrate that only the more refined grids (form baseline and upwards) are able to accurately show the tip and root vortices.

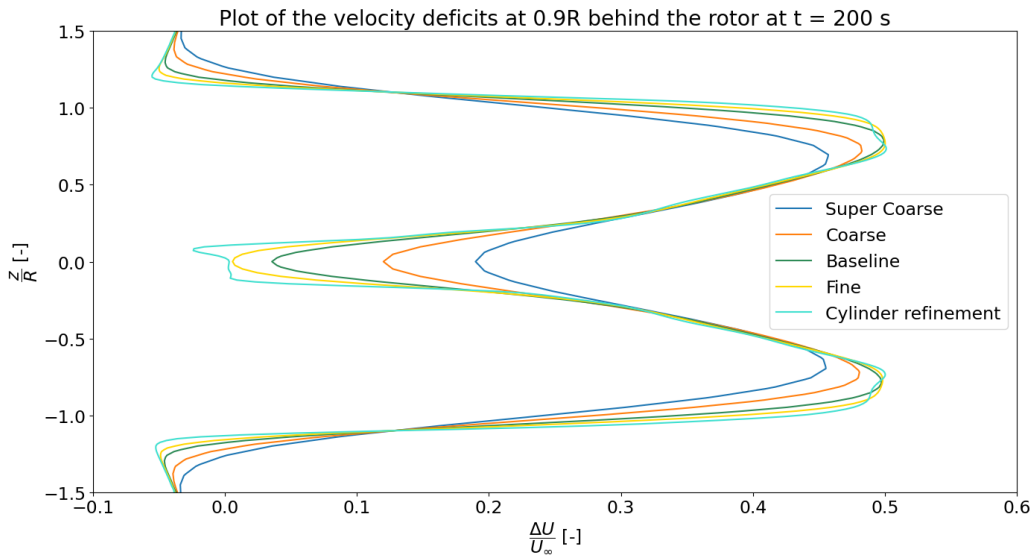

Figure 5.7: Zoomed in version of the plot of the velocity deficit to compare the cases used to study the grid refinement

It can be concluded that the baseline grid is sufficient enough to use when comparing different cases. The refined cylinder case is however better suited when comparing coefficients with literature since the grid is more refined and thus also more accurate. The fine grid is however better suited to compare wake deficits as there are no oscillations in the results and thus the solution does not need to averaged over time. The coarse and super coarse grids are not to be used as those deviate too much from the refined results. Furthermore, it is not needed to model such a large grid as it can be seen in Figure 5.6 that height of 3 diameters is sufficient already. That also means that the width can be reduced to 3 diameters while keeping the length the same.

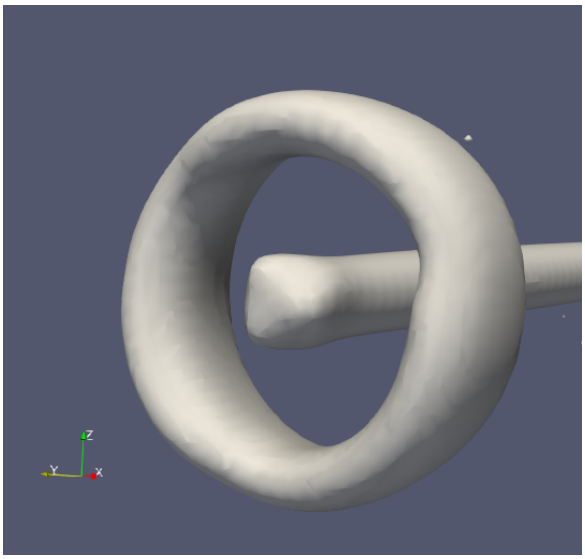

Figure 5.8: Vorticity contour plot of the very coarse grid with Q-criterion = 0.001

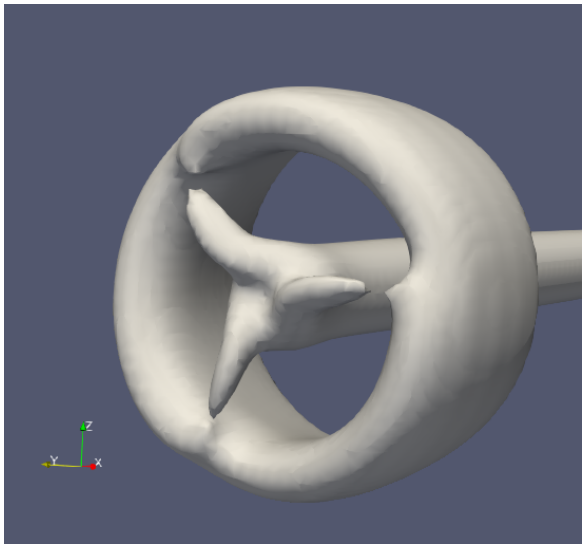

Figure 5.9: Vorticity contour plot of the coarse grid with Q-criterion = 0.001

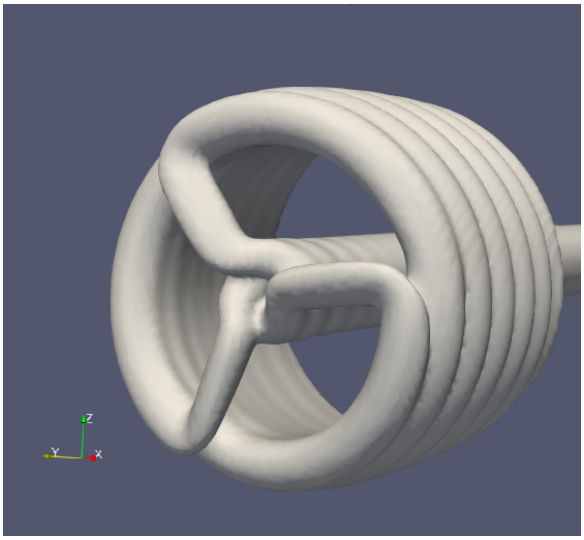

Figure 5.10: Vorticity contour plot of the baseline grid with Q-criterion = 0.001

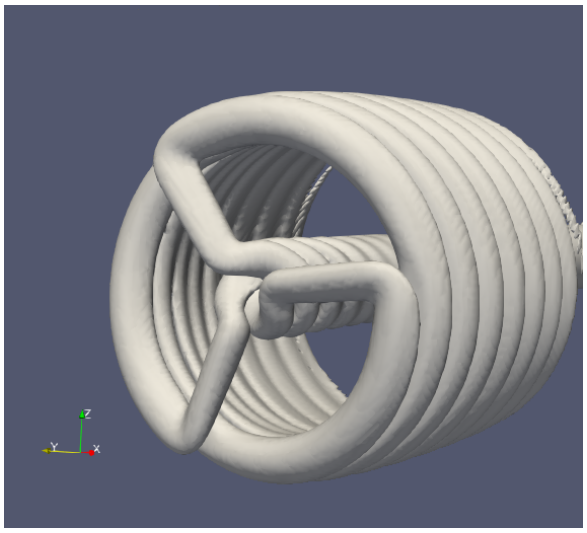

Figure 5.11: Vorticity contour plot of the fine grid with Q-criterion = 0.001

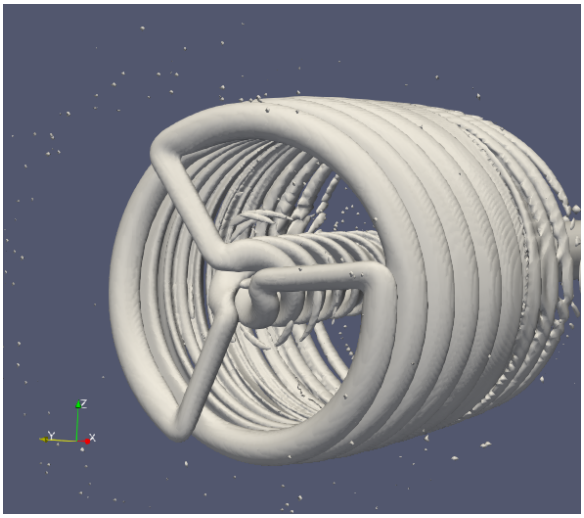

Figure 5.12: Vorticity contour plot of the cylinder refinement grid with Q-criterion = 0.001

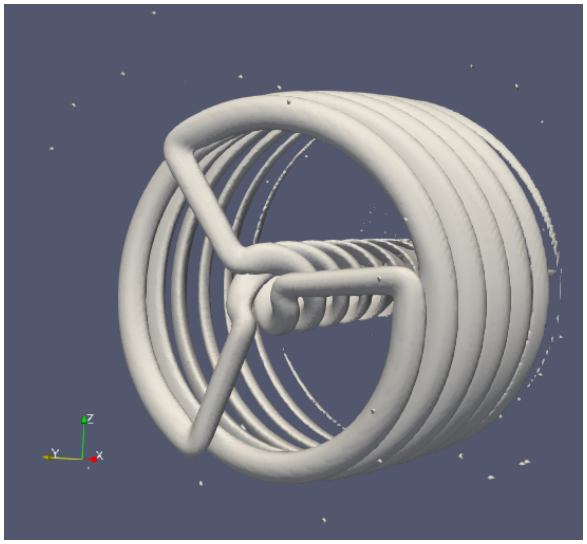

Figure 5.13: Vorticity contour plot of the cylinder refinement grid with Q-criterion = 0.01

5.1.3. Temporal Convergence Study

The time step size was calculated in Equation 5.1 to have a Courant number of 0.75 which is deemed sufficient to reach a stable and converged solution. In literature however [24] the Courant number was chosen significantly smaller to equal 0.1. To determine the effect of changing the Courant number four cases are compared. An overview of these cases can be found in Table 5.4 and the results can be found in Figure 5.14. These results show the velocity deficit at 0.9 R behind the rotor at t = 50 s. The reason why this plot is only shown at 50 s is because with the grid refinement and the low Courant number the simulation time was capped at 50 seconds due to the limited resources available. Therefore these plots do not show steady-state conditions such as the other plots in this chapter but a transient solution which should not matter for this analysis.

Table 5.4: Cases used to study the temporal convergence

Case #	Case definition	dx R1 [m]	dx R2 [m]	dx R3 [m]	dr [m]	dt [s]	Courant [-]	U_∞ [m/s]	TSR [-]	# cells [-]	Tend [s]
Case 03	Baseline	8	4	2	4	0,0222	0,75	9	7,5	4,36E+06	200
Case 04	Fine	6	3	1,5	4	0,0167	0,75	9	7,5	1,01E+07	200
Case 06	Baseline Co 0,10	8	4	2	4	0,0030	0,1	9	7,5	4,36E+06	50
Case 07	Fine Co 0,10	6	3	1,5	4	0,0022	0,1	9	7,5	1,01E+07	50

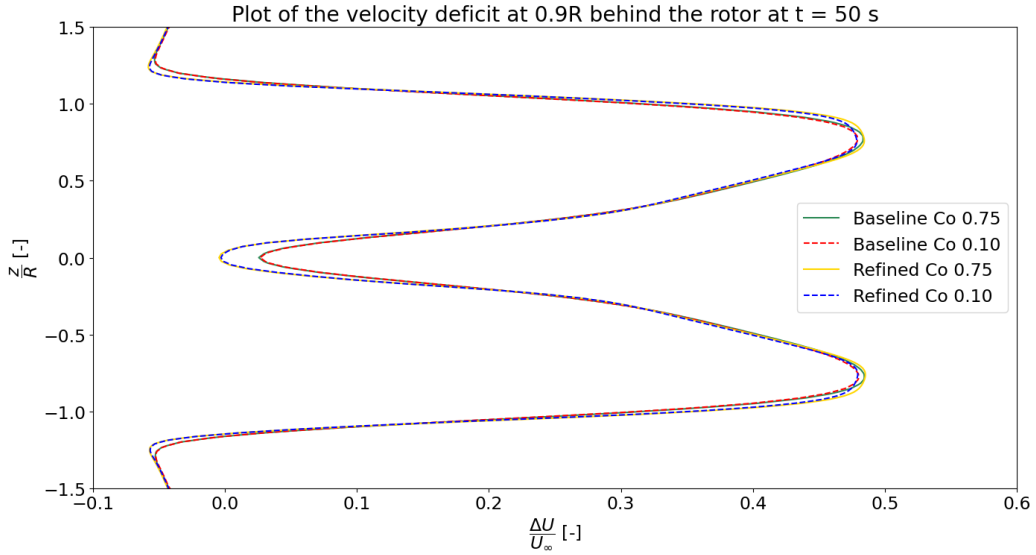

Figure 5.14: Plot of the velocity deficit to compare the cases used to study the temporal convergence

From Figure 5.14 results it becomes clear that having a larger Courant number around 0.75 produces results that deviate little from results with a Courant number of 0.1. Therefore in all the further cases and simulations the Courant number will remain 0.75.

5.1.4. Number of Actuator Elements Study

The optimal number of actuator elements should also be determined. To do this 5 cases are compared with each other that can be found in Table 5.5 and the results can be found in Figure 5.15. Here the results are again plotted as the velocity deficit at 0.9 R behind the rotor but now at the converged steady-state condition again (t = 200 s).

Table 5.5: Cases used to study the number of actuator elements

Case #	Case definition	dx R1 [m]	dx R2 [m]	dx R3 [m]	dr [m]	dt [s]	Courant [-]	U_∞ [m/s]	TSR [-]	# cells [-]	Tend [s]
Case 03	Baseline	8	4	2	4	0,0222	0,75	9	7,5	4,36E+06	200
Case 04	Fine	6	3	1,5	4	0,0167	0,75	9	7,5	1,01E+07	200
Case 08	Baseline with 34 actuator elements	8	4	2	2	0,0222	0,75	9	7,5	4,36E+06	200
Case 09	Fine with 34 actuator elements	6	3	1,5	2	0,0167	0,75	9	7,5	1,01E+07	200
Case 10	Fine with 68 actuator elements	6	3	1,5	1	0,0167	0,75	9	7,5	1,01E+07	200

The results show that having a Δr smaller than Δx does not lead to different results however having a Δr that is larger than Δx can lead results that deviate a bit from the cases where Δr is smaller. However

these differences are quite small. The minimum number of actuator elements is 16 as the span is defined as 16 segments in [23]. Therefore it makes sense that having more elements does not drastically change the results. To illustrate this, it is useful to compare the lift coefficient curve over the span of the blades for the different cases as shown in Figure 5.16.

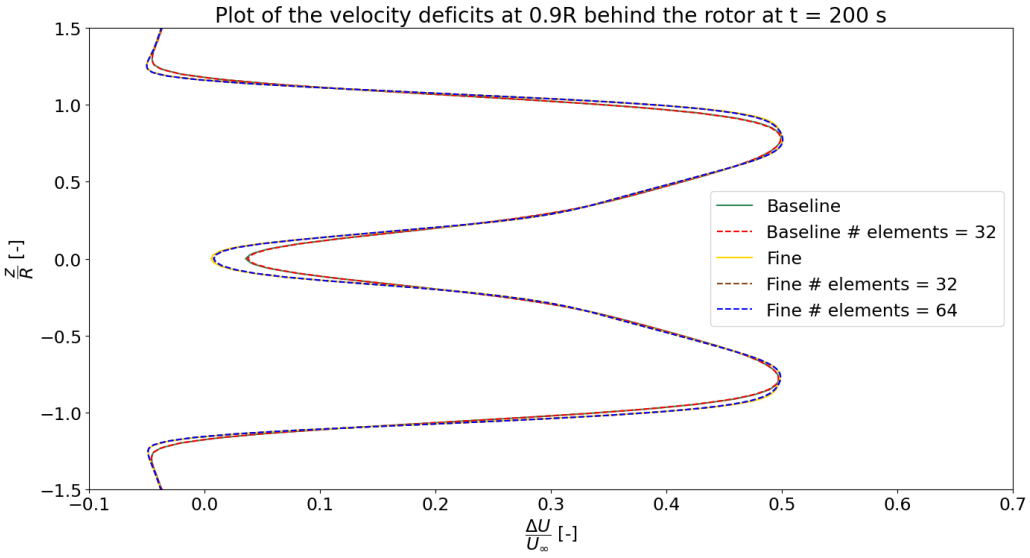

Figure 5.15: Plot of the velocity deficit to compare the cases used to study the number of actuator elements

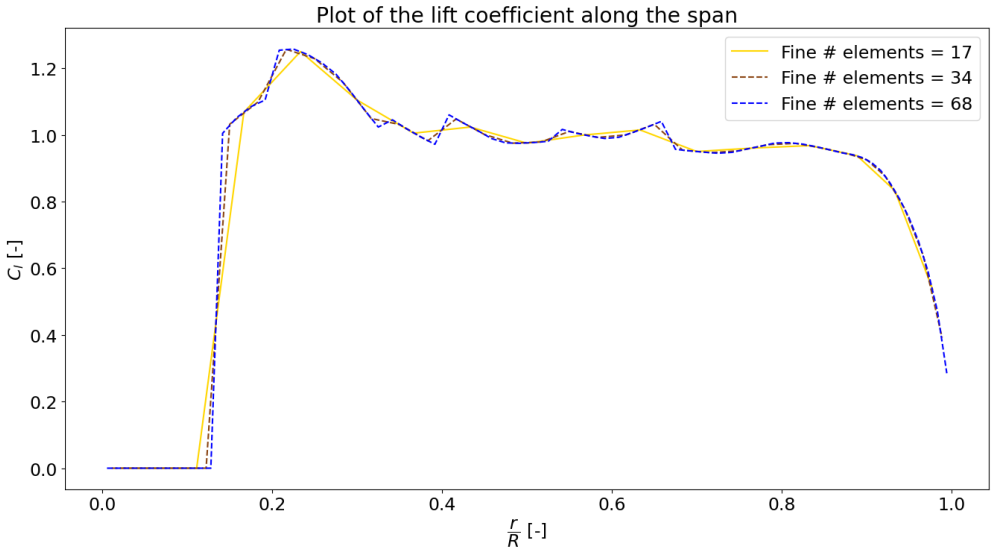

Figure 5.16: Plot of the lift coefficient along the span to compare the cases used to study the number of actuator elements

Figure 5.16 shows that the difference between 16 elements and 32 elements is noticeable but the results between 32 and 64 elements are almost identical. Therefore it can be concluded that setting the number of elements at 32 is preferred to have more accurate results for a small increase in computational time.

5.1.5. Verification Study

To check whether the results obtained from the ALM are what is expected from literature, a verification study is performed. Here the results are compared with the results in the article [24]. The choice of

free stream velocity, TSR and the location to analyse the velocity deficit (0.9 R) were taken from this article to compare the results under the same conditions. These results are already shown in the cases above but are shown again with the results from the article in Figure 5.17.

As shown in Figure 5.17, there is a large difference between the coarse and the fine grid from the article where the fine grid has a much lower velocity deficit than the coarse grid. This is the first major difference when comparing results where the refined grid does have lower wake deficit at the roots (at hub height) but has a larger wake deficit as the tips. The shape of the curves are however very similar and the values of the baseline or refined case Figure 5.17 seem to always lie somewhere between the red (Tabib coarse) and black (Tabib fine) line.

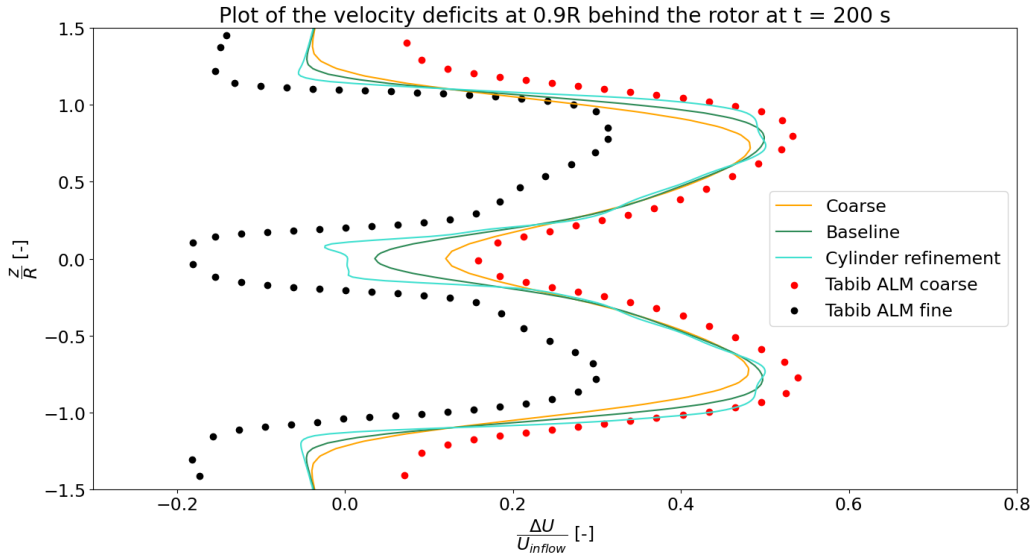

Figure 5.17: Velocity deficit plot of the coarse, baseline and refined grid (case 02)

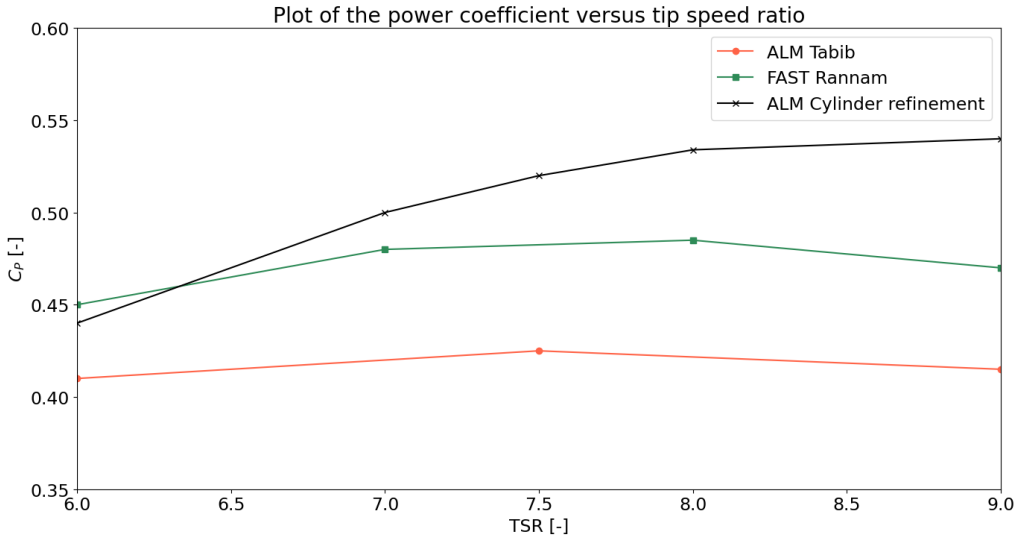

Figure 5.18: C_p versus TSR plot used to verify the results from ALM with data from [24]

A second comparison can be done using the power coefficient that is calculated versus the TSR which is the same method that is used in the aforementioned article as verification. The results can be found

in Figure 5.18 where the results obtained from the ALM model for the cylinder refinement case are compared with the results found in [24]. The power coefficients are in the neighborhood of each other where the ALM Tabib results has the same trend as the FAST Rannam results. The power coefficient from the cylinder refinement, while starting off between the other two, starts to deviate as it has a C_p peak which is around a TSR of 9. The ALM cylinder refinement C_P vs TSR plot will be discussed in more detail in the comparison between the different fidelity methods (see section 5.4). For now, it should be noted that although the results are in the neighborhood of each other, the C_P peak value is higher for the obtained ALM results and also occurs at a higher TSR value.

5.1.6. Effect of the Ground, Tower and Hub

All the cases mentioned before did not model the tower, the hub and ground as a wall boundary. It should be analysed whether the effect of including these elements is significant or whether leaving them out is a reasonable approximation that saves computing power. The computational grid is adjusted to have a wall boundary condition at the ground and the rotor is now only 90 meters from the ground (at the hub height). The computational grid is changed as shown below with the same grid sizes as the Baseline grid. Note that the size of this grid is much smaller than the baseline grid as the wind turbine is currently on the ground and therefore some of the cells that used to be the bottom part of the second and third region are now eliminated.

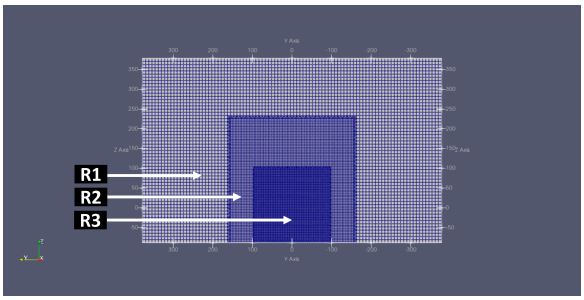

Figure 5.19: Cross-sectional front view of the new computational grid of the NREL 5-MW RWT including the ground as a wall boundary

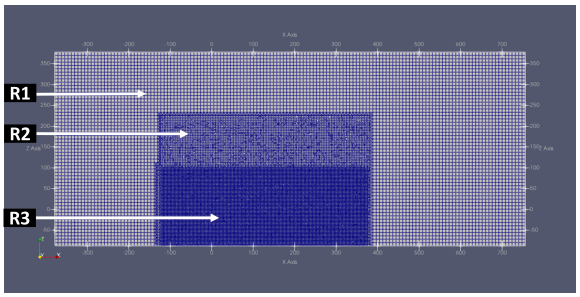

Figure 5.20: Cross-sectional side view of the new computational grid of the NREL 5-MW RWT including the ground as a wall boundary

The cases analysed in this section can be found in Table 5.6. The results of including the ground and the results of including the ground, tower and hub simultaneously can be found in Figure 5.21 where once again the velocity deficit is plotted at 0.9 R.

Table 5.6: Cases used to study the effect ground, tower and hub

Case #	Case name	dx R1 [m]	dx R2 [m]	dx R3 [m]	dx R4 [m]	dr [m]	dt [s]	Courant [-]	U_∞ [m/s]	TSR [-]	# cells [-]	Tend [s]
Case 03	Baseline	8	4	2	NA	4	0,0222	0,75	9	7,5	4,36E+06	200
Case 11	Baseline ground wall boundary	8	4	2	NA	4	0,0222	0,75	9	7,5	3,19E+06	200
Case 12	Baseline ground wall boundary, tower and hub	8	4	2	NA	4	0,0222	0,75	9	7,5	3,19E+06	200

The effect of including the ground wall boundary condition are clear from figure Figure 5.21. It seems that including the ground causes the flow to increase speed and reduce the velocity deficit near the ground. This is to be expected since adding a fixed wall boundary would reduce the area that the flow is moving through and thus increases the velocity due to the conservation of mass (continuity equation). Then, the effect of including the tower and hub as well as the ground is visible in the yellow line in Figure 5.21. The hub causes the flow deficit to increase at hub height ($\frac{x}{R}$) and the tower causes the wake deficit to increase below the hub height up to the ground. The ground itself again speeds up the flow near the ground but this is less visible due to the tower.

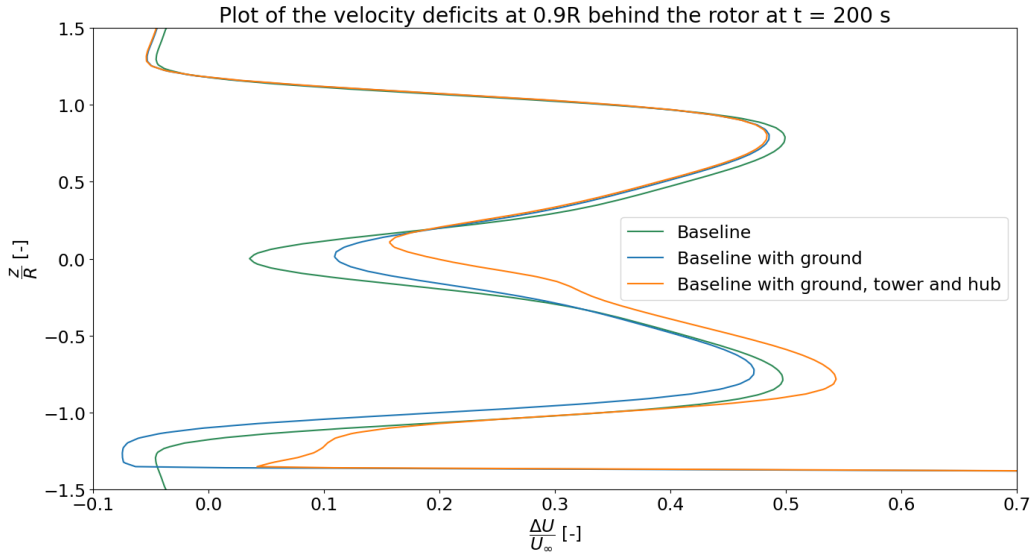

Figure 5.21: Velocity deficit plot to study the effect of including the ground, tower and hub in the baseline case

It can be concluded that including the ground wall boundary condition causes the velocity deficit plot to lose its symmetry but the results will be more realistic. Also including the hub and the tower has a clear effect on the wake deficit plot and it can therefore be argued that these should be included in wake simulations especially when determining the effect of a wake on the performance of another downstream wind turbine. However when determining the performance parameters of a single wind turbine it would be better to not include these elements since then the sole effect of the rotor extracting energy from the flow can be determined.

5.1.7. Conclusion

The NREL 5-MW RWT aerodynamic analysis has been performed using the actuator line method in OpenFOAM. The analysis shows that the total grid size can be reduced and that a cylinder refinement near the turbine is a good method to obtain high accuracy while keeping the number of cells relatively low. A Courant number of 0.75 and having an actuator element for every two cells across the span of the blade are deemed to be optimal in terms of computational cost and accuracy. Including the tower, hub and adding the ground wall boundary have significant effects on the wake deficit which are useful to include when studying the effects of another downwind turbine. However when determining the performance parameters of a single wind turbine it would be better to not include these elements since then the sole effect of the rotor extracting energy from the flow can be determined.

The results of the ALM are verified using the article [24]. The power coefficients obtained are larger than those mentioned in the article but the wake deficit plot aligns well with the article which means that the model works as expected.

5.2. Blade Element Momentum Theory (BEM) of the NREL 5-MW RWT

This RWT has been analysed to great extent using OpenFAST and therefore this is not meant to bring new information at light but rather to use this information for comparison. The setup of BEM in OpenFAST is done in AeroDyn15 and it has several input variables of which most are set to default and the flow velocity, tip speed ratio, etc. are set to the same value as the ALM (see subsection 5.1.1) for a fair comparison. The results will not be showed here but rather in the discussion of the different fidelity methods (see section 5.4).

5.3. Free Vortex Wake (FVW) Method of the NREL 5-MW RWT

This section will analyse the NREL 5-MW RWT in OpenFAST [4] using the cOnvecting LAgrangian Filaments (OLAF) module. Since this method is also used in OpenFAST the input files can be kept exactly the same except for the wake module type (this should be set to OLAF) and an OLAF input file should be used.

In this OLAF input file most variables can be kept as default but there are some guidelines with respect to the time step and the wake length [1]. In the guidelines, it is recommended to have 2 revolutions for the near wake length, 10 revolutions for the far wake length and 3 revolutions for the free far wake length.

The guidelines recommend to use an azimuthal discretization, $\Delta\psi$, of 6 degrees of one rotor revolution. This, together with the the rotational speed, Ω, makes it possible to determine the time step of the OLAF calculations as shown in Equation 5.2.

$$\Delta t = \frac{\Delta\psi_{deg}}{6 \cdot \Omega_{RPM}} \tag{5.2}$$

The azimuthal discretization, together with the prescribed lengths of the wakes, can also be used to determine the number of panels for the different wakes as shown in Equation 5.3. For the near wake rotations this is Equation 5.4, for the far wake rotations this is Equation 5.5 and for the far wake rotations that are considered free this is shown in Equation 5.6. Note that the number of panels do not depend on the rotational speed of the rotor but the time step does. Therefore, only the time step has to be adjusted for each TSR.

$$N_{panels} = N_{revolutions} \cdot \frac{360}{\Delta\psi_{deg}} \tag{5.3}$$

$$N_{NW_{panels}} = 2 \cdot \frac{360}{\Delta\psi_{deg}} \tag{5.4}$$

$$N_{FW_{panels}} = 10 \cdot \frac{360}{\Delta\psi_{deg}} \tag{5.5}$$

$$N_{FFW_{panels}} = 3 \cdot \frac{360}{\Delta\psi_{deg}} \tag{5.6}$$

The results for power and thrust coefficients versus TSR are again not shown here but will be showed in the discussion of the different fidelity methods (see section 5.4). However, the wake visualisation will be shown here where in Figure 5.22, the lifting line representation can be seen with the circulation value of each element.

The near wake is visualised only for one blade (otherwise the image becomes too crowded) in Figure 5.23 where also the circulation can be seen for each shed and trailing vorticity. In Figure 5.24, the far wake is visualized as well (for only one blade) where it can be seen that at a given point the wake starts to collapse. Finally, both the near and the far wake are plotted for all three blades in Figure 5.25 which shows how crowded the image becomes due to the trailing vortices. These images indicate how the wake is formed and how it breaks down without needing a large amount of computational time.

[1] https://openfast.readthedocs.io/en/dev/source/user/aerodyn-olaf/RunningOLAF.html

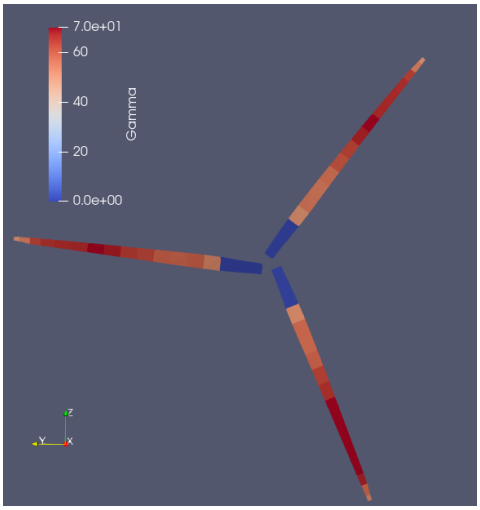

Figure 5.22: Visualization of the lifting lines

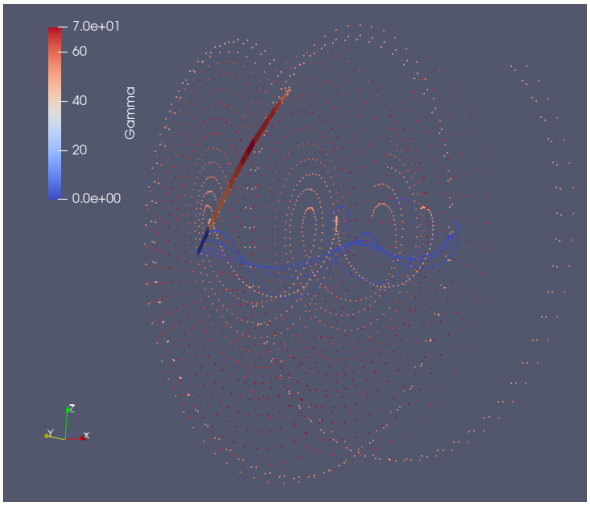

Figure 5.23: Visualization of the near wake for only one blade

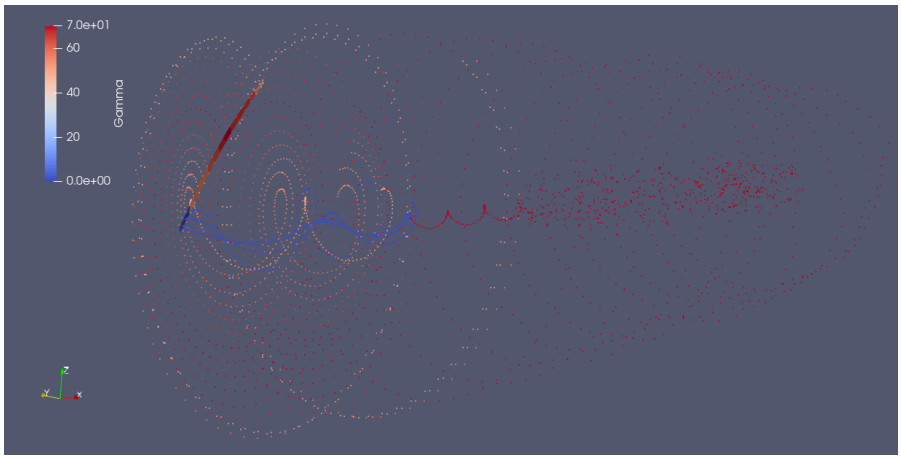

Figure 5.24: Visualization of both the near wake and the far wake for only one blade

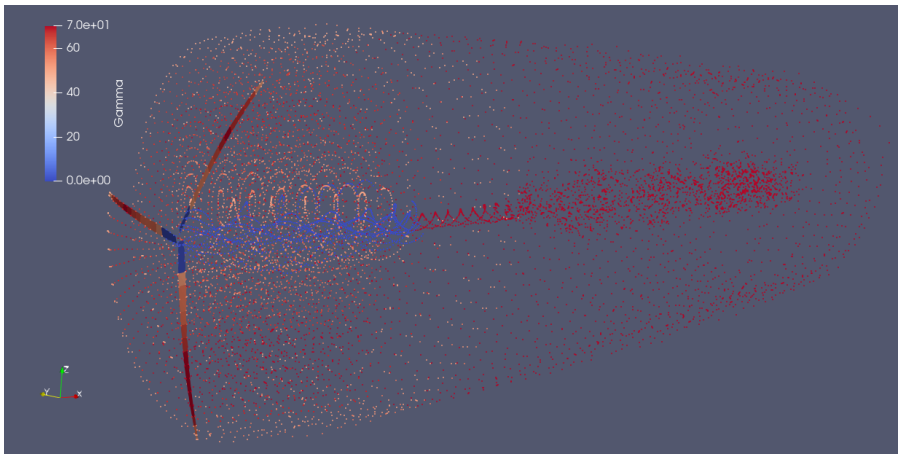

Figure 5.25: A complete visualization of both the near and the far wake for all blades

5.4. Discussion of the Results of the Varying Fidelity Methods

Now that both the high-fidelity and low-fidelity tools are explained, it time to compare the results of the different fidelity models and discuss any significant differences. The first comparison is the C_p versus TSR plot which is shown in Figure 5.26. From this figure it becomes clear that the power coefficient values lie close together but there are some differences. The smallest difference equals 6.8 % at TSR 6, the largest difference equals 31% at TSR 15 and the average deviation equals 16.6 %. What is also noticeable is that the peaks are different for each method both in size and TSR location. BEM has the lowest peak at the lowest TSR and ALM has the highest peak at the highest TSR while the FVW (OLAF) is in the middle. This can be explained by the fact that the FVW is also in the middle of the two in terms of fidelity and therefore it is also expected that the results are in the middle.

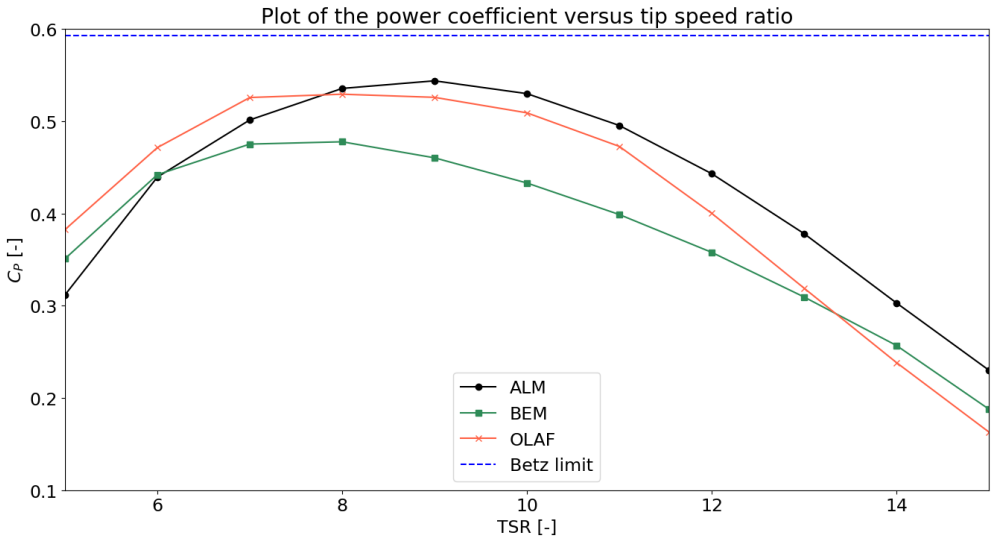

Figure 5.26: C_P versus TSR plot used to compare the results of the ALM, OLAF and BEM

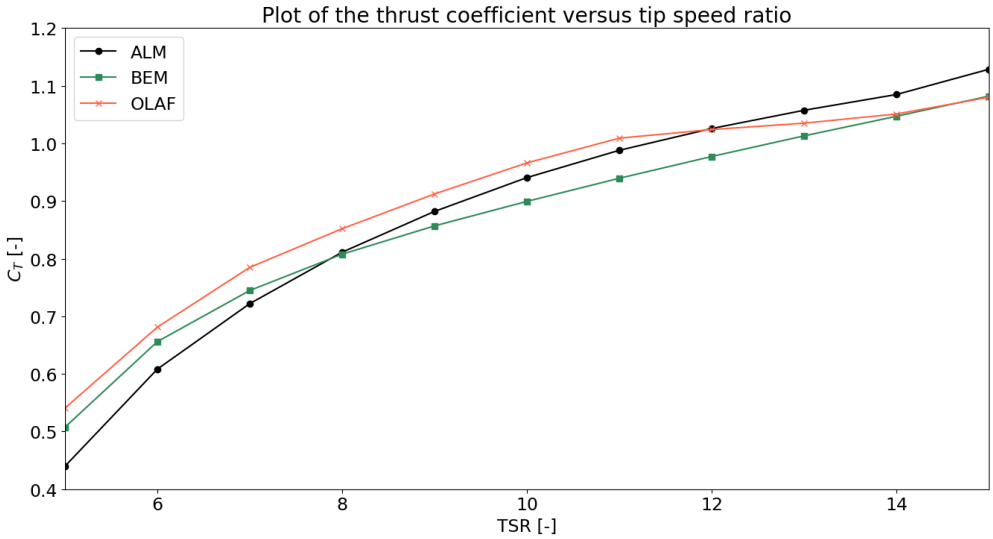

Figure 5.27: C_T versus TSR plot used to compare the results of the ALM, OLAF and BEM

Also the C_t versus TSR plot can be used to compare the tools. This plot is shown in Figure 5.27 and it shows that all three models have similar trends. For most TSRs the FVW OLAF gives the highest thrust coefficient and BEM the lowest thrust coefficient but the values lie much closer together than the power coefficient plot. The smallest difference is at TSR 14 with 3.5 %, the largest difference is at TSR 5 with 18.5 % and the average deviation is 7.1 %.

In [27], a similar comparison is performed where BEM, OLAF and ALM are compared on a different turbine but with a similar power output (although a different library for ALM is used, namely SOWFA instead of TurbinesFOAM). In their work they analysed the effect of changing the turbulence intensity, shear exponent and the yaw misalignment. However for the case of zero yaw misalignment and with uniform inflow conditions (figure 6a), the results show similarities with the results found for the NREL 5-MW. Indeed the OLAF and ALM simulations have the same power output which is higher than the BEM simulations. This shows that the results as show in Figure 5.26 are in line with what can be found in literature.

Wake visualizations can be performed for both the ALM and FVW. The difference between the two is that the ALM uses a contour plot with a certain threshold of the Q-criterion while the FVW simply plots the shed and trailing vorticity which forms the wake. The wake visualization for different grid sizes in ALM has already been discussed in subsection 5.1.2 where it became clear that using the baseline or higher grids are best to visualize the wake. Here the plot of refined grid with Q-criterion of 0.001 is shown again in Figure 5.28 because it has the best visualization of each tip and root vortex. The wake visualization for the FVW has already been discussed in section 5.3 and the last plot will be shown here again but without colour in Figure 5.29. Comparing Figure 5.28 and Figure 5.29, shows that the wake for the FVW can be visualized much further downstream and is also able to visualize the blade trailing and shed vortices instead of only the tip and root vortices. The advantage of the ALM vorticity contour however is that it contains much more information than just the circulation of each vortex as it is also possible to visualize more such as show streamlines and to calculate other variables such as the turbulence intensity and pressure. Nevertheless, the ALM simulation takes 140 times longer to run for the same processing power so it is useful to have a very fast wake visualization tool which produces a similar wake propagation. Of course, the ALM simulation can be run in parallel and when more processors are available the computational time can be reduced but it still takes 7 times longer to run than an OLAF simulation.

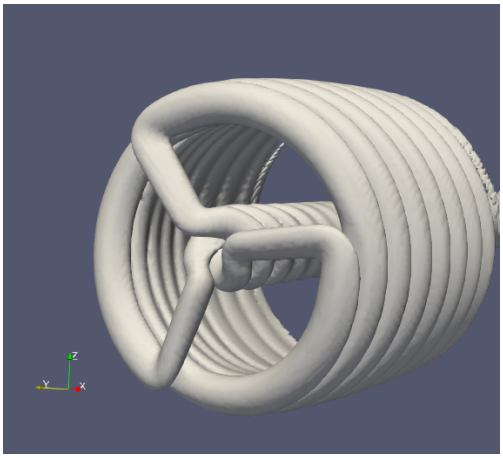

Figure 5.28: ALM vorticity contour plot of the fine grid with Q-criterion = 0.001

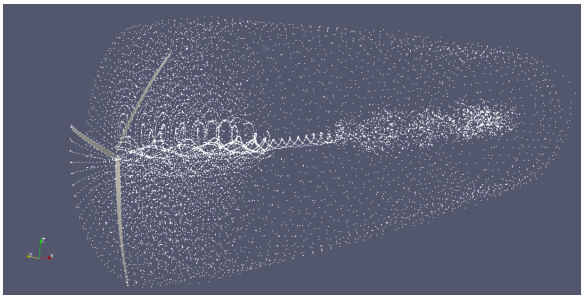

Figure 5.29: OLAF wake visualization of both the near and the far wake

5.5. Conclusion

Three different aerodynamic analysis have been performed on the NREL 5-MW RWT, each with a different fidelity. The ALM has been optimized for this RWT and the model has been verified using literature. The BEM and OLAF tools are widely used and this RWT is a baseline case for the software which means that the results are already verified.

The results of the ALM show a close correlation with the C_P and C_T versus TSR curves of BEM and OLAF, where it overestimates the peak of the C_P relative to BEM but the trend is similar. The ALM shows a better alignment with OLAF than with BEM which makes sense as both use wake calculations to estimate the wake instead of only using a global momentum balance. This is also in line with literature where the power for ALM and OLAF is also found to be higher than for BEM ([27], figure 6a). The C_T versus TSR plot for all three methods lie close together with an average deviation of 7.1 %. This also makes sense, as each method uses blade elements and the same 2D blade element data which is required to calculate the C_T.

Comparing the wake visualizations shows that FVW can visualize the wake much further downstream and it is also able to visualize the blade trailing and the shed vortices instead of only the tip and root vortices. The ALM is however able to also plot streamlines and calculate variables such as pressure which makes it a better analysis tool but also more computationally expensive. The ALM cylinder refinement takes 140 times longer to run for the same processing power as compared to the FVW, so it is useful to have a very fast wake visualization tool which produces a similar wake as the expensive but high-fidelity CFD tool.

6

Aerodynamic Analysis of the IEA 15-MW RWT

This chapter contains the aerodynamic analysis of the IEA 15-MW RWT using varying fidelity methods. The layout of this chapter is similar as the layout of the previous chapter where the NREL 5-MW RWT is analysed. First the actuator line method is analysed in section 6.1. Secondly the blade element momentum (BEM) theory is analysed in section 6.2 and lastly the free vortex wake (FVW) method is analysed in section 6.3. A comparison and discussion of the results of the different fidelity methods is presented in section 6.4 and a conclusion is provided in section 6.5.

6.1. Actuator Line Method (ALM) of the IEA 15-MW RWT

In the previous chapter the NREL 5-MW was extensively studied using the ALM to understand the effect of the grid refinement, Courant number, number of actuator elements, including the ground as a wall boundary and including the tower and the hub as actuator elements as well. The conclusions were that the baseline case has sufficient refinement at a Courant number of 0.75 and that it is best to use the dedicated minimum number of actuator elements while excluding the ground, tower and hub in the analysis. This means that the analysis of the IEA 15-MW RWT does not start from scratch but can build open what was already discovered from the NREL 5-MW RWT. Therefore, only two studies will be performed here again. The first one is another grid refinement study to identify if there is again a grid convergence. Secondly, the number of actuator elements will be analysed because this turbine has a continuous chord, twist, etc. distribution instead of a discrete distribution as was the case or the NREL 5-MW.

This section starts off with an explanation of the numerical setup, after which the two studies are discussed. Unfortunately, no similar analysis has been performed already and therefore it is not possible to verify the results of this RWT specifically. Of course the software and method used was already verified in the previous chapter.

6.1.1. Numerical Setup

A similar setup, with the same solver and models, is used for the IEA 15-MW as for the NREL 5-MW which is explained in subsection 5.1.1. This was done on purpose since the results for the NREL 5-MW have been verified and thus it is possible to adjust the model to the 15-MW for which verification is not yet possible.

The baseline computational setup for the IEA 15-MW is outlined as shown in Figure 6.1 and Figure 6.2. The differences here as compared with the NREL 5-MW is that there is an additional region. The reason for this is because the same resolution is desired at the inner regions for both turbines but since the IEA 15-MW is much larger in size this will result in too many cells when scaling directly (well beyond 20 million cells). Therefore, the inner regions will keep the same resolution but the outer region will lose in resolution. In addition, the inner region is relatively smaller in the streamwise direction to also reduce

the number of cells. These adjustments are deemed acceptable as it was found in the grid study of the NREL 5-MW (see subsection 5.1.1) that these regions offer little to the accuracy of the models.

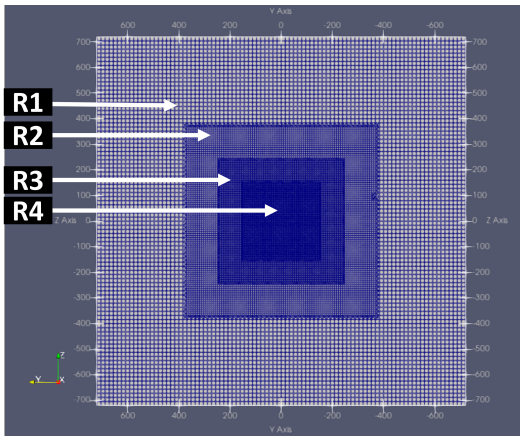

Figure 6.1: Cross-sectional front view of the baseline computational grid of the IEA 15-MW RWT

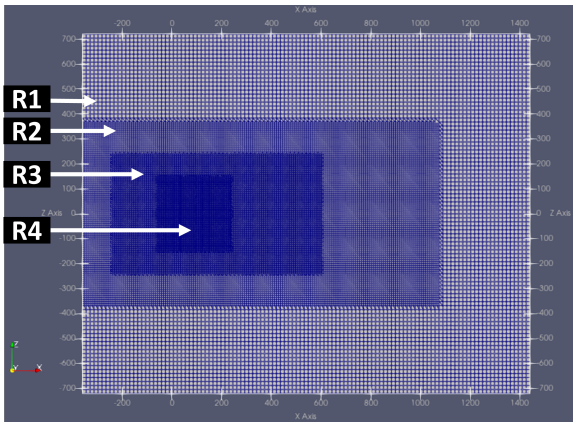

Figure 6.2: Cross-sectional side view of the baseline computational grid of the IEA 15-MW RWT

The same Courant number and simulation time are used for the IEA 15-MW as for the NREL 5-MW but a different TSR is used since both RWT are analysed at each respective design TSR. For the NREL 5-MW RWT the design TSR is 7.5 and for the IEA 15-MW RWT the design TSR equals 9. An overview of all the cases that will be analysed for the IEA 15-MW are shown in Table 6.1.

Table 6.1: Overview of all the cases analyzed in this section

Case #	Case name	dx R1 [m]	dx R2 [m]	dx R3 [m]	dx R4 [m]	dr [m]	dt [s]	Courant [-]	U_∞ [m/s]	TSR [-]	# cells [-]	Tend [s]
Case 01	Very course	16	8	4	4	2.4	0,03704	0,75	9	9	5,55E+06	200
Case 02	Baseline	16	8	4	2	2.4	0,01852	0,75	9	9	9,05E+06	200
Case 03	Baseline # elements 100	16	8	4	2	1.2	0,01852	0,75	9	9	9,05E+06	200
Case 04	Baseline # elements 150	16	8	4	2	0.8	0,01852	0,75	9	9	9,05E+06	200

6.1.2. Grid Refinement Study

The first study is to find out whether the baseline case is again sufficient for aerodynamic analysis as was the case for the NREL 5-MW. To do this, two cases have been set up with the same grid resolution near the turbine as for the NREL 5-MW RWT. A very course grid and a baseline grid are made that have a grid resolution near the turbine of 4 m and 2 m, respectively. The very course grid already has 5.5 million cells and the baseline grid reaches 9 million cells. For reference, these were 2 million and 4.5 million respectively for the 5-MW. As explained in the numerical setup above, the inner grid regions were made smaller for the 15-MW and the outer grid region was coarsened more to keep the total number of cells under 10 million. This is also why there is no analysis of a fine or very fine mesh. It would lead to a drastic increase in computational effort while it has already been showed in the previous chapter that the results have already converged for the baseline grid. In Figure 6.3 the velocity deficit plot of the very coarse grid and the baseline grid can be seen at 0.9 R and at t = 200 s.

This figure shows that even though the very coarse grid is twice as coarse is this region near the turbine, the results coincide well. Apart from the region near the hub there is a sufficient correspondence of the very coarse grid to the baseline grid to suggest convergence. Ideally another finer case should be added to confirm this but due to the computational power required that is not feasible. However it can be stated that since the same analysis has been performed for the NREL 5-MW for which the baseline grid was deemed sufficient, that this grid could be considered sufficient for the 15-MW grid as well, even with the adjustments.

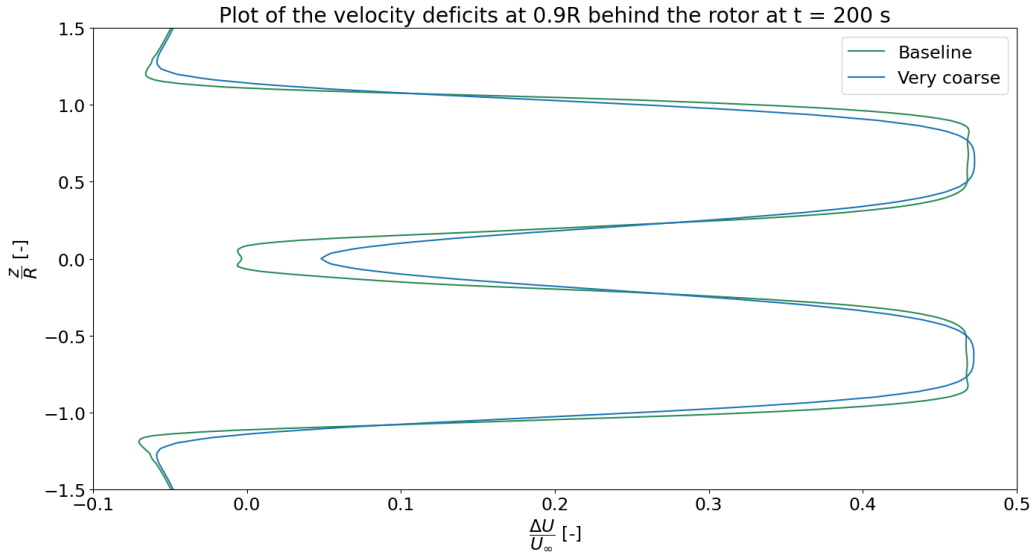

Figure 6.3: Plot of the velocity deficit to compare the cases used to study the grid refinement

A similar conclusion can be drawn when analysing the visualization of the wake for both grids using vorticity contours. The vorticity contour of the very course and the baseline grid can be found in Figure 6.4 and Figure 6.5, respectively. Both figures show the important parameters such as the blades, the tip vortices and the root vortices. These are better visualized by the baseline grid but the differences are not large. Therefore, here it can again be concluded that using the baseline grid is sufficient for a wake analysis.

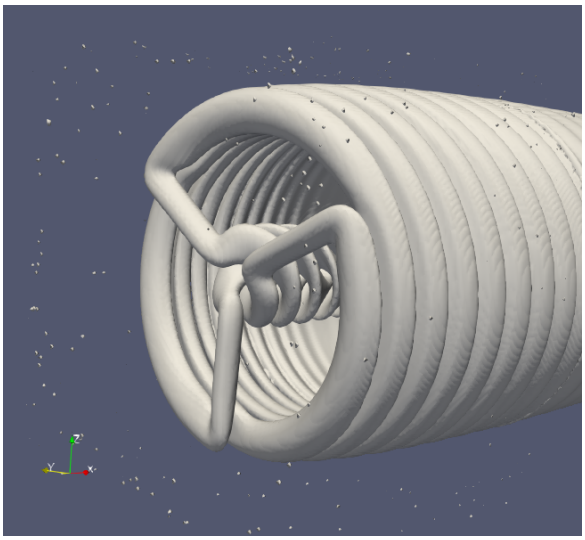

Figure 6.4: Vorticity contour plot of the very coarse grid with Q-criterion = 0.0001

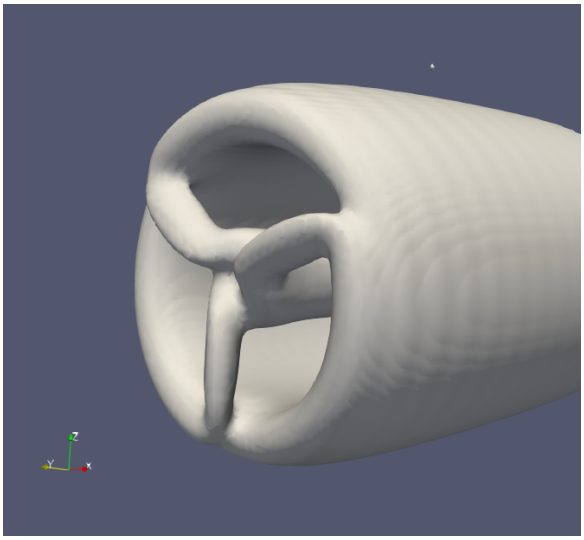

Figure 6.5: Vorticity contour plot of the baseline grid with Q-criterion = 0.0001

6.1.3. Number of Actuator Elements Study

The IEA 15-MW has a continuous chord and twist distribution which the NREL 5-MW did not have. In the OpenFAST input files for the IEA for this RWT there are 50 elements defined along the span which gives a dr of 2.4 whereas for the NREL 5-MW this dr was 3.7. For the NREL 5-MW an analysis was performed in subsection 5.1.4 to find out whether decreasing the dr led to better results and this did not happen. Since the 15-MW RWT has a finer element distribution it is worth again analysing whether increasing the number of elements leads to different results. The results are plotted in Figure 6.6.

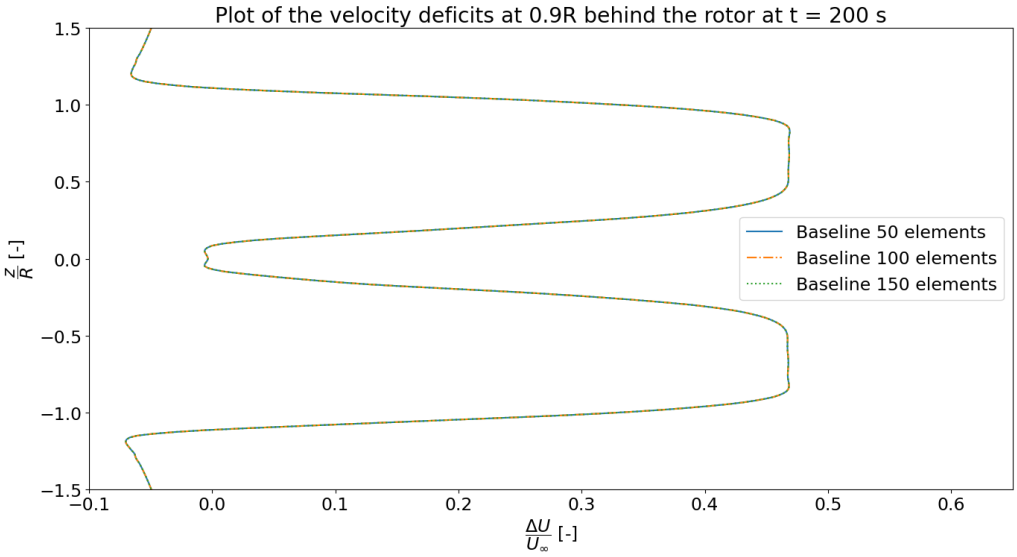

Figure 6.6: Plot of the velocity deficit to compare the cases used to study the number of actuator elements

The plot shows that just like with the NREL 5-MW RWT there does not seem to be an added advantage to including more actuator elements beyond the definition of the reference turbine. In the case for the IEA 15-MW there are 50 predefined elements and therefore it is sufficient to keep using these 50 elements.

6.1.4. Conclusion

The IEA 15-MW RWT aerodynamic analysis has been performed using the ALM based on the knowledge gained from the similar analysis done for the NREL 5-MW RWT in section 5.1. The same conclusions can be drawn from the analysis of the IEA 15-MW which is that the baseline computational grid is sufficient for the aerodynamic analysis and that having a larger number of elements does not lead to different results.

6.2. Blade Element Momentum Theory (BEM) of the IEA 15-MW RWT

Just as with the NREL 5-MW RWT this RWT also has predefined BEM input files available for OpenFAST [1]. These files are used and adjusted so to have the same operating conditions as the ALM case for a fair comparison. The power and thrust coefficient plots are compared with the definition of the turbine in Figure 6.7 and Figure 6.8, respectively. These figures show that the two lines align well. This which makes sense as both lines in the figure use the BEM module of OpenFAST. In section 6.4, the power and thrust coefficient plots of the ALM and FVW will also be shown to compare the different results from different the fidelity models.

[1] https://github.com/IEAWindTask37/IEA-15-240-RWT

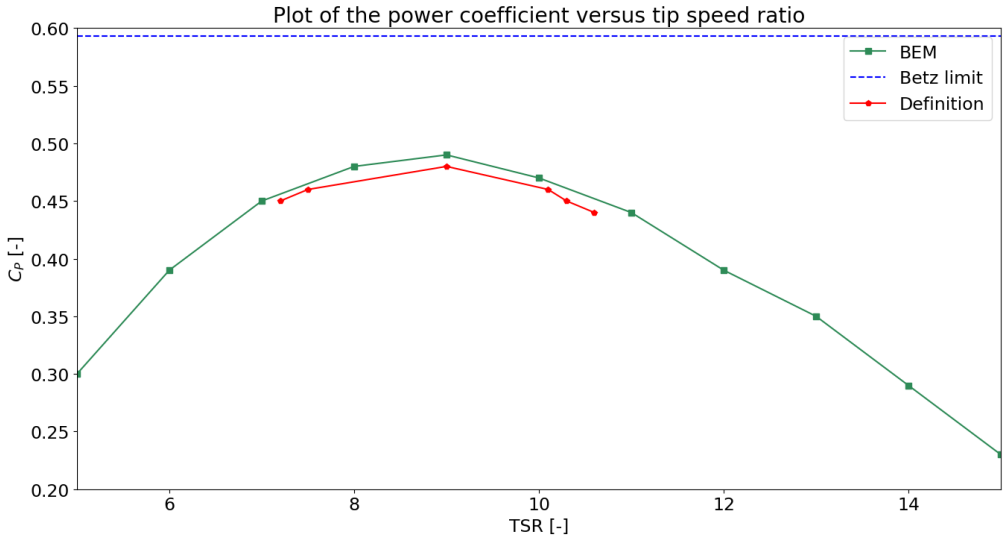

Figure 6.7: C_P versus TSR plot used to compare the results of BEM with the definition of the RWT as defined in [2]

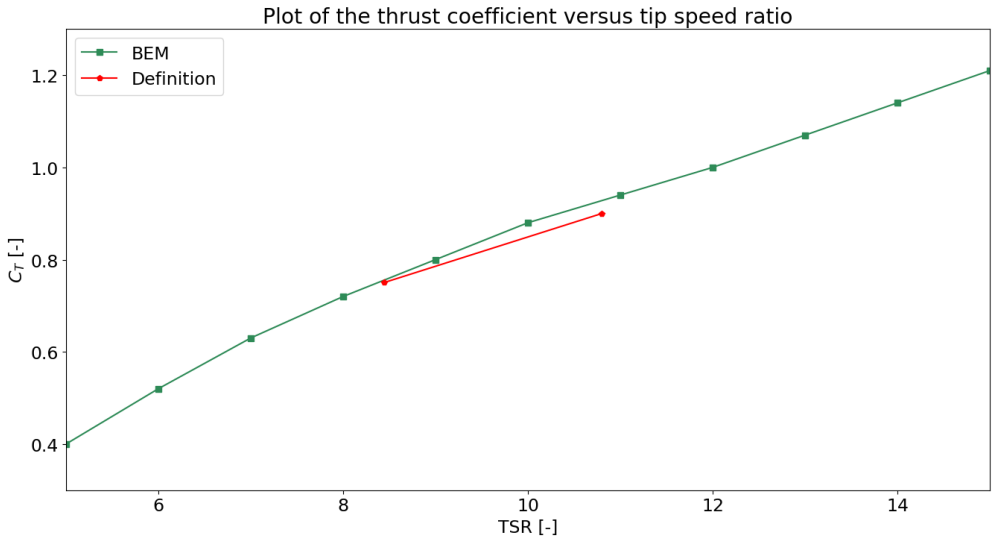

Figure 6.8: C_T versus TSR plot used to compare the results of BEM with the definition of the RWT as defined in [2]

6.3. Free Vortex Wake (FVW) Method of the IEA 15-MW RWT

The free vortex wake (FVW) methods used here is also the model OLAF just as for the NREL 5-MW RWT. OLAF is a wake module in OpenFAST which makes it possible to use the same input files as for BEM but then an additional OLAF input file has to be made.

For this OLAF input file, the same guidelines apply as explained in section 5.3. The only difference now is that the required step size for BEM is much smaller for the 15-MW than for the 5-MW. This already has a large effect on the BEM simulation time which increased from only a minute to 30-45 minutes per simulation. For OLAF this effect is felt much more since the simulation for the 5 MW already took multiple hours. There is no straightforward way to reduce the simulation time as the guideline values for the OLAF simulations must be adhered to. This guideline value for the time step size can be calculated as shown in Equation 6.1 where the azimuthal discretization is set to 6 degrees of one rotor revolution.

$$\Delta t = \frac{\Delta \psi_{deg}}{6 \cdot \Omega_{RPM}} \tag{6.1}$$

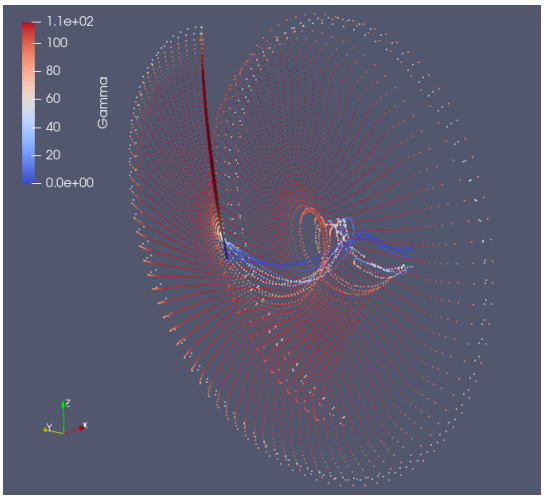

Figure 6.9: Visualization of the near wake for only one blade

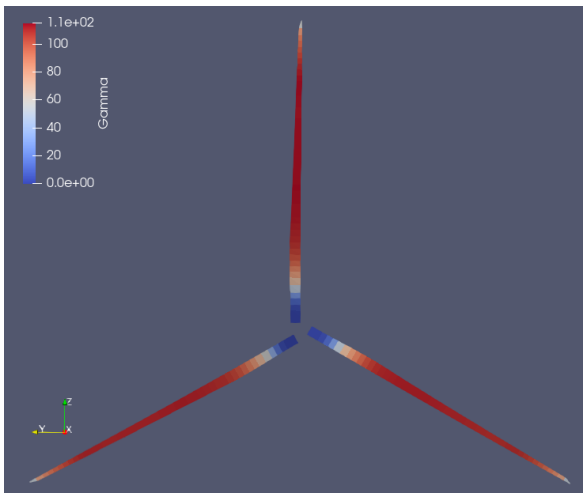

Figure 6.10: Visualization of the lifting lines

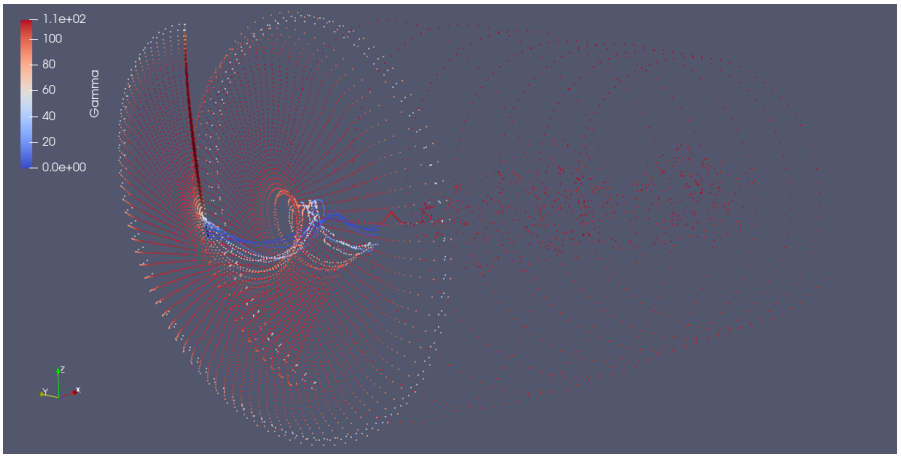

Figure 6.11: Visualization of both the near wake and the far wake for only one blade

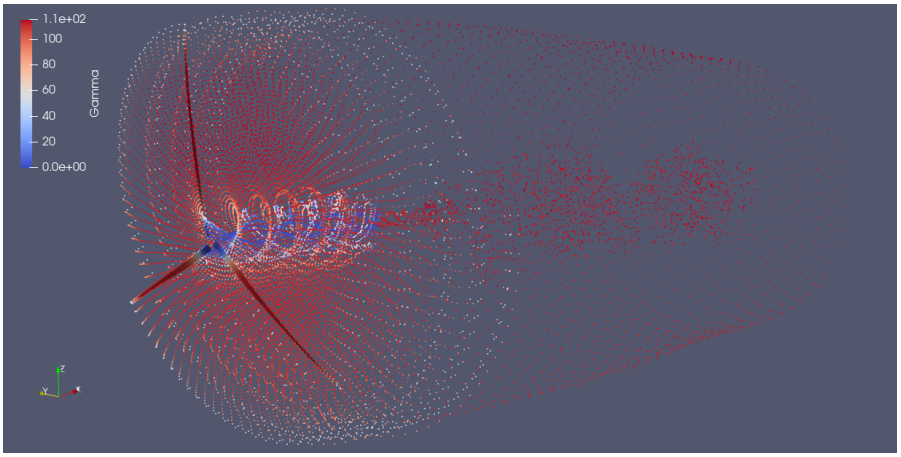

Figure 6.12: A complete visualization of both the near and the far wake for all blades

This leads to similar figures as with the NREL 5-MW. It is again possible to visualize the circulation distribution of the near wake using points as shown in Figure 6.9. Here the near wake is again only visualized for one blade to avoid an overcrowded image. In Figure 6.10, the lifting lines are shown with the circulation of each blade element. The far wake is shown in Figure 6.11 which shows a very stable wake for the entire duration of the simulation (which are set to 10 revolutions). In Figure 6.12, the complete view of the wake due to the three blades is shown which is a too crowded plot to analyse details but it does show the symmetry in the wake caused by the three blades.

6.4. Discussion of the Results of the Varying Fidelity Methods

The high-fidelity and low-fidelity methods are discussed and so it is possible to analyse the performance parameters that the different methods give. First of all, the power coefficient is analysed along the range of tip speed ratios. This is shown in Figure 6.13.

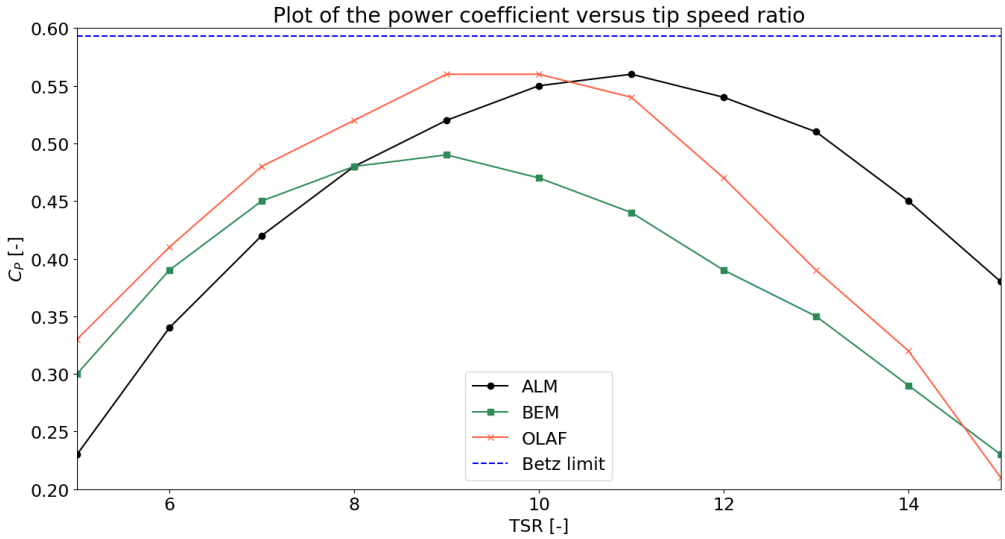

Figure 6.13: C_P versus TSR plot used to compare the results of ALM, OLAF and BEM

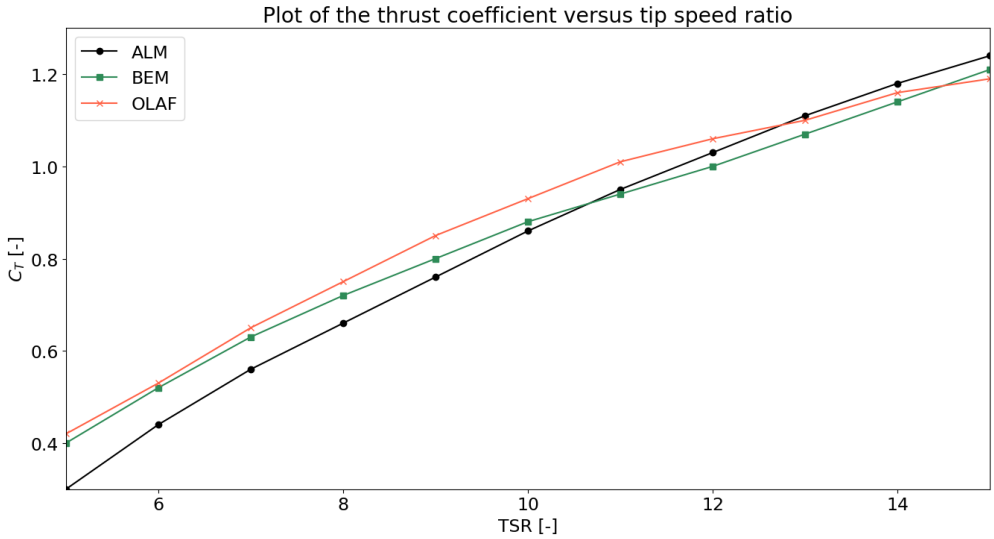

Figure 6.14: C_T versus TSR plot used to compare the results of the BEM with the definition of the RWT as defined in [2]

This figure shows that there are some large differences, especially for higher tip speed ratios. The smallest difference equals 8.0 % at the TSR of 8, the largest difference equals 46.5 % at the TSR of 15 and the average deviation equals 23.9 %. Apart from the substantial deviations there are also some similarities. For instance, OLAF and BEM have their maximum power coefficient peak at the same TSR while ALM and OLAF have the same value for the maximum power coefficient.

The thrust coefficient versus TSR is shown in Figure 6.14. This figure show much less deviations than the previous plot. All three curves have a similar trend and lie close together. The smallest difference equals 4.6 % at the TSR of 14, the largest difference equals 27.7 % at the TSR of 5 and the average deviation equals 10.4 %.

Besides the performance parameters, also the wake visualization can be analysed. In the previous chapter the wake visualisation of the NREL 5-MW RWT was analysed and there the main conclusion was that both tools are used for different reasons. Now however, the FVW OLAF simulation of the IEA 15-MW RWT takes much longer to run. In fact, it even takes longer to run than the ALM simulation (57 hours for FVW versus 36 hours for ALM, but note that the ALM simulation is run in parallel with 20 processors whereas the FVW simulation is only run with 1 processor). The ALM simulation of the IEA 15-MW provided a similar wake visualization as was found for the NREL 5-MW RWT with a similar computational effort. It then becomes difficult to root for a FVW simulation of the IEA 15-MW RWT as the main advantage of OLAF over ALM was its computation time. Seeing as the ALM simulation contains much more information of the wake such as turbulence intensities and pressure distributions, the preference would be to choose ALM over OLAF.

6.5. Conclusion

Three different fidelity tools were used to analyse the IEA 15-MW RWT. The basis for the numerical setup of the ALM simulation was made by verifying the model using the NREL 5-MW RWT. For the BEM and OLAF simulations there were (just like for the NREL 5-MW RWT) input files provided for the tool OpenFAST which is a verified tool on its own.

The results of studies performed on the numerical setup of the ALM provide similar conclusions as was the case for the NREL 5-MW RWT. This means that the method of first verifying the numerical setup for the NREL 5-MW and then expanding it to the IEA 15-MW worked well. The values for the thrust coefficient versus the TSR range coincide well which as explained before makes sense since each method use blade elements and the same 2D blade element data. The values of power coefficient on the other hand coincide much less. There are several similarities to be found however which makes this C_P versus TSR analysis interesting for the comparison with the NREL 5-MW RWT in the next chapter.

The ALM has a preference when it comes to performing wake visualizations for the IEA 15-MW RWT. The main reasons for this are that the FVW OLAF takes longer to perform a simulation towards convergence and the results contain much less information. The main advantage of using OLAF for wake visualization would be that it is a fast tool to visualize where the wake is going and how it breaks down. If the OLAF simulations take longer than the ALM simulations then the advantages of using OLAF over ALM are lost.

7

Aerodynamic Comparison of the NREL 5-MW RWT and the IEA 15-MW RWT

This chapter contains the aerodynamic comparison of the RWTs analysed in the previous two chapters. In addition, it will also introduce a downscaled version of the IEA 15-MW to a 5-MW version. The first section will analyse the performance parameters, the second section will analyse the velocity deficit plots, the wake visualizations are analysed in the third section and the fourth section analyses the velocity profiles. Finally, the last section provides a discussion and conclusion.

7.1. Comparison of Performance Parameters

This section compares the performance parameters of the NREL 5-MW RWT and the IEA 5-MW RWT. Two performance parameters will be compared starting with the thrust coefficient which is plotted versus the TSR and can be seen for the NREL 5-MW and the IEA 5-MW in Figure 7.1 and Figure 7.2, respectively.

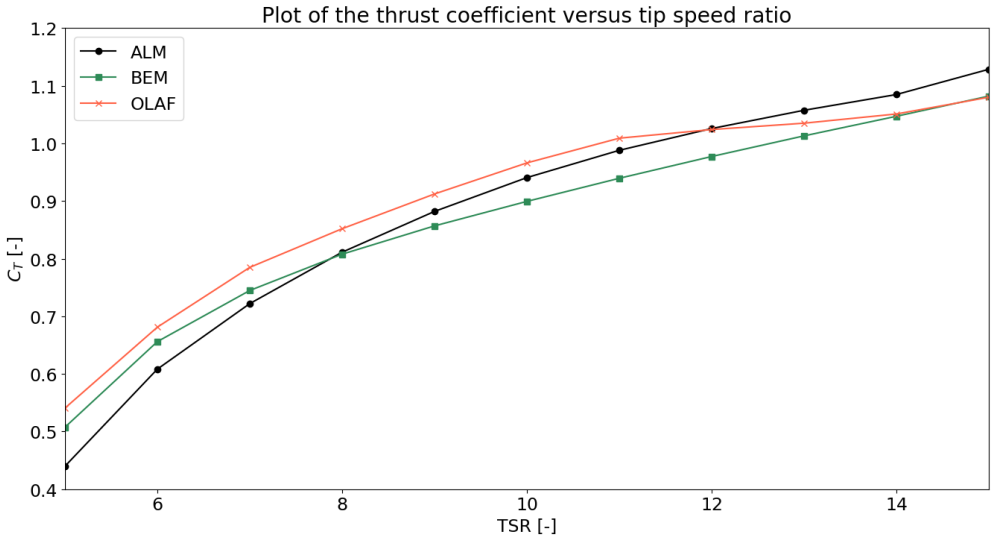

Figure 7.1: c_T versus TSR plot of the NREL 5-MW RWT

Figure 7.2: C_T versus TSR plot of the IEA 15-MW RWT

These two figures show that there is a similar trend for both turbines with the different fidelity models. The FVW OLAF has a higher thrust coefficient for the most TSR values, ALM starts lower but ends up with the highest thrust coefficient and BEM has multiple intersections with ALM OLAF while never having the highest thrust coefficient but usually lying somewhere in between both fidelities. In terms of the deviations, both turbines have the largest deviation at a TSR of 5 but the IEA 15-MW has a 46.6 % higher average maximum deviation than the NREL 5-MW. Comparing these figures shows that there is not one clear outlier. Sometimes the maximum deviation is between ALM and OLAF, sometimes between ALM and BEM and other times between OLAF and BEM. In general, the values are close together and the trends are similar for both plots. It becomes a slightly different story when comparing the power coefficient curves below.

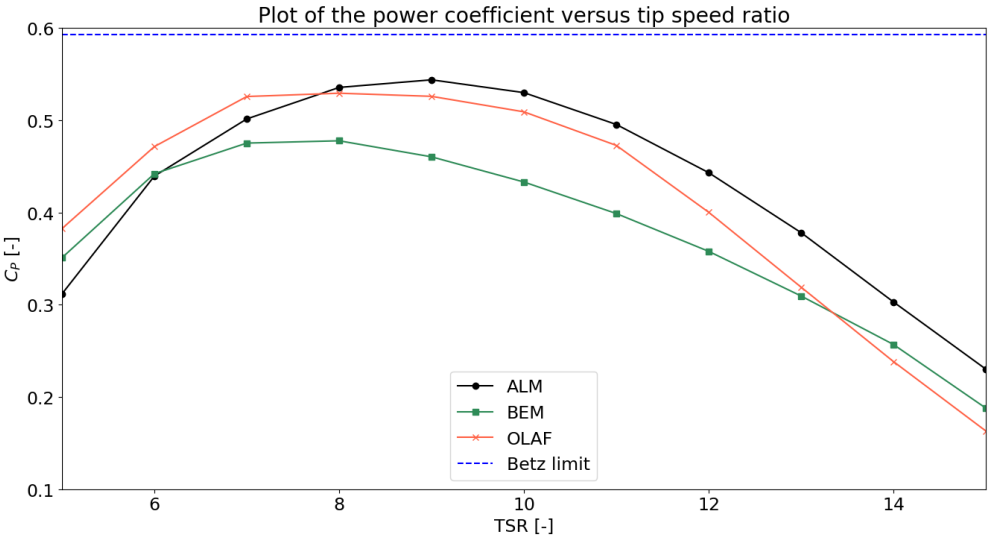

Figure 7.3: C_P versus TSR plot of the NREL 5-MW RWT

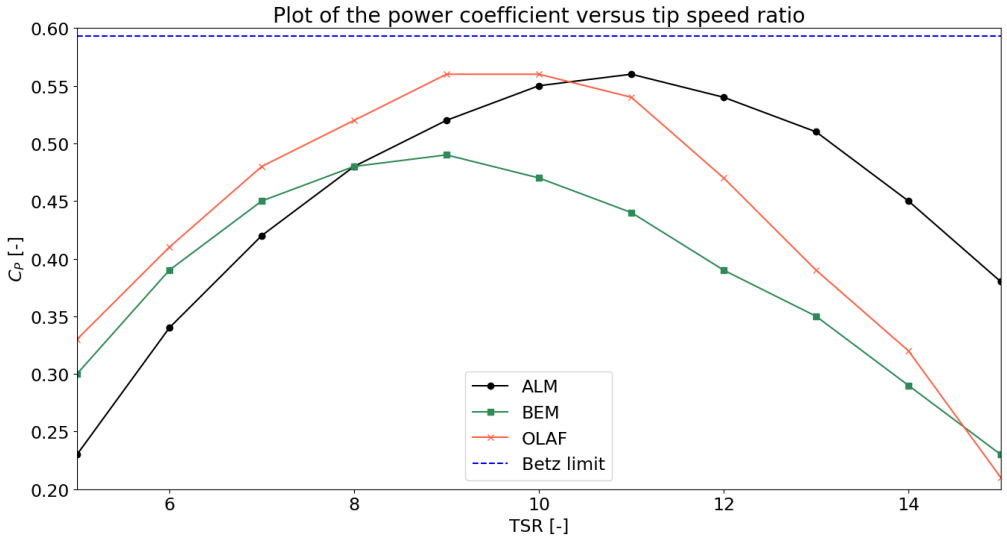

Figure 7.4: C_P versus TSR plot of the IEA 15-MW RWT

The power coefficient versus TSR is plotted for the NREL 5-MW and the IEA 5-MW in Figure 7.3 and Figure 7.4, respectively. At first glance it might seem that these differences between these two figures are much larger than was the case for the thrust coefficient plots. However, the difference is average maximum deviation is also 46.6 % for the power coefficient plots which illustrates that the differences are similar. There are also similarities to be found when comparing the two power coefficient plots for the two turbines. In both figures, OLAF and BEM have the maximum power coefficient at the same TSR but the maximum C_p value of OLAF coincides with the maximum C_P value of ALM (which is shifted with a TSR value of 1.5 to the right). Besides that, both figures also have the maximum deviation at the TSR value of 15, ALM start with a lower C_P value but ends higher for higher TSR values and OLAF drops rapidly at the TSR value of 11, in both figures. In general, it can be said that both C_P versus TSR plots show the same trends between the different fidelities however the average maximum deviation is significantly higher (46.6 %) for the IEA 15-MW.

To identify where these differences might be coming from, a scaled-down turbine is developed which turns the IEA 15-MW into a 5-MW turbine. This is only done for the ALM simulation to check whether the differences would be coming from the increase in size. The scaling relations shown in Equation 7.1 are used as explained in [28] (chapter 7). The down-scaling is limited by the Reynolds number but since the Reynolds number is above 50,000 for both turbines this should not be an issue [28]. In this equation, P is the power, A is the area, R is the radius, c is the chord of a blade elements and dr is the spanwise length of the same element.

$$\frac{P_2}{P_1} = \frac{A_2}{A_1} = \frac{R_2^2}{R_1^2} = \frac{c_2 \cdot dr_2}{c_1 \cdot dr_1} \tag{7.1}$$

Since the power ratio equals one third, this means that the radius of the downscaled turbine equals 69.3 m. The scaling of the computational grid is done linearly which drastically reduces the number of cells (from 9 million to 2 million cells). The results of the thrust and power coefficients can be found in Figure 7.5 and Figure 7.6, respectively. These figures show that there is actually no significant difference between the IEA 15-MW RWT ALM model and the downscaled ALM model (2.2 % for C_P and 1.5 % C_T). This would mean that the difference in fidelities is exactly just that. The NREL 5-MW RWT is better suited to be used across the different fidelities than the IEA 15-MW which can be attributed to the design of the specific turbines. These design parameters are in this case the chord distribution, the twist distribution and the airfoils.

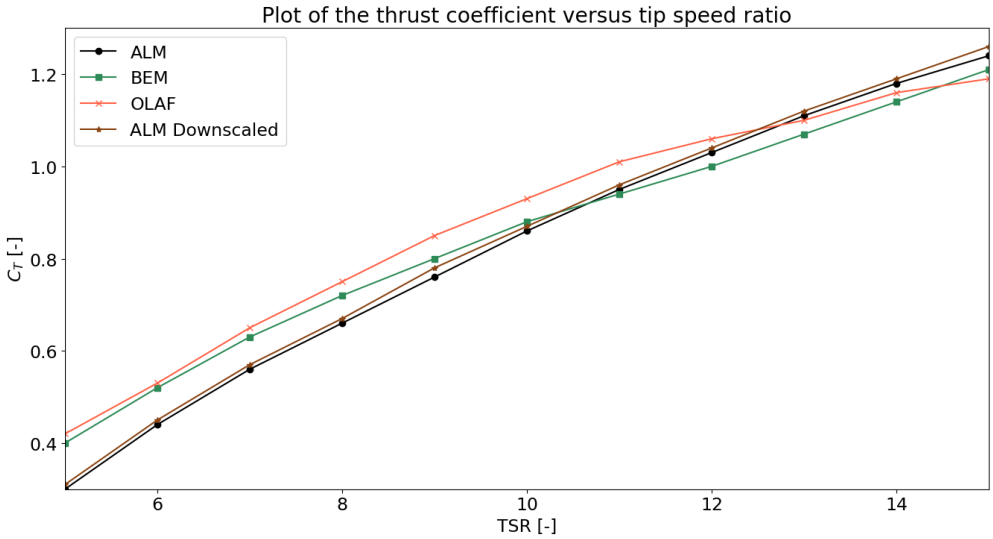

Figure 7.5: C_T versus TSR plot of the IEA 15-MW RWT including the downscaled 5-MW turbine

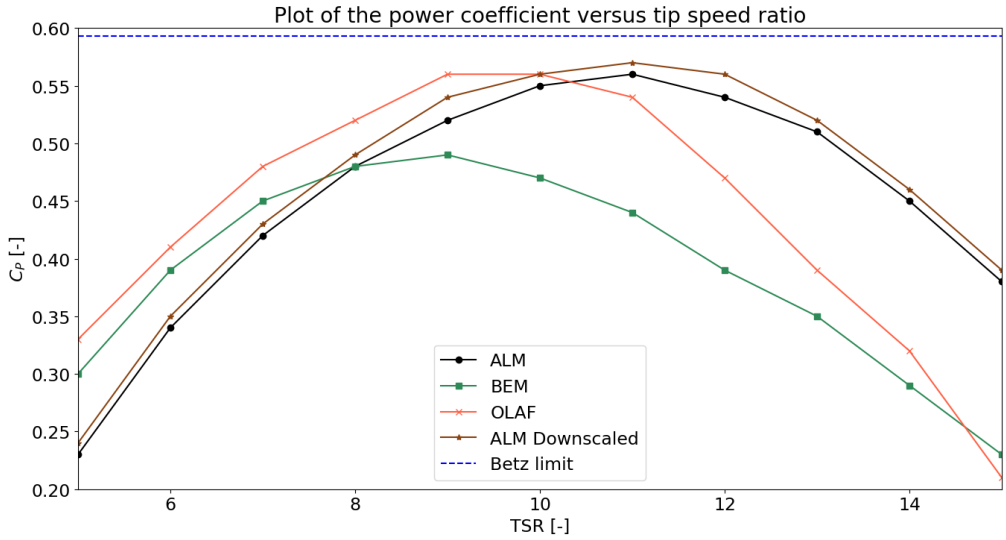

Figure 7.6: C_P versus TSR plot of the IEA 15-MW RWT including the downscaled 5-MW turbine

Plots of the design parameters are shown below for the three turbines. As expected the downscaled version coincides with the IEA 15-MW RWT because the plots are non-dimensional. These figures show that the NREL 5-MW has a higher non-dimensional chord distribution (Figure 7.7), a lower twist distribution (Figure 7.8), a similar drag coefficient distribution (Figure 7.9) and a lower lift coefficient distribution (Figure 7.10).

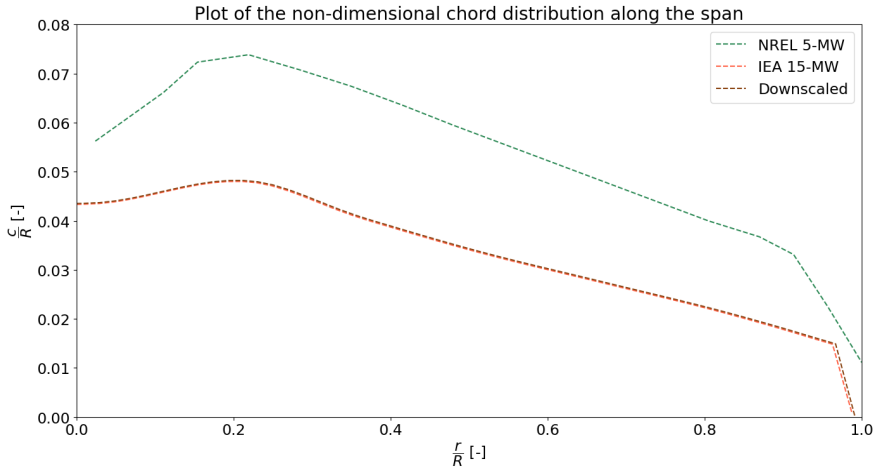

Figure 7.7: Plot of the non-dimensional chord distribution along the span

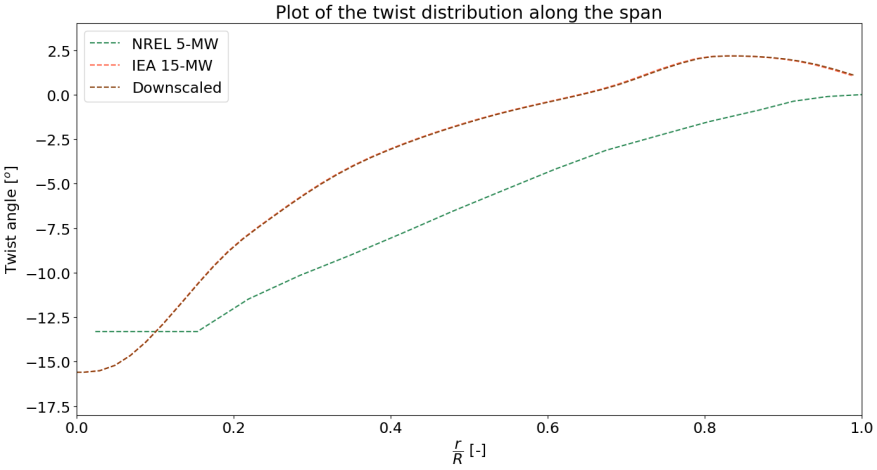

Figure 7.8: Plot of the twist distribution along the span

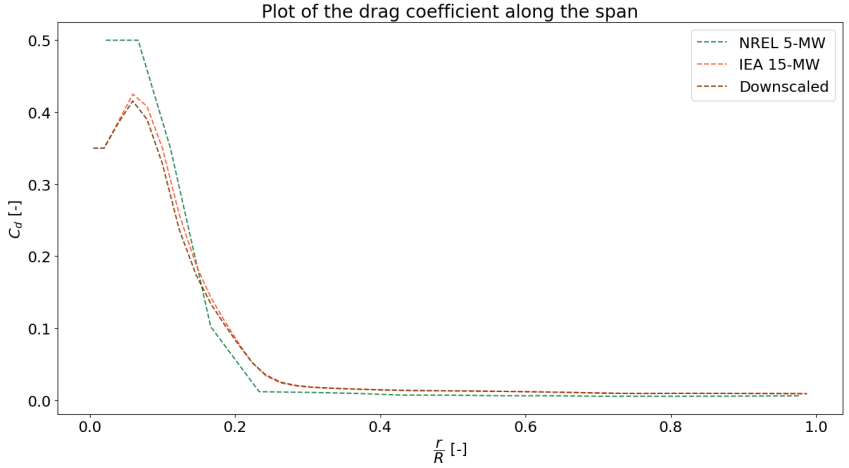

Figure 7.9: Plot of the drag coefficient distribution along the span

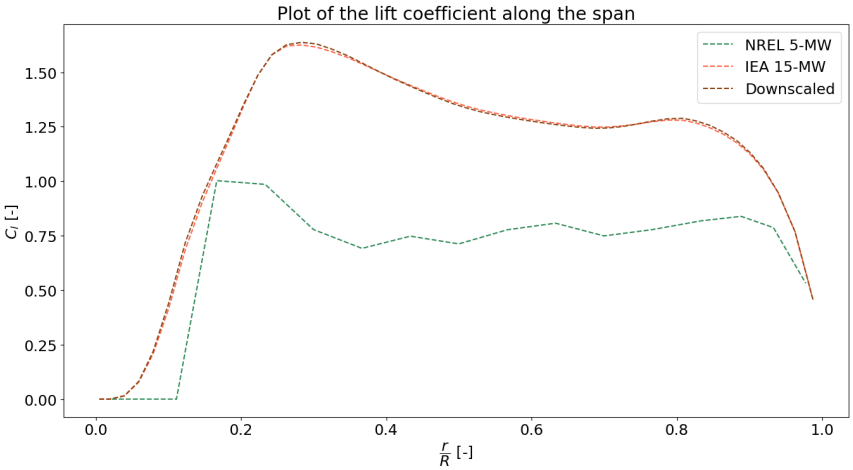

Figure 7.10: Plot of the lift coefficient distribution along the span

7.2. Comparison of Velocity Deficit Plots

The velocity deficit plots of three turbines will be shown this section. Namely the IEA 15-MW RWT, the NREL 5-MW RWT and the downscaled version of the IEA 15-MW RWT to a 5-MW turbine. To allow for a fair comparison each velocity deficit plot is taken at the same distance to radius ratio behind the turbine (for instance 0.9 R in Figure 7.11), at the same time (t = 200 s), with the same uniform inflow conditions and in a region where the resolution is the same (baseline grid, cells of $2mx2mx2m$). The turbines are first compared when each turbine is operating at the same TSR of 9 and later they are compared when each turbine is operating at its design TSR which is also where they have the same C_P of 0.52.

Note that the design TSR as defined in the definition of the RWTs is the same as the TSR where the maximum C_P occurs for the BEM simulations but is therefore different than where the maximum C_P occurs for the ALM simulations. In this report the design TSR always refers to the TSR value as defined in the definitions of the RWTs (I.e. 9 for the IEA 15-MW and 7.5 for the NREL 5-MW).

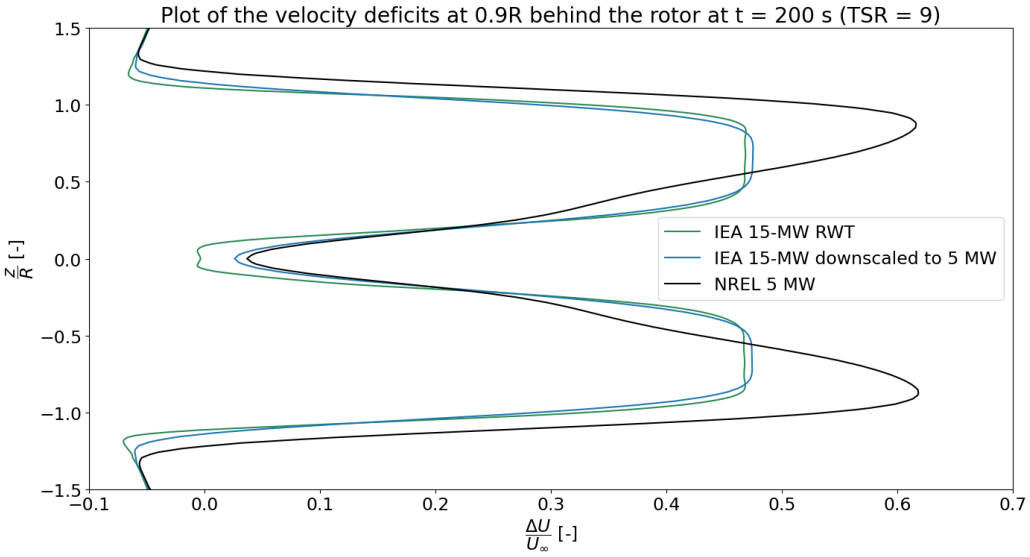

Figure 7.11: Plot of the velocity deficit at a TSR of 9 for the IEA 15-MW RWT, the NREL 5-MW RWT and the downscaled version of the IEA 15-MW to a 5-MW version

In Figure 7.11 the velocity deficit plot of the three turbines operating at a TSR of 9 can be found. This figure shows that the velocity deficit of the NREL 5-MW RWT is much larger at this TSR than for the IEA 15-MW RWT and its downscaled counterpart. This makes sense when looking at the C_P versus TSR curves of these turbines (Figure 5.26 and Figure 6.13, respectively). The NREL 5-MW RWT is at its peak value while the IEA 15-MW RWT is still climbing towards the peak C_P value. The second observation that can be made, is that the downscaled version aligns well with the IEA 15-MW except for some minor deviations at the hub and the tip. This also makes sense as this figure is non-dimensionalized and therefore no scaling effects should be noticeable here.

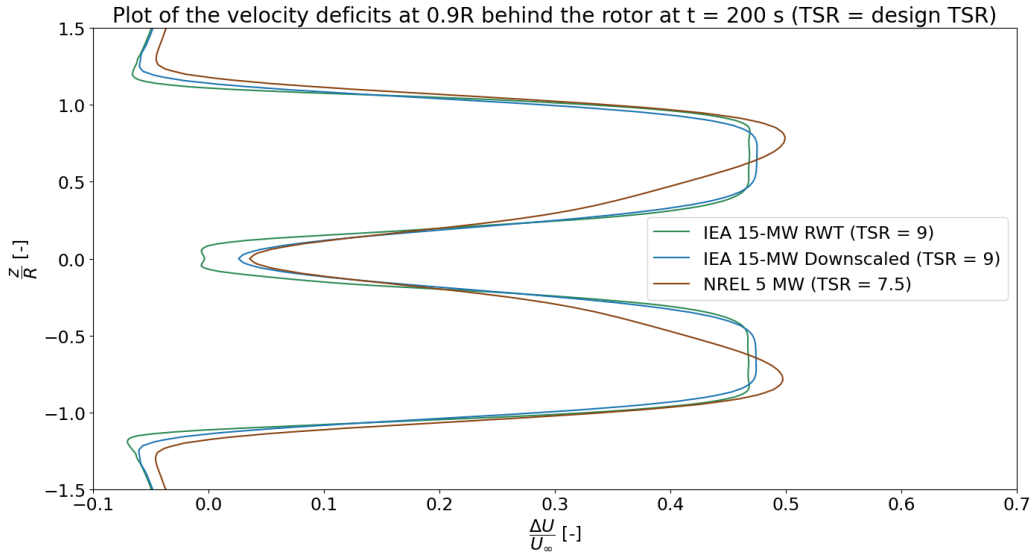

Figure 7.12: The same plot of the previous velocity deficit but now including the the line of the NREL 5-MW RWT at its design TSR of 7.5

In Figure 7.12 the velocity deficit plot of the three turbines operating at a their design TSR can be found. At these TSRs, the turbines have the same power coefficient which aligns with what can be observed in the figure as the velocity deficits are similar. The differences in the curves between the IEA 15-MW RWT and the NREL 5-MW RWT can be attributed to the different choice of airfoils, twist distribution and chord distribution.

7.3. Comparison of Wake Visualization

The different wake visualizations should also be compared to identify differences between the turbines. First, the ALM models are compared and after that the OLAF models are compared.

Each turbine is analysed at its own design TSR. The wake visualization using ALM of the IEA 15-MW RWT for the baseline grid and the coarse grid are shown in Figure 7.13 and Figure 7.14, respectively. For the NREL 5-MW RWT these are shown in Figure 7.15 and Figure 7.16, respectively. Finally, the downscaled version has a wake visualization of the baseline grid as shown in Figure 7.17 and Figure 7.18 shows a comparison of the IEA 15-MW RWT and the downscaled version.

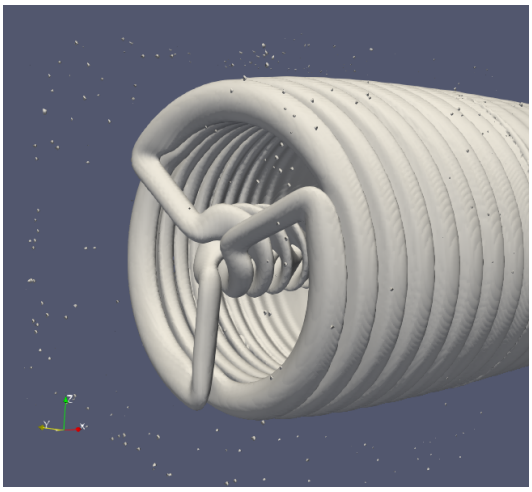

Figure 7.13: Vorticity contour plot of the IEA 15-MW RWT with a very coarse grid and Q-criterion = 0.0001

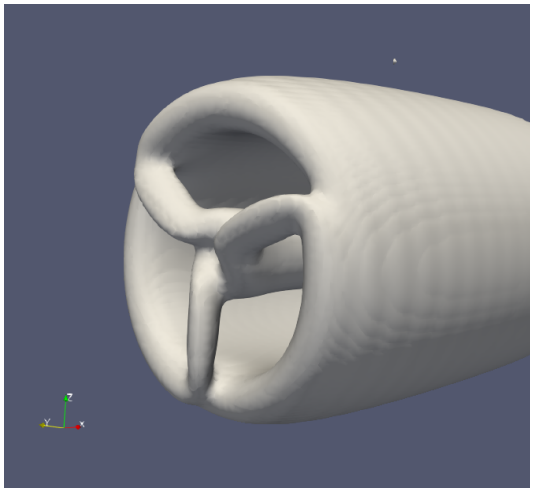

Figure 7.14: Vorticity contour plot of the IEA 15-MW RWT with a baseline grid and Q-criterion = 0.0001

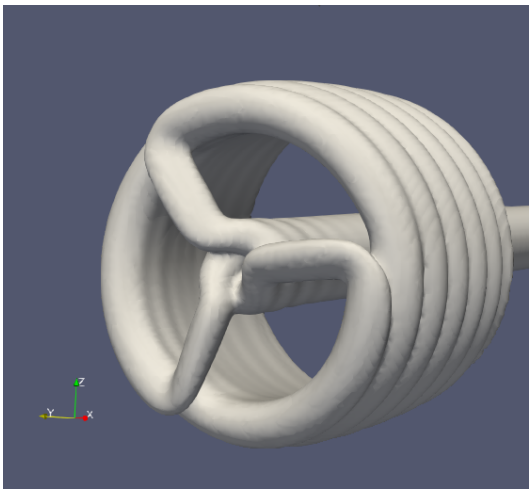

Figure 7.15: Vorticity contour plot of the NREL 5-MW RWT with a very coarse grid and Q-criterion = 0.001

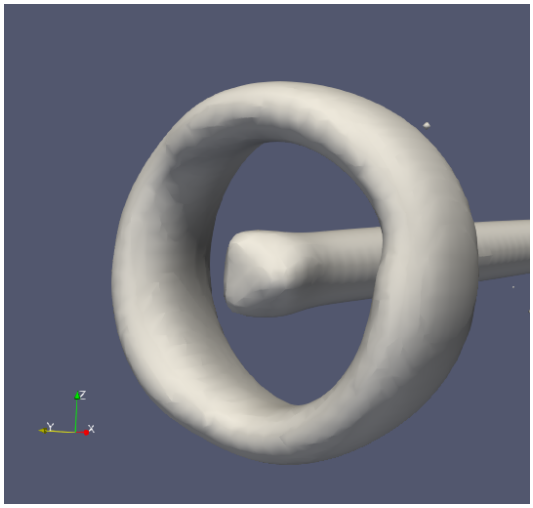

Figure 7.16: Vorticity contour plot of the NREL 5-MW RWT with a very coarse grid and Q-criterion = 0.001

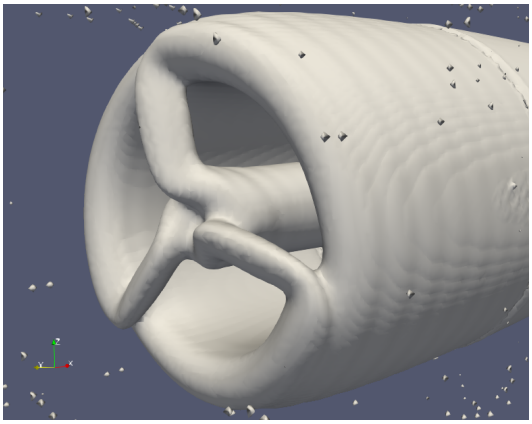

Figure 7.17: Vorticity contour plot of the downscaled version of the IEA 15-MW RWT with a very coarse grid and Q-criterion = 0.0001

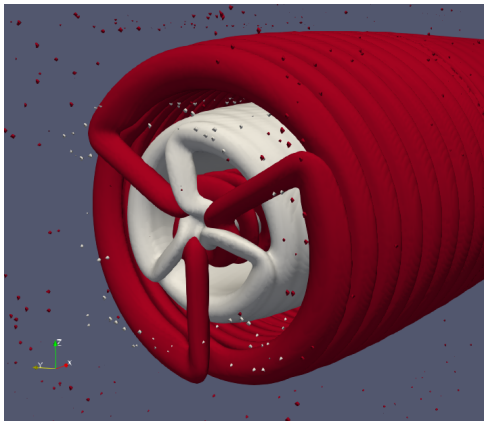

Figure 7.18: Vorticity contour plot of the IEA 15-MW RWT and the downscaled version with a baseline grid and Q-criterion = 0.0001

The IEA 15-MW has a better wake visualization plot than the NREL 5-MW because the vortices and blades are more distinguished. This is true when comparing baseline cases (Figure 7.13 versus Figure 7.15) and also when comparing the very coarse cases (Figure 7.14 versus Figure 7.16). In the performance parameters and velocity deficit comparisons (discussed in section 7.1 and section 7.2, respectively), the differences were not attributed to the change in size but rather to the difference in design parameters. Now however, it is perhaps due to the difference in size while keeping the same resolution, since also the downscaled version of the IEA shows a worse visualization for the same resolution. There is a simple explanation for this. Namely that the resolution should also scale with the grid sizes, to keep the non-dimensional cellsize-over-radius ratio constant instead of keeping the number-of-cells-over-radius ratio (i.e. the resolution) constant. This is illustrated visually in Figure 7.19. Why this is important has to do with the Q-criterion which is used to visualize the vortices in the ALM simulation. The Q-criterion uses the gradient of the velocity tensor and since the number of cells plays a role in the discretization of the velocity gradient, it means that the total number of cells should remain the same (i.e. keep the non-dimensional ratio cellsize-over-radius constant).

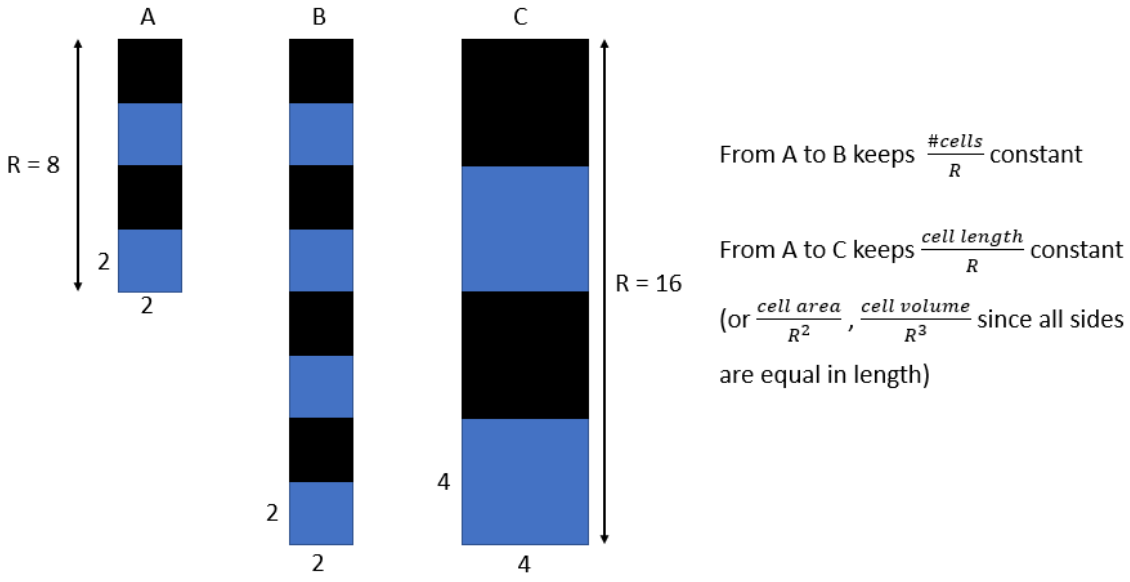

Figure 7.19: Example of two ways to discretize the grid when scaling the turbine

To investigate whether this is indeed the case, the velocity profiles for the three turbines, with the same and with different resolutions, will be analysed in the next section.

For the OLAF wake comparison, the turbines are also analysed at their own design TSR. The two near and far wakes (for only one blade) of the NREL 5-MW RWT and the IEA 15-MW RWT are shown in Figure 7.20 and Figure 7.21, respectively.

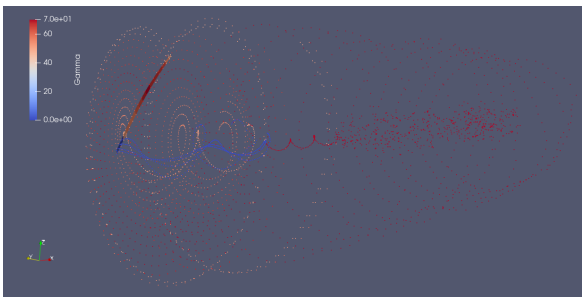

Figure 7.20: Visualization of both the near wake and the far wake of the NREL 5-MW RWT for only one blade

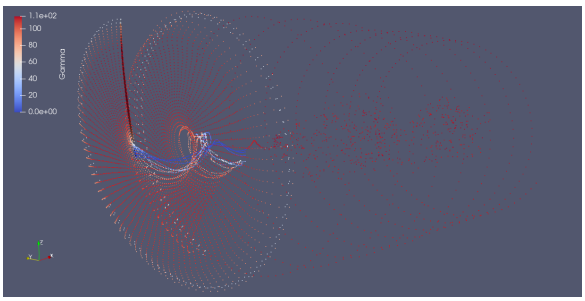

Figure 7.21: Visualization of both the near wake and the far wake of the IEA 15-MW RWT for only one blade

These figures show that the wake of both turbines break down soon in the far wake. These figures also show that the IEA 5-MW RWT has a finer discretization because it has more blade elements for its radius length (50/120 = 0.42 versus 17/63 = 0.27), a lower magnitude in step size and it takes more simulation time to reach convergence. The OLAF simulations take 57 CPU hours for the IEA 15-MW while the NREL 5-MW only takes 1.5 CPU hours to reach 200 seconds of simulation time.

7.4. Comparison of Velocity Profiles

The velocity profile plots of the three turbines are shown below. Each turbine has its velocity profile on the left-hand side and the corresponding grid resolution on the right-hand side. At this point, each plot has the same resolution near the turbine for which a similar velocity profile is expected. However as seen in the figures, the two smaller turbines (Figure 7.24 and Figure 7.26) show less details in the very near wake than the IEA 15-MW RWT (Figure 7.22) for the same resolution. These findings are in line with the ALM wake visualizations of the previous section where it was already shown that the IEA 15-MW RWT has more details for the same resolution than the smaller turbines.

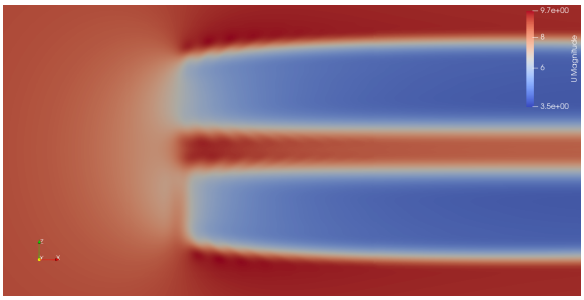

Figure 7.22: Velocity profile plot of the IEA 15-MW RWT with the baseline grid resolution $(2mx2mx2m)$

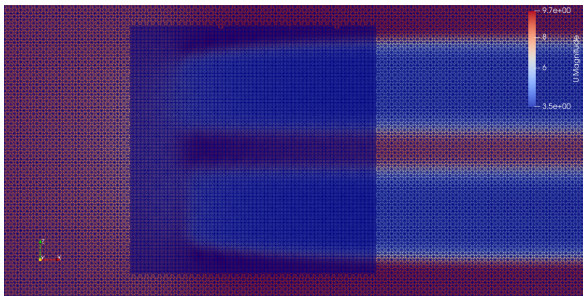

Figure 7.23: Velocity profile plot with overlapping grid of the IEA 15-MW RWT with the baseline grid resolution $(2mx2mx2m)$

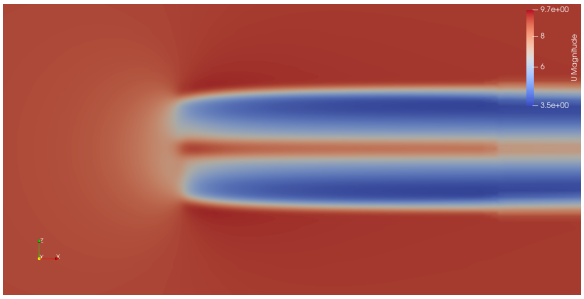

Figure 7.24: Velocity profile plot of the NREL 5-MW RWT with the baseline grid resolution $(2mx2mx2m)$

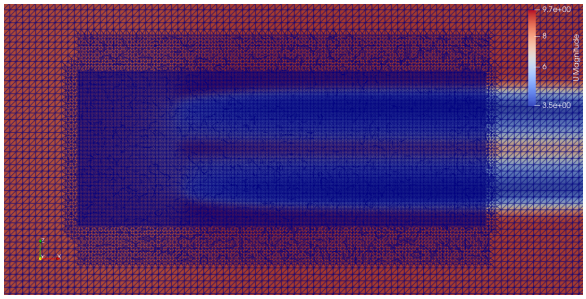

Figure 7.25: Velocity profile plot with overlapping grid of the NREL 5-MW RWT with the baseline grid resolution $(2mx2mx2m)$

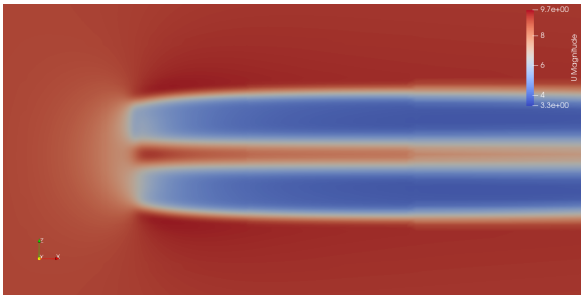

Figure 7.26: Velocity profile plot of the downscaled version of the IEA 15-MW RWT with the baseline grid resolution $(2mx2mx2m)$

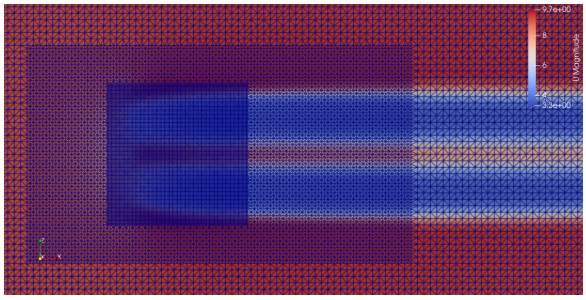

Figure 7.27: Velocity profile plot with overlapping grid of the downscaled version of the IEA 15-MW RWT with the baseline grid resolution $(2mx2mx2m)$

Comparing different resolutions leads to the same conclusions. The velocity profile with a very coarse grid of the IEA 15-MW RWT can be seen in Figure 7.28 and the very fine grid of the NREL 5-MW RWT can be seen in Figure 7.30. This is done to find out if the baseline grid of the IEA 15-MW is more comparable with the more refined grid of the NREL 5-MW than with its baseline counterpart. The same question can be posed for the very coarse grid of the IEA 15-MW RWT.

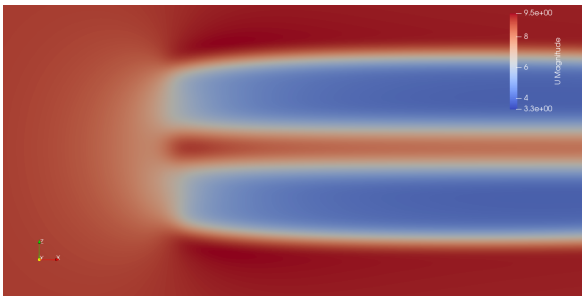

Figure 7.28: Velocity profile plot of the IEA 15-MW RWT with the very coarse grid resolution $(4mx4mx4m)$

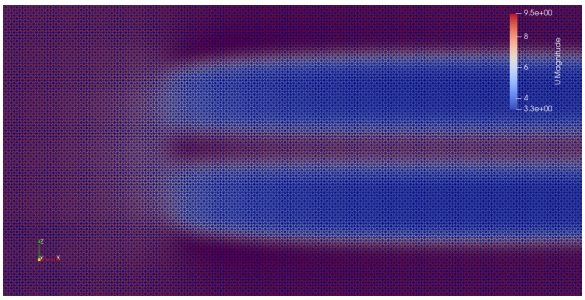

Figure 7.29: Velocity profile plot with overlapping grid of the IEA 15-MW RWT with the very coarse grid resolution $(4mx4mx4m)$

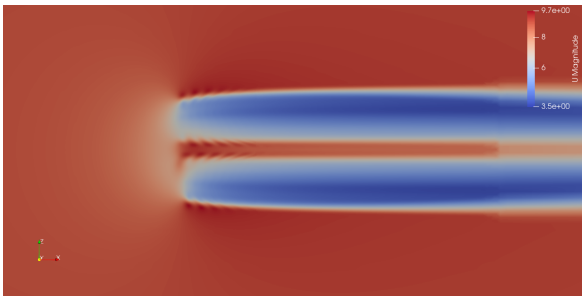

Figure 7.30: Velocity profile plot of the NREL 5-MW RWT with the very fine grid resolution $(1mx1mx1m)$

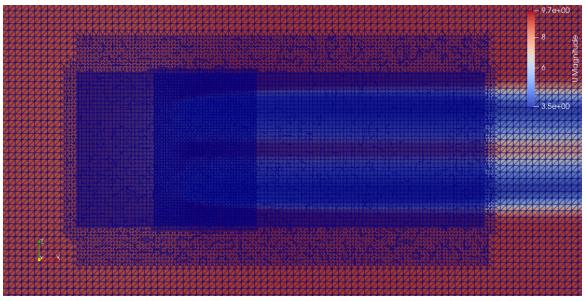

Figure 7.31: Velocity profile plot with overlapping grid of the NREL 5-MW RWT with the very fine grid resolution $(1mx1mx1m)$

When looking at the figures above it is indeed true that the baseline grid of the larger IEA 15-MW RWT compares better with the more refined grid of the smaller NREL 5-MW RWT than with its baseline grid. Similarly, the baseline grid of the smaller NREL 5-MW RWT compares better with the very coarse grid of the larger IEA 15-MW RWT than with its baseline grid. This leads to the conclusion that the resolution should also be scaled with the radius to allow for a fair comparison of the wake.

7.5. Discussion and Conclusion

The differences that can be found across the different fidelity models can be attributed to their assumptions and workings. All three methods use the same airfoil data and make use of blade elements but each method uses a different theory. BEM uses an one dimensional momentum balance, FVW uses a discrete vorticity field and ALM uses the Navier-Stokes equations with a momentum sink.

The thrust coefficient shows much more similarities across the different fidelities than the power coefficient. The main reason for this is because all three methods use the same airfoil data and make use of blade elements. Therefore simulating the blade thrust that is exerted on the flow does not deviate as much as simulating how the flows develops in the wake. Since the power coefficient is based on the wake calculations and since each method has a different wake method this could indeed lead to more differences in the power coefficient than in the thrust coefficient.

The results show that BEM consistently has a lower power coefficient than ALM and OLAF which would mean that it underestimates the reduction in axial velocity. BEM does not calculate a wake but only uses the blade elements in an actuator disk configuration. This makes it fast but does not allow the

wake results to be considered in the iterations towards convergence. The FVW OLAF on the other hand does calculate a wake by using a vorticity field and by doing this it is better suited to calculate the power coefficient of the turbine. Finally, ALM shows more similarity with FVW than with BEM which makes sense since both methods calculate the wake of the blades to determine the power coefficient. However, the ALM has lower a lower C_P for the lower TSR values and a higher C_P for the higher TSR values. The differences are much smaller for the NREL 5-MW than for the IEA 15-MW but it can nevertheless be observed for both turbines.

It is clear that the differences across the fidelities are much larger for the IEA 15-MW RWT than for the NREL 5-MW RWT (46.6 % for both the power and thrust coefficient). Adding a downscaled model to the mix shows that these differences must come from the design of the IEA 15-MW. This turbine is designed to have larger blades where different issues are increasingly important such as control and aero-elasticity. In any case, the design parameters are clearly different as shown in Figure 7.7 to Figure 7.10 which might give reason for why the ALM simulation reach different values and especially at a higher TSR.

The wake of the three turbines are compared using the velocity deficit plots, the wake visualizations and the velocity profiles. From this analysis it can be concluded that the wakes show similar behaviour but that the resolution of the grid cannot be simply kept constant. Having the same resolution for larger turbines as for lower turbines leads to relatively more distinguished plots for the larger turbine (and vice versa). The OLAF simulations of the IEA 15-MW are better visualized due to the higher number of blade elements but this comes at the price of higher computational cost.

To analyse the computational cost, an overview can be found in Table 7.1 where the computation time for each turbine and tool can be seen. This shows that BEM and ALM take about three times longer for the IEA 15-MW RWT than for the NREL 5-MW RWT. OLAF on the other hand, takes 38 times longer for the IEA 15-MW and even requires more time to run than the CFD ALM simulation. The downscaled version of the IEA 15-MW has almost half the computation time of the NREL 5-MW due to a more efficient grid design (fewer cells in the less important outer regions and smaller inner regions). In general however, if the grid resolution for the ALM simulation is also scaled then that would mean that there is not more simulation time required when increasing turbine size (since the total number of cells would remain the same).

Table 7.1: Overview of the computation time required for each turbine and fidelity tool

	BEM (100 seconds)	OLAF (200 seconds)	ALM Baseline (200 seconds with 20 processors on 1 node)
NREL 5-MW	14 min	1,5 h	10,5 h
IEA 15-MW	46 min	57 h	36 h
Downscaled IEA to 5-MW	X	X	6 h

8

Conclusions and Recommendations

This thesis report started off with the main goal to analyse whether a low-fidelity approach is still feasible for an aerodynamic analysis of large wind turbines in comparison with a high-fidelity approach. To do this, first a suitable high-fidelity and low-fidelity aerodynamic analysis methods have to be found. Then the wind turbines have to be chosen. With the analysis methods and the turbines in place it is possible to perform aerodynamic analysis and to compare the results to find similarities and differences across both the turbines and the fidelities. This section will summarize the conclusions given at each step and finally it will provide the final conclusions and recommendations.

8.1. Summary of Conclusions

To find a suitable high-fidelity method, different possibilities were discussed in chapter 2. First, the turbulence model had to be chosen. LES (Large Eddy Simulation) has the advantage over RANS (Reynolds-Averaged Navier-Stokes) that it is able to calculate the unsteady, anisotropic turbulent flows of the wake but this higher accuracy comes with a higher computational cost. Therefore, it was chosen to use RANS instead of LES because the computational time for performing an LES simulation would be out of the scope of this thesis project. Secondly, a modelling approach of the turbine had to be chosen where the ALM (Actuator Line Method) was deemed to be the optimal choice for this thesis project because the focus lies on performing near wake calculations. The BRM (Blade Resolved Method) would be better suited for blade calculations and the ADM (Actuator Disk Method) would be better suited for wind farm calculations. Finally, a solver had to be chosen for which OpenFOAM was deemed best because it is well documented, it has available libraries for ALM and because it is open-source.

Two low-fidelity methods were chosen in chapter 3. First of all, the BEM (Blade Element Momentum) theory was deemed a good choice because it is a widely applied low-fidelity method to analyse the performance parameters of wind turbines. BEM will be applied in OpenFAST because it is widely used by the wind energy community, it is open-source and it has the input variables of the NREL reference wind turbines readily available. Secondly, the FVW (Free Vortex Wake) method was chosen as another low to mid fidelity model since it is higher in fidelity than BEM but still lower in fidelity than ALM. OLAF will also be applied in OpenFAST because there is a wake module available called OLAF (cOnvecting LAgrangian Filaments) for which only an additional OLAF input file is required but apart from that the same input files can be just as for BEM.

The two turbines that were used for the analysis are the NREL 5-MW RWT (Reference Wind Turbine) and the IEA 15-MW RWT. The NREL 5-MW RWT was chosen because a lot of research has been conducted on this turbine and therefore it is possible to verify the results found for the three methods. The IEA 15-MW RWT was chosen since it is a newly proposed turbine with little research done so far on it. Therefore this analysis can provide useful information to the wind energy community. The idea is to first complete an analysis and verification of the NREL 5-MW RWT and then to apply the same tools and methods on the IEA 15-MW RWT. This should provide data which can be used to compare the results across both the turbines and the fidelities.

The results of the NREL 5-MW RWT were analysed in section 5.4. In general, the baseline grid was deemed sufficient from the grid refinement study and the results show a good agreement for the thrust and power coefficient. The ALM shows a better alignment with OLAF than with BEM which makes sense as both use wake calculations to estimate the wake instead of only using a global momentum balance. This is also in line with literature where the power for ALM and OLAF is also found to be higher than for BEM ([27], figure 6a). The C_T versus TSR plot for all three methods lie close together with an average deviation of 7.1 %. This also makes sense, as each method uses blade elements and the same 2D blade element data which is required to calculate the C_T. In terms of wake visualization, the VFW OLAF is 140 times faster than ALM for the same processing power which makes it a valuable tool to visualize the wake but for a more elaborate wake analysis the ALM is required which can only takes 7 times longer to run when run in parallel.

The results of the IEA 15-MW RWT, analysed in chapter 6, tell a slightly different story. First of all, the average maximum deviation for the thrust and power coefficient have both increased with 46.6 % when comparing with the NREL 5-MW RWT. Besides that, the OLAF simulations, which were useful for the NREL 5-MW to visually the wake, take much longer for the IEA 15-MW RWT as shown in Table 7.1. The main advantage of using OLAF for wake visualization would be that it is a fast tool to visualize where the wake is going and how it breaks down. If the OLAF simulations take longer to run than the ALM simulations then the advantages of using OLAF over ALM are lost.

A comparison of the performance parameters is given in section 7.1. As stated before the average maximum deviation for the C_T and C_P have both increased with 46.6 % but there are also a large number of similarities to be found. In general, it can be said that both C_P and C_T versus TSR plots show the same trends between the different fidelities however the average maximum deviation is significantly higher for the IEA 15-MW than for the NREL 5-MW. Adding a downscaled model to the mix shows that these differences must come from the design of the IEA 15-MW. This turbine is designed to have larger blades where different issues are increasingly important such as control and aero-elasticity. In any case, the design parameters are clearly different as shown in Figure 7.7 to Figure 7.10 which might give reason for why the ALM simulation reach different values and especially at a higher TSR.

A comparison of the wake and the resolution of the numerical setup is given by comparing the velocity deficits, the wake visualizations and the velocity profiles. In general, it can be concluded that the wakes show similar behaviour but that the resolution of the grid cannot be simply kept constant for the ALM simulations. Having the same resolution for larger turbines as for lower turbines leads to relatively more distinguished plots for the larger turbine (and vice versa). The OLAF simulations of the IEA 15-MW are better visualized due to the higher number of blade elements but this comes at the price of higher computational cost. This higher computational cost is not considered to be entirely worth it as the simulation takes longer than the ALM simulation. Since the ALM simulation contains much more information of the wake such as turbulence intensities and pressure distributions, the preference would be to choose ALM over OLAF for the IEA 15-MW RWT.

8.2. Final Conclusions

To reach the goal of this thesis project, the research questions must be answered as described in chapter 1. The two research questions are repeated below.

1. *How does the IEA 15-MW RWT compare with the previous NREL 5-MW RWT in terms of the steady state analysis and the unsteady wake simulation?*

2. *How well do different fidelity models perform in analysing the 15-MW RWT?*

To answer the first question, the 15-MW RWT does show more complex aerodynamics for the ALM simulations depending if the resolution is also scaled with the rotor size. Using the same resolution for both turbines leads to more flow details in the near wake of the larger IEA 15-MW RWT. If this is not the case however then both turbines show a very similar wake for the ALM wake visualizations. It is a slightly different story for the FWV OLAF as the aerodynamics can be said to be more complex because

the larger IEA 15-MW RWT requires a smaller time step to run and also has a finer blade element discretization. This causes the OLAF simulations to take 38 times longer to reach convergence while the ALM simulations only take 3 times longer.

The second question can also be answered. First of all, there are indeed significant differences in the performance parameters when using different fidelity models which also increase significantly for the IEA 15-MW RWT when comparing with the NREL 5-MW RWT, as shown in section 7.1. There are however also significant similarities. The most important one is that the C_P versus TSR plot of both turbines show that OLAF and BEM have the maximum power coefficient at the same TSR but the maximum C_p value of OLAF coincides with the maximum C_P value of ALM (which is shifted with a TSR value of 1.5 to the right). It was already discussed that these differences could be coming from the fact that the IEA 15-MW RWT is designed as a large turbine for which other fields also play a role such as control and aero-elasticity. It could very well be that, due to these different design parameters, the low-fidelity methods are less suitable to be used especially for high TSR values. It seems from the comparisons done that the use of CFD is already critical for analysing the IEA 15-MW RWT for high TSR values (TSR 12 and higher).

8.3. Recommendations

For further research it is recommended to study if the findings are in agreement to other findings in the field once more articles are published of the IEA 15-MW RWT. In addition, it would be useful to also include an even higher fidelity in the mix to identify if the ALM is indeed on the right track. For instance, since this thesis focused on the wake analysis, a similar study can be performed to perform a blade analysis. Such studies could use a blade resolved method and/or a large eddy simulation. These would specifically be useful to analyse the unsteady blade effects such as separation, transition and stall. Adding different turbines to the analysis could also provide useful information to identify if the deviation of the results can indeed be attributed to the design of large turbines or whether the findings here are only specific for the IEA 15-MW RWT. For these turbines also grid refinement studies should be performed, to support or undermine the conclusion that, when scaling, the resolution should also scale with the grid sizes, to keep the non-dimensional cellsize-over-radius ratio constant instead of keeping the number-of-cells-over-radius ratio (i.e. the resolution) constant.

In addition, aero-elastic effects were not studied in this thesis project which is something that will also play an increasingly important role for larger turbines. Therefore, it is also recommended to extent this study to include the effects of aero-elasticity for the three different fidelity methods. It becomes interesting to check whether the differences between across fidelities and turbines will increase, decrease, or stay the same.

Finally, this thesis project only used uniform inflow conditions but the IEA wind task 47 suggests that the effect of shear and veer are driving variables as to why the industrial design codes could not be sufficient anymore to design the larger wind turbines which is why it is also recommended to study the effects of adding shear and veer. Here it is again interesting to check in the differences across fidelities and turbines will change and to which degree.

Bibliography

[1] Gerard Schepers. “Avatar: Advanced aerodynamic tools of large rotors”. In: *33rd Wind Energy Symposium*. 2015, p. 0497.

[2] Evan Gaertner et al. *Definition of the IEA 15-Megawatt Offshore Reference Wind Turbine*. Tech. rep. International Energy Agency, 2020. URL: https://www.nrel.gov/docs/fy20osti/75698.pdf.

[3] ESI Group. “OpenFOAM”. In: *last accessed http://www.openfoam.com* (September 1, 2021).

[4] NREL. “OpenFAST”. In: *last accessed http://github.com/OpenFAST/openfast* (September 1, 2021).

[5] Tony Burton et al. *Wind energy handbook*. John Wiley & Sons, 2011.

[6] Benjamin Sanderse, SP Van der Pijl, and Barry Koren. “Review of computational fluid dynamics for wind turbine wake aerodynamics”. In: *Wind energy* 14.7 (2011), pp. 799–819.

[7] J Boussinesq. “Theorie de l’ecoulement tourbillant”. In: *Mem. Acad. Sci.* 23 (1877), p. 46.

[8] Joseph Smagorinsky. “General circulation experiments with the primitive equations: I. The basic experiment”. In: *Monthly weather review* 91.3 (1963), pp. 99–164.

[9] Luis A Martínez-Tossas. “Wind turbine modeling for computational fluid dynamics”. PhD thesis. 2012.

[10] Idriss Ammara, Christophe Leclerc, and Christian Masson. “A viscous three-dimensional differential / actuator disk method for the aerodynamic analysis of wind farms”. In: *J. Sol. Energy Eng.* 124.4 (2002), pp. 345–356.

[11] Niels Troldborg. “Actuator line modeling of wind turbine wakes”. In: (2009).

[12] PE Réthoré. “Wind Turbine Wake in Atmospheric Turbulence Ph. D”. PhD thesis. thesis Risø, 2009.

[13] Jens Norkær Sorensen and Wen Zhong Shen. “Numerical modeling of wind turbine wakes”. In: *J. Fluids Eng.* 124.2 (2002), pp. 393–399.

[14] Ye Zhang, Shuanghou Deng, and Xiaofang Wang. “RANS and DDES simulations of a horizontal-axis wind turbine under stalled flow condition using OpenFOAM”. In: *Energy* 167 (2019), pp. 1155–1163.

[15] Anshul Mittal et al. “Blade-resolved simulations of a model wind turbine: effect of temporal convergence”. In: *Wind Energy* 19.10 (2016), pp. 1761–1783.

[16] M Salman Siddiqui et al. “Numerical investigation of modeling frameworks and geometric approximations on NREL 5 MW wind turbine”. In: *Renewable Energy* 132 (2019), pp. 1058–1075.

[17] M Salman Siddiqui et al. “Numerical analysis of NREL 5MW wind turbine: A study towards a better understanding of wake characteristic and torque generation mechanism”. In: *Journal of Physics: Conference Series*. Vol. 753. 3. IOP Publishing. 2016, p. 032059.

[18] Niels Troldborg et al. “Comparison of wind turbine wake properties in non-sheared inflow predicted by different computational fluid dynamics rotor models”. In: *Wind Energy* 18.7 (2015), pp. 1239–1250.

[19] Jordan M Wilson et al. “Comparisons of horizontal-axis wind turbine wake interaction models”. In: *Journal of Solar Energy Engineering* 137.3 (2015).

[20] Pete Bachant et al. *turbinesFoam/turbinesFoam: v0.0.8*. Version v0.0.8. Mar. 2018. DOI: 10.5281/zenodo.1210366. URL: https://doi.org/10.5281/zenodo.1210366.

[21] Jennifer Rinker et al. “Comparison of loads from HAWC2 and OpenFAST for the IEA Wind 15 MW Reference Wind Turbine”. In: *Journal of Physics: Conference Series*. Vol. 1618. 5. IOP Publishing. 2020, p. 052052.

[22] Kelsey Shaler, Emmanuel Branlard, and Andy Platt. “OLAF User’s Guide and Theory Manual”. In: (2020).

[23] Jason Jonkman et al. *Definition of a 5-MW reference wind turbine for offshore system development*. Tech. rep. National Renewable Energy Lab.(NREL), Golden, CO (United States), 2009.

[24] Mandar Tabib et al. “Industrial scale turbine and associated wake development-comparison of RANS based Actuator Line Vs Sliding Mesh Interface Vs Multiple Reference Frame method.” In: *Energy Procedia* 137 (2017), pp. 487–496.

[25] Xu Ning et al. “Numerical Study of Wake Interaction and its Effect on Wind Turbine Aerodynamics Based on Actuator Line Model”. In: *The 29th International Ocean and Polar Engineering Conference*. OnePetro. 2019.

[26] Néstor Ramos-García et al. “Investigation of the floating IEA Wind 15 MW RWT using vortex methods Part I: Flow regimes and wake recovery”. In: *Wind Energy* (2021).

[27] Kelsey Shaler et al. “Comparison of Free Vortex Wake and BEM Structural Results Against Large Eddy Simulations Results for Highly Flexible Turbines Under Challenging Inflow Conditions”. In: *Wind Energy Science Discussions* (2022), pp. 1–22.

[28] Robert Gasch and Jochen Twele. “Scaling wind turbines and rules of similarity”. In: *Wind Power Plants*. Springer, 2012, pp. 257–271.